



UNIVERSIDAD DE ANTIOQUIA
Medellín (Colombia)

Study of core collapse neutrino signals and constraints on neutrino masses from a future Galactic Supernova

A dissertation submitted in partial satisfaction
of the requirements for the degree
Doctor in Physics

by
Jorge I. Zuluaga

Thesis director
Prof. Enrico Nardi

January 2005

Abstract

We study the sensitivity to neutrino masses of a Galactic supernova neutrino signal as could be measured with the detectors presently in operation and with future large volume water Čerencov and scintillator detectors.

The analysis uses the full statistics of neutrino events. The method proposed uses the principles of Bayesian inference reasoning and has shown a remarkably independence of astrophysical assumptions.

We show that, after accounting for the uncertainties in the detailed astrophysical description of the neutrino signal and taking into account the effects of neutrino oscillations in the supernova mantle, detectors presently in operation can have enough sensitivity to reveal a neutrino mass (or to set upper limits) at the level of 1 eV. This is sensibly better than present results from tritium β -decay experiments, competitive with the most conservative limits from neutrinoless double β -decay and less precise but remarkably less dependent from prior assumptions than cosmological measurements.

Future megaton water Čerencov detectors and large volume scintillator detectors will allow for about a factor of two improvement in the sensitivity; however, they will not be competitive with the next generation of tritium β -decay and neutrinoless double β -decay experiments.

Using the codes developed to perform the generation of synthetic supernova signals and their analysis we created a computer package, SUNG (SUpernova Neutrino Generation tool, <http://urania.udea.edu.co/sungweb>), aimed to offer a general purpose solution to perform calculations in supernova neutrino studies.

*Nothing is built on stone;
all is built on sand,
but we must build as if the sand were stone.*
Jorge Luis Borges

Acknowledgments

First I want to express my gratitude to all the institutions that made possible the realization of this work. The *Universidad de Antioquia* that provided an initial financial support through the *Fondo de Becas Doctorales de la Vicerrectoría de Docencia* and to *COLCIENCIAS* and its *Programa de Apoyo a la Comunidad Científica Nacional a través de los Programas de Doctorado* for providing the fellowship that allowed me to complete my Ph.D. studies.

I also want to thank to the *Posgrado de Física* and the *Grupo de Fenomenología de Interacciones Fundamentales* of the Universidad de Antioquia for providing partial economical support for my visits to institutes abroad.

Special thanks go to the Abdus Salam ICTP in Trieste (Italy) that I had the pleasure to visit several times during the development of this work, for the nice hospitality and for the economical support provided for my travel and living expenses. The Abdus Salam ICTP has always been for me the ideal place to meet and interact with experienced scientists of all nationalities, and this has been fundamental for opening my mind. A special acknowledgment goes to Professor Alexei Smirnov for the comments and suggestions he made during a seminar I gave in one of my visits. I also want to acknowledge the precious support that the staff of the Abdus Salam ICTP Computer Division gave me that allowed me to optimize the use of the computational facilities of the Center.

I am very grateful to the *Laboratori Nazionali di Frascati* (INFN-LNF) in Frascati-Rome (Italy) where I had the opportunity to spend a period of six months during my *Pasantía Doctoral*. In particular it is a pleasure to acknowledge the INFN-LNF Theory Group for the kind hospitality and for the partial economical support they provided me during my stay in such a beautiful place. I also thank the Laboratori Nazionali del Gran Sasso (INFN-LNGS) for the kind invitation to give a seminar and present the preliminary results of this work. Special thanks go to Professor Francesco Vissani for his useful comments and quite valuable suggestions, as well as for the visit that he personally organized for me to the amazing LNGS underground installations.

I am specially indebted to my advisor, Professor Enrico Nardi, not only for his constant guidance during all these years and for his inspiring collaboration, but also for his continuous support and advice and for his huge patience in proofreading the manuscript of this thesis.

Many other people has contributed directly and indirectly to this work. Specially I

want to thank to Juan Jose Quiros for loan me his laptop to write the final version of this work in a more quit environment and my friend Jorge Johnson who help me in the organization of the computer codes in order to prepare a public version of the same codes (SUNG).

To my friends, parents and brothers that always encouraged me despite the circumstantial difficulties faced during these years.

And for their love and support in any possible way I owe my deepest thanks to my family (Olga, Andres and Daniel, *mis muñecos*) who always was there (and even follow me to Frascati) giving a profound sense to all my efforts. Words cannot express my gratitude and love for them. This work is dedicated to them.

Jorge Zuluaga
January, 2005

Table of Contents

1	Introduction	1
2	Neutrino fluxes and spectra	7
2.1	Evolution of Neutrino fluxes	8
2.1.1	Fast rising - the shock breakout	8
2.1.2	Flux maximum - accretion, mantle cooling and explosion	9
2.1.3	Decay - Kelvin-Helmholtz cooling	10
2.1.4	Analytical flux model	10
2.2	Neutrino Spectra	14
2.2.1	Electron neutrinos and antineutrinos	14
2.2.2	Non-electron neutrinos	15
2.2.3	Spectral pinching	16
2.3	Hierarchy of average energies	21
3	Simulation of a supernova neutrino signal	24
3.1	Oscillations of supernova neutrinos	25
3.1.1	Neutrino Oscillations - Basic facts	25
3.1.2	Neutrino mixing parameters - experimental values and limits	29
3.1.3	Neutrino Oscillations in the Supernova Mantle	29
3.1.4	Initial conditions	30
3.1.5	Neutrino oscillations in the Earth	34

3.2	The neutrino signal formalism	35
3.2.1	Neutrino Detection	36
3.3	Characteristics expected for the signal	44
3.3.1	Number of events	45
3.3.2	Time-integrated spectrum	46
3.3.3	Energy-integrated time profile	47
3.4	Generation of full statistics signals	47
4	Mass limits with Supernova Neutrinos	52
4.1	Time-of-flight delay of supernova neutrinos	52
4.2	Neutrino mass and the TOF delay	53
4.2.1	Time spread of the signal	53
4.2.2	Timing events	55
4.2.3	Detailed analysis of a signal	56
4.3	Basic description of method	56
4.4	Formalism for the signal analysis	58
4.4.1	The Likelihood Function	60
4.4.2	Posterior probabilities	60
4.4.3	Best-fit value and neutrino mass limits	61
4.5	Construction of the Likelihood Function	64
4.5.1	Neutrino spectrum	64
4.5.2	Detection cross-section	66
4.5.3	Flux model	66
4.5.4	LF regularization	71
4.6	Likelihood marginalization	77
5	Results and discussion	80
5.1	Description of tests	80
5.2	Results of the maximum likelihood analysis	84
5.2.1	Best-fit values and limits on m_ν^2	85
5.2.2	Fit to the flux model	90

5.3	Quantifying the sensitivity of the method	93
5.4	Additional remarks on the method	98
5.5	Summary and Conclusions	101
A	Bayesian Inference: basic definitions	104
A.1	Basic principles	104
A.2	Bayes theorem	105
A.3	The marginalization procedure	106
A.3.1	Marginalization of a normal pdf	107
A.4	Credible regions	108
B	SUNG: SUpernova Neutrino Generation tool	110
B.1	Package structure	111
B.2	Methods and Algorithms	112
B.2.1	Manipulation of Supernova simulations	112
B.2.2	Expected signal properties	113
B.2.3	Signal generation	114
C	List of symbols and abbreviations	116
C.1	List of symbols	116
C.2	List of abbreviations	119
References	120

List of Figures

1.1	Schematic illustration of the collapse of a massive star core and the onset of the explosion	
2.1	Neutrino fluxes evolution	9
2.2	Schematic analytical fits of $\bar{\nu}_e$ fluxes from two supernova simulations	12
2.3	Supernova neutrino fluxes from three different self-consistent simulations	13
2.4	$\bar{\nu}_e$ spectrum at 100 msec	15
2.5	Schematic representation of ν_x transport	17
2.6	Relation between pinching p , α and the effective degeneracy parameter η	19
2.7	α parameter evolution	20
2.8	Mean energy evolution from three different supernova simulations . .	22
3.1	Contours of equal neutrino jump probability across a resonance region	38
3.2	Jumping probability P_H (\bar{P}_H for inverted hierarchy)	39
3.3	Schematic illustration of how transition probabilities are computed .	40
3.4	Oscillation probability p_{\oplus} in the Earth mantle	41
3.5	Oscillation probability p_{\oplus} when neutrino traverse the mantle and core	42
3.6	Comparison between inverse β process cross-sections	43
3.7	Distribution of events in a supernova signal	46
3.8	Time integrated spectrum for two different supernova model and oscillations schemes	48
3.9	Energy integrated time-profile	49
3.10	Neutrino detected rate	51

4.1	TOF delay induced by a non-zero neutrino mass as a function of neutrino mass and supernova model	57
4.2	Schematic explanation of the method strategy	59
4.3	Schematic illustration of the determination of mass limits from the posterior probabilities	63
4.4	Schematic illustration of the spectral parameter estimation using overlapped time windows	64
4.5	Results of the spectral parameters estimation for 40 synthetic signals	68
4.6	Behavior of the flux model I	70
4.7	Behavior of the flux model II	72
4.8	Schematic illustration of the two-step process used to evaluate the likelihood function of a given signal	73
4.9	Schematic illustration of the problem introduced because the detected neutrino energies are discrete	74
4.10	Time profile of \tilde{f} for a 10 MeV neutrino using three different schemes of regularization	76
4.11	Illustration of the profile likelihood computation for m_ν^2	78
4.12	Contours of the log-LF compared with the contours of a Gaussian distribution	79
5.1	Luminosity, mean energy and α -parameter for $\bar{\nu}_e$ and $\bar{\nu}_x$ in the supernova models used in the study	81
5.2	First set of band plots for tests performed with supernova model I	86
5.3	Second sets of band plots for tests performed with supernova model I	87
5.4	First set of band plots for tests performed with supernova model II	88
5.5	Second set of band plots for tests performed with supernova model II	89
5.6	Fits to the flux model for various sets of input conditions using supernova model I	91
5.7	Fits to the flux model for various sets of input conditions using supernova model II	92
5.8	Two ways to quantify the sensitivity of the method	95
5.9	Relation between the number of events in the signal and the sensitivity of the method	96
5.10	Upper bounds obtained when two different prior probability on neutrino mass are used	99
5.11	Present and future of mass limits	103

List of Tables

3.1	Transition probabilities	33
3.2	The relevant $\bar{\nu}_e$ detection parameters for present and proposed large volume detectors	44
4.1	Limits on the neutrino mass from supernova neutrinos	57
5.1	Results for \bar{m}_{up} and $\sqrt{m_{\text{min}}^2}$ under different emission and detection conditions	97

CHAPTER **1**

Introduction

Supernovae (SN) and neutrinos form one of the most interesting (and strange) couples in Astrophysics and Fundamental Physics. The first ones are the most energetic explosions in the Universe after the Big-Bang while the second ones are the lightest and most elusive (massive) elementary particles.

This strange relation was probably first recognized in the early 1940s [1] and arises from the fact that neutrinos are produced in huge quantities by the nuclear processes which dominate the evolution of a dying massive star.

When the iron core of a massive star $M \gtrsim 10 M_{\odot}$ reaches a critical mass $M_c \simeq 1.0 M_{\odot} (Y_e/0.4)^2$ [2] by accumulation of the residual material produced in the “melting” of silicon, it becomes unstable and starts to collapse. Density and temperature of the very compressed material rise rapidly during the fast implosion of the core. When temperature is high enough the heavy nuclei synthesized during the whole stellar life start to be dissociated through photon processes:



This endothermic photodisintegration processes start to drain energy from the core and trigger the collapse. Additionally electron capture on proton produces electron neutrinos and reduces the electron degeneracy pressure:



Collapse is not forever. When the inner part of the stellar core reaches nuclear densities $\rho > 3 - 8 \times 10^{14} \text{ g/cm}^3$ it suddenly stops. Not all the core feels the

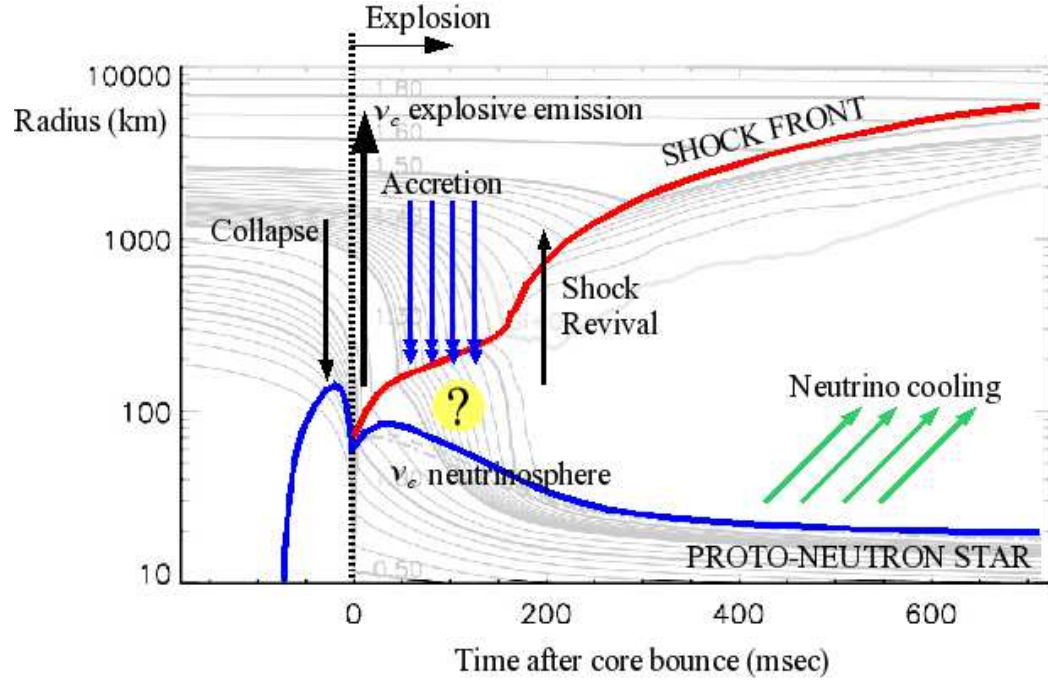


Figure 1.1: *Schematic illustration of the collapse of a massive star core and the onset of the explosion, superposed to a diagram of the evolution of mass-shells from a supernova simulation [3]. The question-mark in the region between the neutrino-sphere (neutrino last scattering surface) and the stalled shock wave during the accretion phase indicates our present ignorance about the exact mechanisms that concur to produce the revival of the explosion.*

interruption (collapse velocities above the inner core are faster than acoustic waves) and matter continues infalling. In less than 1 msec a hydrodynamic shock wave forms and starts to move outwards sweeping the falling matter and reversing the collapse: the core bounces (see fig. 1.1).

At the very high densities of the collapsing stellar core neutrinos are trapped in the first hundreds kilometers where production and absorption processes are very fast. After a few milliseconds from the core bounce the shock wave reaches the region where neutrinos stream out freely. Electron neutrino luminosity suddenly increases by around a factor of 10 in less than 1 msec and the fluxes of $\nu_{\mu,\tau}$, $\bar{\nu}_{\mu,\tau}$ are turned on (see sect. 2.1). Neutrino “fireworks” start.

In tens of seconds more than 10^{58} neutrinos of all flavors with energies in the range

10-50 MeV, are emitted carrying out almost all the gravitational binding energy released in the core collapse:

$$E_B \approx 3 \times 10^{53} \text{ erg} \left(\frac{10 \text{ km}}{R_{\text{NS}}} \right) \left(\frac{M_{\text{NS}}}{1.4 M_{\odot}} \right), \quad (1.3)$$

where R_{NS} and M_{NS} is the final mass of the neutron star formed in the process.

In the inner regions of the massive star the future of the shock wave is uncertain. More than thirty years of core collapse simulations show that before leaving the core, the shock wave looses completely its energy through photodisintegration of nuclear matter, and becomes an almost static accretion front. Then what produces the supernova explosion? No complete consensus still exists in the answer of this important question [4, 5, 6] although for sure, as was first realized twenty years ago [7], neutrinos do play a central role. The absorption in the stalled accretion shock of even a small fraction of the huge neutrino flux coming from the inner regions can be enough to revive the shock wave and restart the explosion, hundred of milliseconds after the initial core bounce.

This delayed explosion scenario is by now the preferred way to explain to the “supernova explosion enigma”. However self consistent hydrodynamic simulations have not yet been able to obtain a successful explosion [4, 5, 6]. The problem does not seem to be the mechanism in itself, in the sense that it is generally accepted that the delayed explosion occurs, and that neutrinos play a central role. More likely, other concomitant processes (convection, rotation, magnetic fields, etc.) could give the “last kick”. However the processes at the moment are not completely understood.

In summary, neutrinos are copiously produced in supernova and (together with other not well understood concomitant processes) could finally trigger the explosion itself. However supernova neutrinos can actually do more than producing the explosion. The detection of these neutrinos can open a door to understand the physics of supernova by giving us an unique “snapshot” of the core collapse processes in a way that no other signal (except perhaps the still undetected gravitational radiation) can do.

Supernova neutrinos are also very interesting for particle physics. On one hand they travel along huge distances, even in the astronomical sense (10 kpc is a typical number which is $\sim 10^8$ times larger than the Earth-Sun distance), and any small neutrino mass will produce a tiny (but detectable) time delay among neutrinos of very different energies. On the other hand, its energy is in the right range to make neutrino oscillations across the Earth “visible”, allowing to measure neutrino mixing parameters with unprecedented sensitivity.

In this work we will concentrate on the supernova neutrino potential to give us information on the absolute scale of neutrino masses.

During the past few years, atmospheric [8, 9, 10, 11, 12] and solar [13, 14, 15, 16, 17, 18, 19, 20, 21] neutrino experiments provided strong evidences for neutrino flavor oscillations and therefore for non vanishing neutrino masses. The KamLAND results [22, 23] on the depletion of the $\bar{\nu}_e$ flux from nuclear power plants in Japan, and the K2K indication of a reduction in the ν_μ flux from the KEK accelerator [24], gave a final confirmation of this picture.

However, to date all the evidences for neutrino masses come from oscillation experiments, that are only sensitive to squared mass differences and cannot give any information on the absolute scale of these masses. The challenge of measuring the absolute value of neutrino masses is presently being addressed by means of a remarkably large number of different approaches, ranging from laboratory experiments to a plethora of methods that relay on astrophysical and cosmological considerations (for recent reviews see [25, 26]).

From the study of the end-point of the electron spectrum in tritium β -decay, laboratory experiments have set the limit $m_{\nu_e} < 2.2$ eV [27, 28]. If neutrinos are Majorana particles, the non observation of neutrino-less double β decay can constrain a particular combination of the three neutrino masses. Interpretation of these experimental results is affected by theoretical uncertainties related to nuclear matrix elements calculations. This is reflected in some model dependence of the corresponding limits, that lie in the range $m_\nu^{\text{eff}} < 0.2 - 1.3$ eV [29, 30, 31, 26].

Tight bounds $\sum_i m_{\nu_i} < 0.6 - 1.8$ eV have been recently set using WMAP observations of cosmic microwave background anisotropies, galaxies redshift surveys and other cosmological data (for a recent review see [32] and references therein). However, these limits become much looser if the set of assumptions on which they rely is relaxed (see [33, 34, 35] for discussions on this point), and might even be completely evaded in exotic scenarios where neutrinos can annihilate into hypothetical light bosons, implying a suppression of their contribution to the cosmic matter density and negligible effects on structure formation at large scales [36].

Zatsepin [37] was probably the first to realize that information on a neutrino mass could be provided by the detection of neutrinos from a Supernova explosion. Other early (independent) contributions in studying the potential of supernova were put forth in refs. [38, 39, 40]. The basic idea relies on the time-of-flight (TOF) delay Δt_{tof} that a neutrino of mass m_ν and energy E_ν traveling a distance L would suffer with respect to a massless particle:

$$\Delta t_{\text{tof}} \simeq \frac{1}{2} \frac{m_\nu^2}{E_\nu^2} L. \quad (1.4)$$

Indeed, already in the past, the detection of about two dozens of neutrinos from SN1987 [41, 42, 43] allowed to set upper limits on m_ν . Due to the low statistics, the model independent bounds derived were only at the level of $m_{\bar{\nu}_e} < 30 \text{ eV}$ [44] while more stringent limits could be obtained only under specific assumptions [45, 46, 47, 48]. More recently, a detailed reexamination of the SN1987 neutrino signal based on a rigorous statistical analysis of the sparse data and on a Bayesian treatment of prior informations on the SN explosion mechanism, yielded the tighter bound $m_{\bar{\nu}_e} < 5.7 \text{ eV}$ [49].

The first observation of neutrinos from a SN triggered in the years following 1987 an intense research work aimed to refine the methods for neutrino mass measurements, in view of a future explosion within our Galaxy. With respect to SN1987, the time delay of neutrinos from a Galactic SN would be reduced by a factor of a few due to the shorter SN-earth distance. However, the neutrino flux on Earth would increase as the square of this factor and, most importantly, the large volumes of the neutrino detectors presently in operation will yield a huge gain in statistics. In recent years several proposal have been put forth to identify the best ways to measure the neutrino time-of-flight delays, given the present experimental facilities. Often, these approaches rely on the identification of “timing” events that are used as benchmarks for measuring the neutrino delays, as for example the emission of gravitational waves in coincidence with the neutrino burst [50, 51], the short duration ν_e neutronization peak that could allow to identify time smearing effects [51], the sudden steep raise of the neutrino luminosity due to neutrino-sphere shock-wave breakout [52], the abrupt interruption of the neutrino flux due to a further collapse of the star core into a black hole [53, 54]. The more robust and less model dependent limits achievable with these methods are at the level of $m_\nu \lesssim 3 \text{ eV}$. Tighter limits are obtained only under specific assumptions for the original profiles of the SN neutrino emission, or for the astrophysical mechanisms that give rise to the benchmarks events.

In this thesis we present a new approach to the measurement of the absolute scale of neutrino mass from a future Galactic supernova signal. The new method proposed, which is formally based on the principles of Bayesian reasoning, is rather independent on specific astrophysical assumptions and makes use of the whole statistics of the signal. The method has been tested under a wide range of different conditions for the neutrino emission, mixing schemes and for different present and planned neutrino detectors. The detailed results of such tests are presented in this dissertation and allow us to conclude that even with an approximate description of the neutrino flux

and spectrum, competitive mass limits can still be obtained from the analysis of the next Galactic supernova signal.

We have organized this dissertation in four main chapters. In chapter 2 we review the information available about the expected characteristics of the emitted neutrino fluxes and spectra. We have put special attention on those characteristics that can be identified as robust predictions regarding the supernova neutrino emission. We discuss in some detail how the physical processes involved in the core collapse, shock wave emergence and revival determine these robust features. Chapter 3 is dedicated to “construct” the detected signal according to the informations acquired in chapter 2. The effect of neutrino oscillations are also taken into account in this step. Neutrino flavor oscillations are determinant to model in a correct way an observed supernova signal. Although our aim will not be that of studying oscillations signatures in supernova, the description of this phenomenon is an obligatory aspect of any description of a neutrino signal. Using these informations we describe the procedure to construct a neutrino signal, and we evaluate the expected main properties of the signal under several mixing and detection conditions. Chapter 4 is devoted to explain with more detail the different methods that have been devised to measure or constrain a neutrino mass studying supernova neutrino. More importantly, we describe in this chapter with full detail the statistical method that we have put forth to measure a neutrino mass from the analysis of the whole statistics in a future supernova signal. The method has been tested with the procedures described in the final chapter 5, where the results obtained from such tests are presented in full detail. A comprehensive comparison of various results and an analysis of the conclusions that can be drawn from our study is also contained in this last chapter.

In Appendix A we describe the main ideas and mathematical formalism of the Bayesian approach to data analysis. Appendix B is devoted to present a simple computer tool (publicly available) that has been designed specifically to generate synthetic supernova signals. Some of the underlying algorithms and numerical techniques used in the development of our computer codes are also presented in this appendix.

A complete list of symbols and abbreviations used along the text is given in Appendix C.

CHAPTER 2

Neutrino fluxes and spectra

Before proceeding to construct numerical simulations of a Supernova neutrino signal it is necessary to establish which are the features of the neutrino emitted signal for which the theory is reliable and which features are more uncertain.

Although different Supernova simulations produce neutrino signals with different sets of properties, there are a set of overall features common to almost every result:

1. The neutrino luminosities and fluxes evolve with time in a rather well understood way. In the first tens of milliseconds the luminosity and flux of all neutrino flavors increase rapidly. After this, the luminosity and flux stabilize in their maxima and start to decay slowly for several hundred of milliseconds. A slow decay on a time-scale of several seconds follows and finally the signal turns off.
2. The supernova core is the only place besides the early Universe where neutrinos are in thermal equilibrium. The observational consequence of this fact is the emission of a quasi-thermal neutrino spectrum.
3. The average energies of different neutrino flavors are hierarchical, i.e. muon- and tau-(anti)neutrinos (hereafter we will refer them globally as ν_x) have a harder spectrum than the electron antineutrinos ($\bar{\nu}_e$) which in turn are hotter than the electron neutrinos (ν_e).

Despite the wide range of detailed results obtained in supernova simulations during the last three decades, we can be confident that a future supernova signal will exhibit these properties.

In this chapter we will describe in some detail these robust features of the neutrino emission from supernovae, its physical motivation and how they are supported by self-consistent supernova simulations. In order to be prepared for the chapters where this information will be used to generate and analyze realistic supernova signals, we have attempted to translate some of the described properties into analytical expressions.

A more comprehensive and complete description of the emitted neutrino properties can be found in refs. [55, 56, 57] and references therein.

2.1 Evolution of Neutrino fluxes

One of the best known features of neutrino emission from Supernovae is the way the neutrino fluxes evolve with time (we are interested only in times after the core-bounce).

Although the detailed time structure and some of the time-scales of the neutrino fluxes differ from one simulation to another, it is possible to recognize the existence of mainly three different phases in the evolution of the rates. Each of these phases are directly related to well known physical processes in the collapsed core of the star.

The main phases of neutrino's fluxes evolution is illustrated in figure 2.1.

2.1.1 Fast rising - the shock breakout

Once the inner region of the collapsing stellar core reach supra-nuclear densities a hydrodynamical shock wave forms and starts to travel out. After less than few milliseconds the shock wave reach the region of the core where neutrinos escape freely. A sudden increase in the plasma temperature produced by the energy deposited by the shock, together with the sudden transition from coherent scattering on “iron” nuclei to scattering on nucleons produce a huge release of electron neutrinos (the *prompt neutrino burst* or *deleptonization burst*).

The shock breakout turn on the emission of ν_x in less than 1 msec (neutrino-sphere crossing time of the shock wave [56]). After this turn-on the heat from the shocked material above the neutrino-sphere and below the shock wave produces a steadily increase in the flux that last from 20 to 50 msec (see figure 2.1)

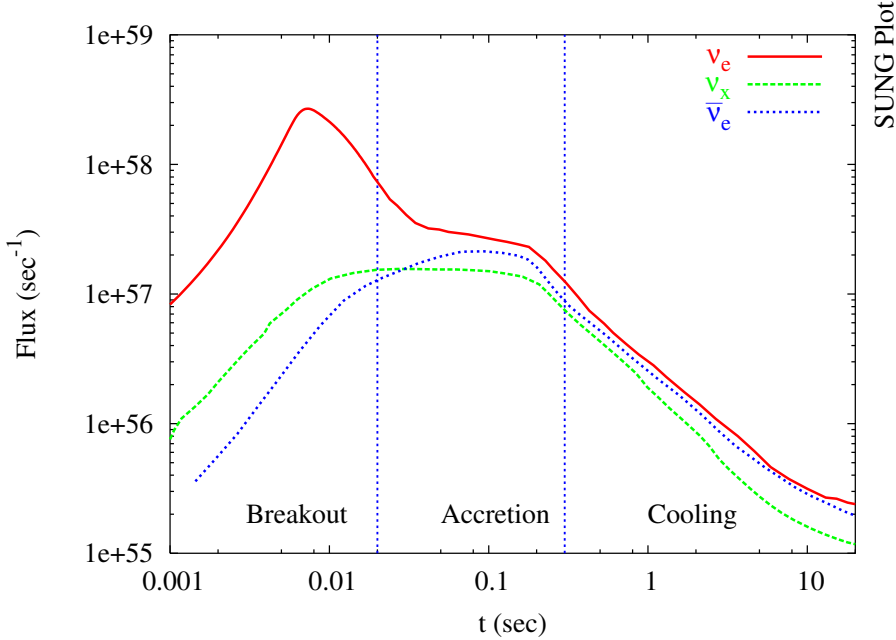


Figure 2.1: *Neutrino fluxes evolution could be described with three main phases: shock breakout (fast rising), accretion and mantle cooling (maximum and plateau) and Kelvin-Helmholtz cooling (decay). The fluxes were taken from simulations by Totani et al. [52].*

2.1.2 Flux maximum - accretion, mantle cooling and explosion

Neutrino emission and nuclear dissociation consume energy of the emergent shock wave. Even before it leaves the iron core, the shock wave becomes an almost stationary accretion front. In these conditions a new source of neutrinos appears. The inner core (protoneutron star) emits its heat through neutrinos in a steady fashion. The same thing happens to the hot material below the accretion front (core mantle). However, as new material is accreted in the stalled shock, it is dissociated and produce extra ν_e by electron capture on protons. The hot material in the shock front also produces electron-positron pairs and the capture of positrons on neutrons, in the neutron rich material of the mantle, creates an additional $\bar{\nu}_e$ flux. The emission of neutrinos during this phase is characterized by a slow decay in the flux on a time-scale of one hundred of milliseconds.

The emission of neutrinos by accretion is suddenly truncated when the shock wave revives and the delayed explosion starts.

2.1.3 Decay - Kelvin-Helmholtz cooling

Once the revitalized shock wave emerges a more stable and long phase starts. The gravitational binding energy of the newly formed protoneutron star (1.3) is radiated as neutrinos on time-scales comparable with the diffusion time-scale (*Kelvin-Helmholtz cooling*).

This phase is characterized by a power law decrease in the neutrino flux and the emission of an important fraction of the protoneutron star binding energy. The Kelvin-Helmholtz cooling phase last for tens of seconds to minutes and it ends when the material of the newly formed neutron star becomes transparent to neutrinos.

As was mentioned before this basic description of the overall features of the emitted neutrino flux is a robust prediction of supernova models. Its global features have been confirmed by the observation of the neutrino signal from SN1987A. The initial short burst of neutrinos (~ 1 sec) observed in the signal is consistent with an accretion phase [49] and the observed total duration of the signal (~ 10 sec) confirms the emission of neutrinos from a cooling neutron star [58].

2.1.4 Analytical flux model

In order to quantify the overall features of the flux described above it is possible to construct a simplified model for the neutrino emission. Such a model will be an useful tool to understand the characteristics of fluxes obtained in simulations. In section 4.5.3, we will start with this analytical approximation to construct a test model to analyze a realistic neutrino signal.

We can recognize two main components in neutrino emission:

- *Cooling component.* On a crude level of approximation neutrino emission from the supernova core and mantle could be written in terms of the Stefan-Boltzmann law (see [59] for a detailed discussion),

$$\frac{dn^{\text{em}}}{dt} = 4\pi R_{\text{eff}}(t)^2 \int F(E; T_{\text{eff}}(t)) dE = C_c R_{\text{eff}}(t)^2 T_{\text{eff}}(t)^4, \quad (2.1)$$

where R_{eff} is the effective radius where neutrinos are emitted and a quasi-thermal spectral distribution $F(E; T_{\text{eff}}(t))$ is assumed, with $T_{\text{eff}}(t)$ as the spectral temperature. C_c is a constant in which we have absorbed geometrical and physical terms.

- *Accretion component.* When accretion starts an additional contribution to the flux is turned on. β -processes producing ν_e and $\bar{\nu}_e$ neutrinos in the accreting matter are in local thermal equilibrium (LTE) and thus neutrino spectra could be also described as thermal with a temperature equal to the accreted material temperature T_a . The neutrino emission rate per unit of mass of accreted material will be given by [49],

$$\frac{dn^{\text{em}}}{dt} \sim M_a(t) \int E^2 F(E; T_a) dE = C_a(T_a) M_a(t). \quad (2.2)$$

The E^2 term arises from the energy dependence of the β -processes cross-section. $C_a(T_a)$ is a parameter depending on the spectral temperature of the accreted matter that can be assumed constant in time. $M_a(t)$ is the mass of accreted material at time t .

When the cooling emission component (2.1) and the accretion component (2.2) are summed up the total flux on ν_e and $\bar{\nu}_e$ is

$$\frac{dn^{\text{em}}}{dt} = C_c R_{\text{eff}}(t)^2 T_{\text{eff}}(t)^4 + C_a(T_a) M_a(t). \quad (2.3)$$

As can be seen the temporal evolution of neutrino flux is a function of the temporal evolution of the effective emission radius R_{eff} , the effective thermal temperature T_{eff} and the rate of matter accretion M_a . Different phenomenological models could be formulated to describe the behavior of this quantities. For the cooling component it is common to use a exponential cooling law, i.e. $T_{\text{eff}} = T_o e^{-t/4\tau}$ and assume an almost constant effective neutrino-sphere radius. This kind of models seems to fit well the gross behavior of the SN1987A signal [58]. In a more complete and detailed reanalysis of SN1987A signal Loredo and Lamb [49] has recently found that a power-law cooling model, $T(t) = T_o(1 + t/4\gamma\tau)^{-\gamma}$ which is capable to reproduce a wide range of cooling behaviors (e.g. when $\gamma \rightarrow \infty$ we obtain an exponential cooling) could fit even better the signal [49].

For the accretion component a truncated power law decay for the mass of accreted matter, $M_a(t) = M_o e^{-(t/t_a)^{n_a}} (1 + t/t_b)^{-n_b}$, seems to fit well supernova simulations results [49].

Using the preferred phenomenological models the final neutrino flux for times posterior to the shock breakout (2.3) is written as

$$\frac{dn^{\text{em}}}{dt} = C \frac{1}{(1 + t/\gamma\tau)^\gamma} + \frac{e^{(-t/t_a)^{n_a}}}{(1 + t/t_b)^{n_b}}, \quad (2.4)$$

where $C \equiv C_c T_o$ and $A \equiv C_a(T_a) M_o$ and we have reparametrized the cooling component in terms of $n_c = 4\gamma$ and $t_c = \gamma\tau$. Note that this flux does not behave properly for $t \rightarrow 0$ since it is aimed to describe the emission of neutrinos for times after the shock breakout. In order to use this analytical approximation to fit a signal we will modify (2.3) in section 4.5.3 to ensure the proper asymptotic behavior of this function.

In figure 2.2 we compare the $\bar{\nu}_e$ and $\bar{\nu}_x$ fluxes from supernova simulations with this analytical model. As can be seen the flux model (2.4) reproduces well the behavior of the flux in the accretion and cooling phases.

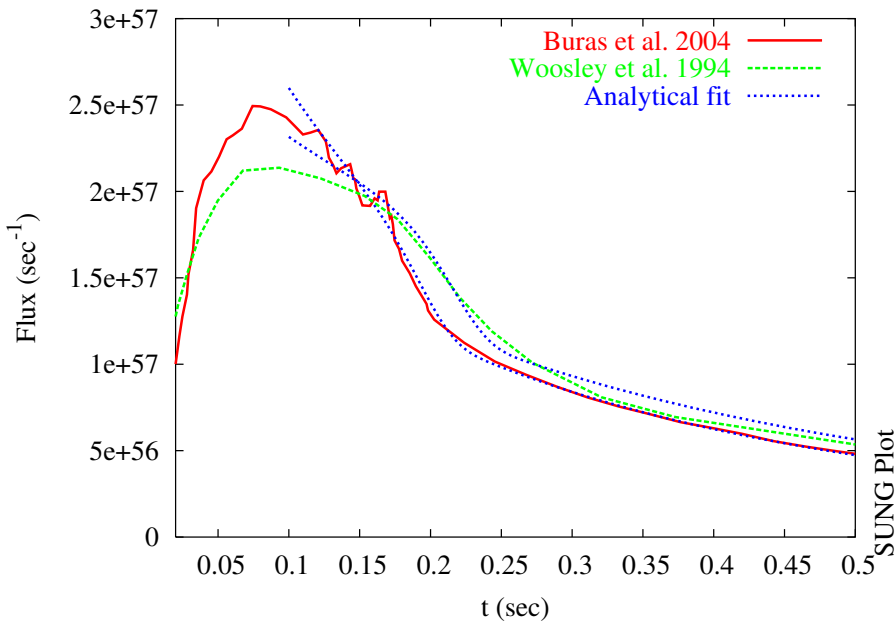


Figure 2.2: Schematic analytical fits of $\bar{\nu}_e$ fluxes from two supernova simulations using the flux model (2.4).

Finally in figure 2.3 we present fluxes of all neutrino flavors coming from three different supernova simulations.

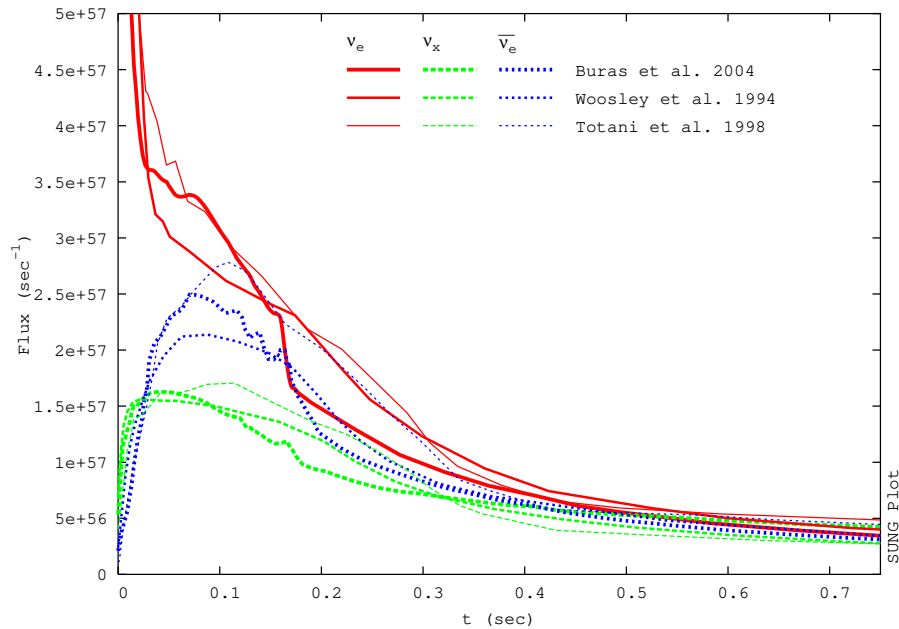


Figure 2.3: *Supernova neutrino fluxes from three different self-consistent simulations: Totani et al. [52], Woosley et al. [60] and Buras et al. [61]. The main overall features of the fluxes described in the text could be recognized here.*

2.2 Neutrino Spectra

Neutrinos trapped inside the inner regions of a supernova core are maintained in thermal equilibrium with the surrounding plasma through inelastic scattering. For this reason it is expected that they will be emitted with a quasi-thermal spectrum characterized by a spectral temperature close to the temperature of the plasma in the region where neutrinos decouple energetically. More than 30 years of analytical and numerical studies of neutrino spectra formation in supernova have confirmed this basic picture. However, the fine details of neutrino transport and emission near to the last scattering surface are highly non trivial and the precise determination of the spectral properties of the emitted neutrinos is not a simple task.

Let us examine here the main features expected for the neutrino spectra and its origin. A more comprehensive and complete discussion could be found in ref. [57] and references therein.

2.2.1 Electron neutrinos and antineutrinos

The production and transport of ν_e and $\bar{\nu}_e$ is simple when compared with the transport of ν_x . Due to the presence of electron and positrons, ν_e and $\bar{\nu}_e$ can undergo charge current reactions (β -processes $ep \leftrightarrow n\nu_e$, $e^+n \leftrightarrow p\bar{\nu}_e$) that are almost absent for all other flavors. With a cross-section much larger than other scattering processes, β -processes dominate completely the transport of ν_e and $\bar{\nu}_e$ inside the supernova core. The continuous creation and capture of neutrinos in these processes inside the core maintain ν_e and $\bar{\nu}_e$ in LTE with the surrounding medium.

Neutrinos diffuse outward until the β -processes become ineffective at the neutrino-sphere. Since the cross section of β -processes are energy dependent the neutrino-sphere radius and therefore the characteristic thermal temperature for ν_e and $\bar{\nu}_e$, are different for neutrinos of different energies. High energy neutrinos will stream out from larger radius with lower temperatures while low energy neutrinos will be radiated from a lower radius and higher temperatures. Therefore the energy distribution of the emitted neutrinos will not be exactly thermal. The emitted neutrino spectra will be “pinched”, i.e. high energy and low energy tails of the spectrum will be depleted due to the different thermal temperatures characteristic of the radius where neutrinos of different energies are emitted (see fig. 2.4).

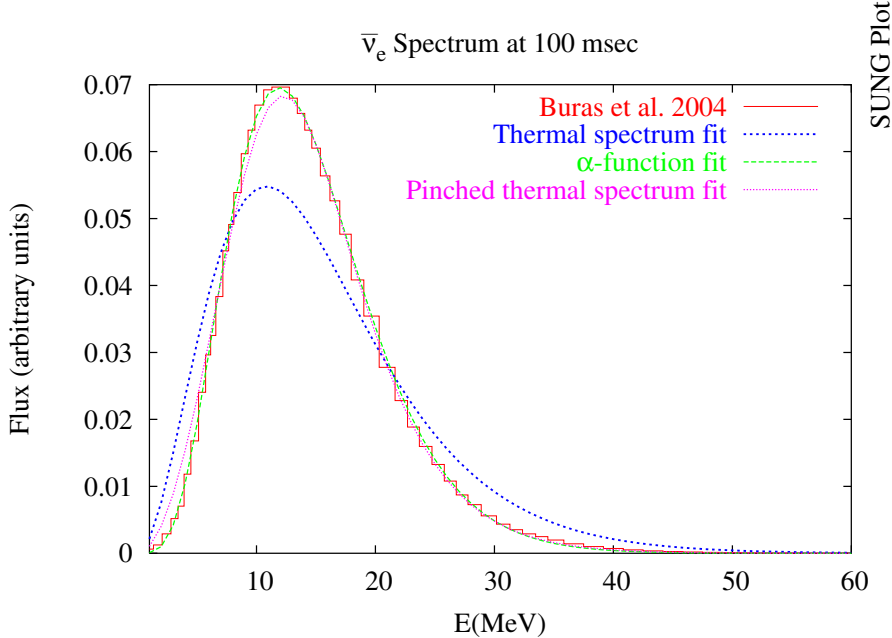


Figure 2.4: $\bar{\nu}_e$ spectrum at 100 msec (accretion and mantle cooling phase) taken from the simulation of Buras et al. [61] (histogram). The dotted curve correspond to a Fermi-Dirac fit with zero chemical potential. The pinching effect, i.e. the depletion of the distribution at high and low energy, can be clearly recognized in the distorted Fermi-Dirac and α -distribution fits. As can be seen, for this particular case the α -distribution fits slightly better the spectrum than the pinched Fermi-Dirac.

2.2.2 Non-electron neutrinos

The emission of ν_x from the supernova requires a more complicated description. In this case different neutral current reactions play comparable roles in the neutrino transport.

ν_x can undergo three kind of processes: creation reactions, energy exchange scattering and isoenergetic scattering.

Deep inside the core neutrinos are created and annihilated through three main processes: nuclear bremsstrahlung $NN \leftrightarrow NN\nu\nu$, electron-positron annihilation $ee^+ \leftrightarrow \nu_x\nu_x$ and neutrino-neutrino annihilation $\nu_e\bar{\nu}_e \leftrightarrow \nu_x\nu_x$. There, neutrinos are in LTE and trapped. At a given radius creation/annihilation processes freeze out and no more neutrinos are created. This condition defines what is called the *number sphere*. The emergent neutrino total flux is fixed in this layer. Outside the number

sphere neutrinos still undergo energy exchange scattering on electrons, positrons and nucleons and maintain some thermal contact with the plasma. When density and temperature is lower inelastic scattering on nucleons and e^\pm becomes inefficient and neutrinos decouple energetically from the surrounding medium. This condition defines the so-called *energy sphere*. Above the energy sphere neutrinos still interact strongly with the plasma through elastic scattering on nucleons. Finally at some radius elastic scattering becomes in turn inefficient and neutrinos stream out from the neutrino-sphere or *transport sphere*. In figure 2.5 we illustrate schematically this process.

What will be the emergent energy distribution of ν_x ? Naively one could think that since thermal contact is maintained only inside the energy-sphere neutrino average energy will be related with the plasma temperature at that layer. However the energy dependence of the nucleon scattering outside the number-sphere acts as a filter [62] lowering the average energy to 50-60% its value close to the energy sphere.

The complex interplay of all factors which determine the emergent ν_x flux makes harder to predict exactly which will be the spectral properties of these flavors. We will come back on this issue in section 2.3.

2.2.3 Spectral pinching

The quasi-thermal nature of the neutrino spectra is a robust feature of neutrino emission from a supernova.

There are two ways to quantify the non-thermal distortion (pinching effect) of the neutrino spectra. On one hand it is possible to use higher order momenta of the neutrino energy distribution that contain informations about the high energy tail. Raffelt [62] first quantifies the pinching effect by introducing a “pinching parameter” defined in terms of the ratio of the second and first momentum

$$p \equiv \frac{1}{a} \frac{\langle E^2 \rangle}{\langle E \rangle} \quad (2.5)$$

Where $a \simeq 1.3029$ is a weight constant equal to the ratio of the second and first momentum of a Fermi-Dirac distribution with zero chemical potential. In the absence of any pinching and without degeneracy $p = 1$. A pinched spectrum will be characterized by $p < 1$ while an anti-pinch, i.e. an enhancement of the spectrum tails, corresponds to $p > 1$.

On the other hand has been common in the literature to fit the supernova neutrino spectrum using a Fermi-Dirac distribution with an effective degeneracy parameter

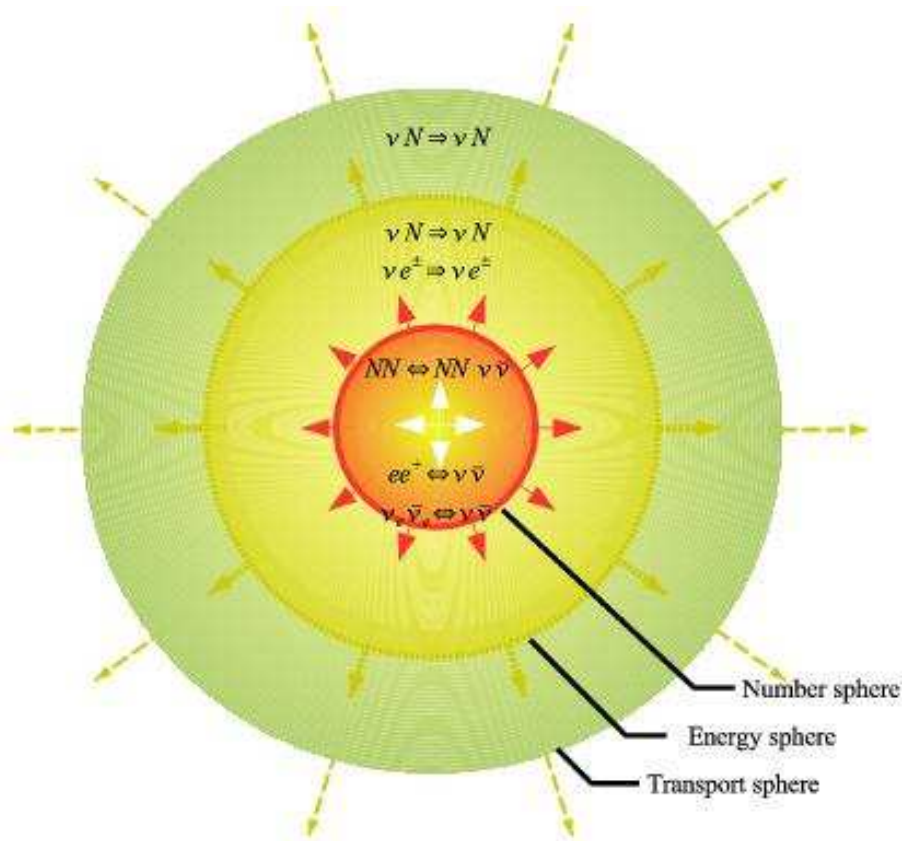


Figure 2.5: *Schematic representation of ν_x transport. Neutrinos are produced and annihilate through nucleon bremsstrahlung and pair processes. When creation/annihilation freeze-out at the number sphere the total flux is fixed (number of arrows). Neutrinos maintain a thermal contact with the medium until they reach the energy sphere (style of lines indicates the neutrino average energy). Finally above the transport sphere (neutrino-sphere) neutrinos freely stream out. Its average energy at this layer (style of arrows) is close to that at the energy sphere.*

η that enters the distribution like an effective chemical potential:

$$F_{\text{FD}}(E; T, \eta) \propto \frac{E^2}{1 + e^{E/T-\eta}}. \quad (2.6)$$

The introduction of η allows to fit the distorted tails of the distribution. Its value could therefore be used as a measure of the spectrum pinching.

Recently an alternative two-parameter distribution has been proposed [3, 63]:

$$F_{\alpha}(E; \bar{\epsilon}, \alpha) = N(\bar{\epsilon}, \alpha) (E/\bar{\epsilon})^{\alpha} e^{-(\alpha+1)E/\bar{\epsilon}}, \quad (2.7)$$

where the normalization constant is given by $N(\bar{\epsilon}, \alpha) = (\alpha + 1)^{\alpha+1}/\Gamma(\alpha + 1)\bar{\epsilon}$. It has been shown that this new distribution, denoted α -distribution, in [3] fits slightly better the neutrino spectra and has the nice property of allowing a simple analytical estimation of the two spectral parameters $\bar{\epsilon}$ and α directly in terms of the first and second momentum of the energy distribution. Using the well known relation $\alpha\Gamma(\alpha) = \Gamma(\alpha + 1)$ it is easy to verify that:

$$\bar{\epsilon} = \langle E \rangle; \quad \frac{2 + \alpha}{1 + \alpha} = \frac{\langle E^2 \rangle}{\langle E \rangle^2}. \quad (2.8)$$

Using these relations, the pinching parameter p could be expressed in terms of α as:

$$ap = (2 + \alpha)/(1 + \alpha). \quad (2.9)$$

Therefore when an α -distribution is used to fit the neutrino spectrum the value of the α parameter can quantify the spectrum pinching.

Figure 2.4 illustrate the quality of fits of a numerical neutrino spectrum with a Fermi-Dirac and an α -distribution.

The relation between p , η and α is depicted in figure 2.6. Typical values for α from a self-consistent supernova simulation are presented in figure 2.7. As can be seen the spectral pinching evolves to lower values as the protoneutron star and the core mantle settles and neutrino emission is confined to more compact regions [3].

Typical ranges for the spectral pinching obtained in simulations are [64, 3]:

$$\begin{aligned} p_{\nu_e} &\simeq 0.88 \div 0.92, \quad \eta_{\nu_e} \simeq 3 \div 5, \quad \alpha_{\nu_e} \simeq 4.0 \div 5.6 \\ p_{\bar{\nu}_e} &\simeq 0.90 \div 0.95, \quad \eta_{\bar{\nu}_e} \simeq 2 \div 4, \quad \alpha_{\bar{\nu}_e} \simeq 3.0 \div 5.0 \\ p_{\nu_x} &\simeq 0.95 \div 1.00, \quad \eta_{\nu_x} \simeq 0 \div 2, \quad \alpha_{\nu_x} \simeq 2.3 \div 3.2 \end{aligned} \quad (2.10)$$

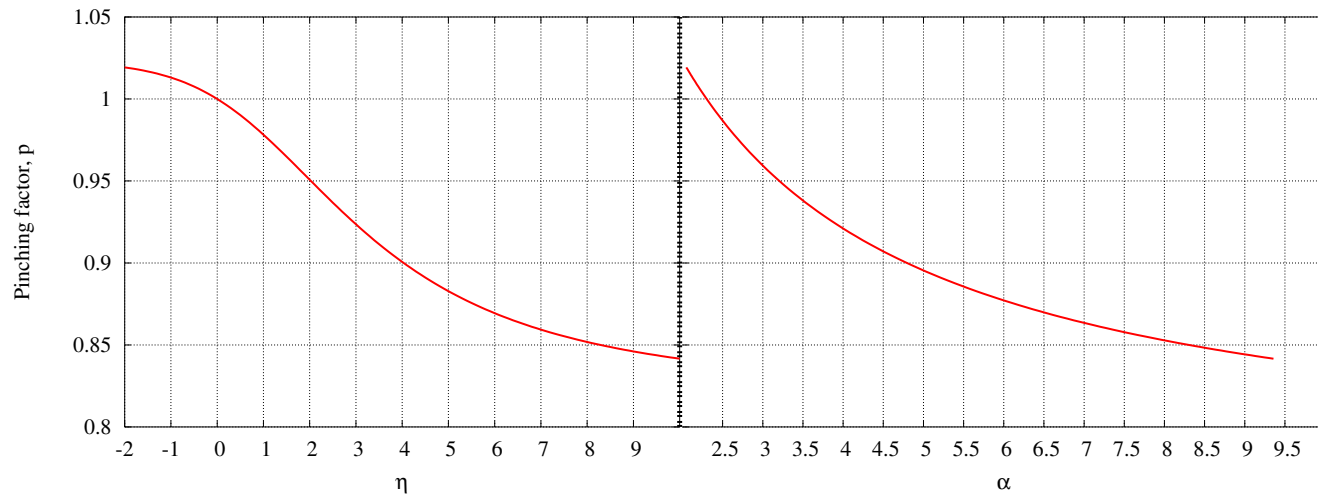


Figure 2.6: *Relation between the pinching parameter p , α and the effective degeneracy parameter η used to quantify the thermal distortion of supernova neutrino spectra.*

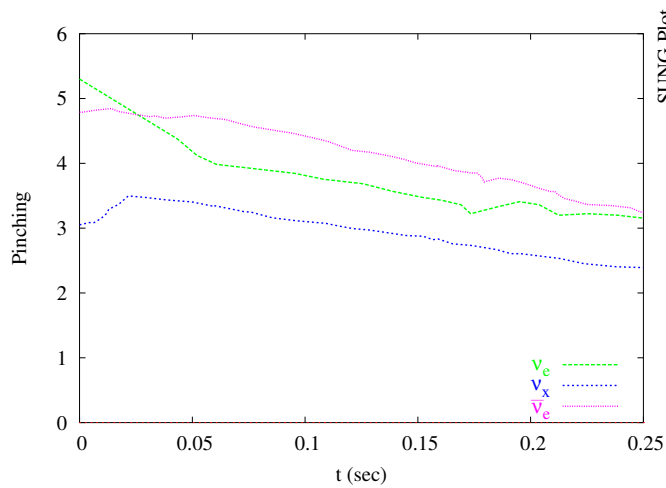


Figure 2.7: *Evolution of the α parameter in the supernova simulation by Buras et al. [61]. The pinching gets reduced at later times when neutrinos are emitted from more compact regions inside the protoneutron star.*

2.3 Hierarchy of average energies

The last robust feature of the emission of neutrinos from supernova is the hierarchy of the average energies of different neutrino flavors.

As was discussed in the previous section the spectral properties of neutrinos emitted from the supernova core are determined by the transport processes near the neutrino-spheres. In the simple case of ν_e and $\bar{\nu}_e$ the average energy is determined by the temperature of the plasma around the neutrino-spheres. Although the cross section for β -processes (the main source of opacity for these flavors) has the same energy dependence for ν_e and $\bar{\nu}_e$, the asymmetry between protons and neutrons in the supernova core produces a significant difference in the opacity of antineutrinos and neutrinos. Since neutrons are more abundant, ν_e decouple from matter at a larger radius than $\bar{\nu}_e$, and therefore has a lower average energy, i.e. $\langle E_{\nu_e} \rangle < \langle E_{\bar{\nu}_e} \rangle$.

The size of the difference between the average energies of ν_e and $\bar{\nu}_e$ depends basically on the core structure (density, temperature and lepton number profile) which determines the position of the respective neutrino-spheres. In supernova simulation typical values ranges from 30% [61, 56] to 50% [60, 52] (see figure 2.8).

On the other hand the transport of ν_x is dominated by neutral current reactions that have smaller rates than the β -processes. This implies that ν_x decouples at a lower radius than $\bar{\nu}_e$ and therefore it is expected that $\langle E_{\nu_x} \rangle > \langle E_{\bar{\nu}_e} \rangle > \langle E_{\nu_e} \rangle$. However the determination of how large are the differences between the average energies of ν_x and $\bar{\nu}_e$ is not easy. If the average energies were only determined by the spectral temperature at the energy-sphere, large differences would be expected. However the filter effect of the elastic reactions outside the energy-sphere for ν_x contribute reducing the average energy. It has been shown in ref. [3] that the final difference will depend on the details of the ν_x transport in that regions.

Most of the self-consistent simulations have made use of simplified descriptions of ν_x transport mainly due to the fact that ν_x does not play an important role in the supernova dynamics. In these simulations the resulting ν_x spectra has typical energies differences that range from 30% up to 100%! (see figures 2.8a,b).

Large spectral differences of this size have been exploited in several works to study the potential information contained on a supernova signal. Minakata et al. [65] have claimed that an inverse hierarchy of neutrino masses could be rejected using the informations contained in the SN1987A signal. Lunardini and Smirnov [66] have derived similar conclusions about the potential of SN1987A signal to give information about neutrino oscillations parameters. The potential of a future supernova signal has also be studied in the presence of large spectral differences [67].

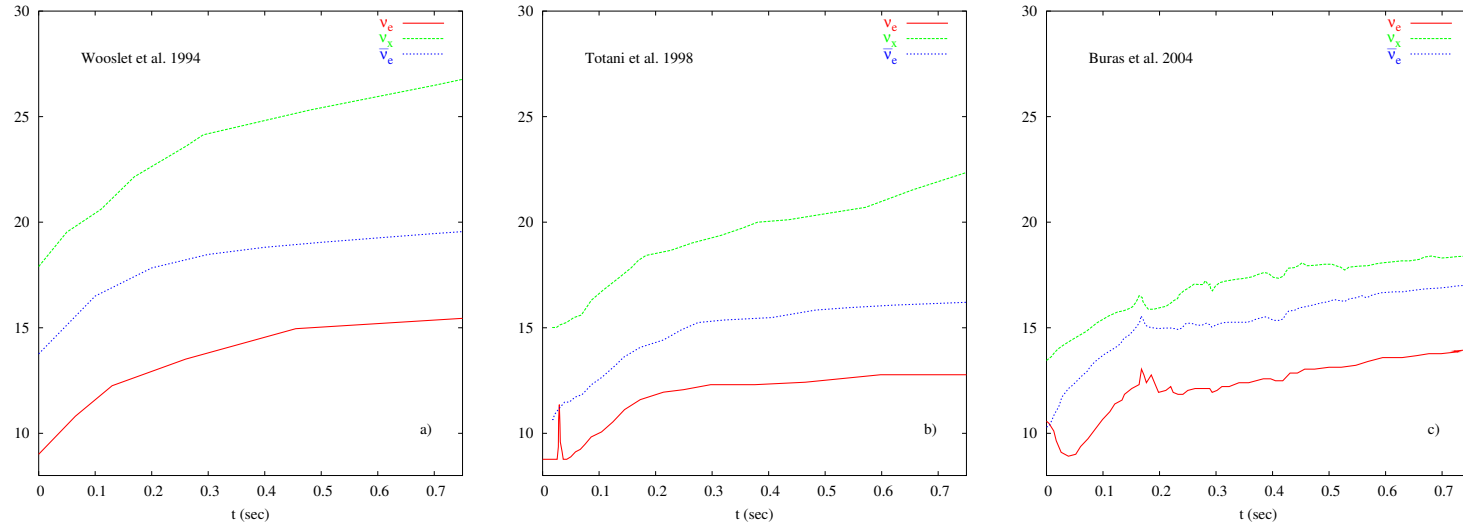


Figure 2.8: *Evolution of the mean energy from three different supernova simulations. It is apparent the big difference between the “standard” result of large spectral differences in simulations where a simplified description of ν_x transport was used (panels a and b) compared with almost equal average energies of ν_x and $\bar{\nu}_e$ when a more precise and complete description of ν_x interactions are included (panel c).*

Recently the inclusion of a detailed description of ν_x microphysics in self-consistent hydrodynamical supernova simulations (see ref. [57] has suggested that the standard picture of large spectral differences could be wrong. Including all the relevant reactions in the ν_x transport, and other effects that had not been taken into account in previous simulations, the ν_x average energy results almost equal to that of $\bar{\nu}_e$. Although a partial hierarchy could still be present (at least during part of the emission) differences will not be larger than 20%, with 10% as a typical value [57]. Panel *c* in figure 2.8 illustrates this point.

We conclude that, according to the most recent results, any attempt to obtain informations on neutrino mixings and their mass hierarchy from a Galactic supernova signal will have to take into account that the differences between the neutrino energies will be probably not very large.

CHAPTER **3**

Simulation of a supernova neutrino signal

Using what we have learned about neutrino emission in Supernova we can now proceed to calculate the expected characteristics of a future supernova signal. One main part of this work regards using this description to create artificial signals that will be later used to test the statistical method that will be presented in the next chapter.

In this chapter we present the theoretical description of a supernova neutrino signal and the general strategies that can be used to generate synthetic realizations of such signals. In section 3.1 we present the most relevant ideas about supernova neutrino oscillations which will play a central role in the determination of the final features of any neutrino signal. Section 3.2 introduces the formalism and describes in some details how we model the neutrino detection process. In section 3.3 we compute the most relevant features of a future supernova neutrino signal, assuming different emission models and oscillation effects and analyze the interplay of the different aspects which are involved in the determination of the signal characteristics. Finally section 3.4 describes the particular strategies, algorithms and numerical techniques used to create synthetic signals.

The material presented in this chapter is a collection of useful results obtained from rather standard descriptions of neutrino propagation and detection phenomenology. We intend just to present synthetically the theoretical results behind the computer codes used in our work.

3.1 Oscillations of supernova neutrinos

Neutrinos will undergo oscillations on their way from the supernova core to a detector. First, when they traverse the outer shells of the stellar core and then when they arrive to the Earth and travel through our planet's mantle and/or core before being detected.

In the last two decades many works has been devoted to study supernova neutrino oscillation phenomenology. Many of these efforts were devoted to understand how neutrino oscillations affected the SN1987A signal [65, 66]. More recently the effect of neutrino oscillations on a supernova signal have been studied in the attempt to determine how the distortions caused by oscillations could be used to estimate and/or constrain the neutrino mixing parameters [67, 68, 69, 70, 71].

Here we will summarize the most relevant facts and predictions of these works. More detailed discussions can be found fro example in refs. [67, 66] and references therein.

3.1.1 Neutrino Oscillations - Basic facts

Neutrinos are produced and detected as weak-interaction (flavor) eigenstates ν_α ($\alpha = e, \mu, \tau$). We know that the flavor eigenstates do not diagonalize the mass matrix, and after being produced they propagate as a superposition of mass eigenstates ν_i ($i = 1, 2, 3$). The flavor and mass neutrino basis are related through a unitary transformation:

$$\vec{\nu}_W = U \vec{\nu}_M, \quad (3.1)$$

where we denote $\vec{\nu}_W = (\nu_e \nu_\mu \nu_\tau)^T$, $\vec{\nu}_M = (\nu_1 \nu_2 \nu_3)^T$ and U is the Maki-Nakagawa-Sakata matrix (MNS). U (whose elements we will denote as $U_{\alpha i}$) can be parameterized in terms of three mixing angles θ_{12} , θ_{23} and θ_{13} , and assuming $\delta = 0$ it reads[72, 73]:

$$U = \begin{pmatrix} c_{12}c_{13} & s_{12}c_{13} & s_{13} \\ -c_{23}s_{12} - s_{23}s_{13}c_{12} & c_{23}c_{12} - s_{23}s_{13}s_{12} & s_{23}c_{13} \\ s_{23}s_{12} - c_{23}s_{13}c_{12} & -s_{23}c_{12} - c_{23}s_{13}s_{12} & c_{23}c_{13} \end{pmatrix}, \quad (3.2)$$

where we have used the notation $c_{ij} = \cos \theta_{ij}$ and $s_{ij} = \sin \theta_{ij}$.

The propagation of an ultra relativistic neutrino mass eigenstate $E \simeq p(1 + m_\nu^2/2E)$ obeys an approximate Schrödinger-like equation of motion[74]:

$$i \frac{d\vec{\nu}_M}{dt} \simeq H_M \vec{\nu}_M, \quad (3.3)$$

where the Hamiltonian in the mass basis is $H_M \equiv (1/2E)\text{diag}(m_1^2, m_2^2, m_3^2)$. In the flavor basis the propagation equation could be obtain from (3.3) applying the transformation (3.1),

$$i \frac{d(U^\dagger \vec{\nu}_W)}{dt} = H_M (U^\dagger \vec{\nu}_W), \quad (3.4)$$

$$i \frac{d\vec{\nu}_W}{dt} = H_W \vec{\nu}_W \quad (3.5)$$

with the Hamiltonian defined as $H_W = U H_M U^\dagger$.

The evolution of a mass eigenstate is given by $\nu_i(t) = \exp[-(m_i^2/2E)t]\nu_i(0)$ and can be used to write down how a neutrino which is produced as a definite flavor eigenstate $\nu_\alpha(0) = \sum U_{\alpha i} \nu_i(0)$ evolves:

$$\nu_\alpha(t) = \sum U_{\alpha i} e^{-i \frac{m_i^2}{2E} t} \nu_i(0). \quad (3.6)$$

We see that the neutrino flavor (given by the particular mix of mass eigenstates) changes along the path, provided the neutrino masses are different. This is the reason underlying neutrino *vacuum oscillations*.

The projection of the neutrino state at t on the flavor basis allows us to find the general *conversion probability* in vacuum:

$$P_{\alpha\beta} \equiv P(\nu_\alpha \rightarrow \nu_\beta) = |\langle \nu_\beta | \nu_\alpha(t) \rangle|^2 \quad (3.7)$$

$$= \left| \sum U_{\beta j} U_{\alpha i}^* \langle \nu_j | \nu_i(0) \rangle \right|^2 \quad (3.8)$$

$$= \sum U_{\beta j}^* U_{\alpha j} U_{\beta i} U_{\alpha i}^* e^{-i \frac{\Delta m_{ij}^2}{2E} t}, \quad (3.9)$$

where $\Delta m_{ij}^2 \equiv m_i^2 - m_j^2$ are the *squared mass differences*. The above equation tells us that a neutrino flavor oscillate with a spatial period $\ell_{\text{osc}} = 4\pi E / \Delta m_{ij}^2$ called the *oscillation length*.

In matter, the effect of coherent neutrino interaction with the medium can be accounted for by adding a potential term to the equation of motion (3.5),

$$i \frac{d\vec{\nu}_W}{dt} = \left[H_W + \begin{pmatrix} V & 0 & 0 \\ 0 & 0 & 0 \\ 0 & 0 & 0 \end{pmatrix} \right] \vec{\nu}_W, \quad (3.10)$$

$$= H_W^{\text{eff}} \vec{\nu}_W \quad (3.11)$$

where $V = \sqrt{2}G_F n_e$ is the effective electron neutrino potential ($-V$ for antineutrinos) that is due to coherent charge current scattering off electrons. In the last equation we have redefined the fields to absorb the neutral current effective potential which is common to all flavors and contributes an overall phase.

With the introduction of the interacting terms the vacuum mixing matrix U does not diagonalize the weak Hamiltonian and therefore the vacuum mass eigenstates are no longer propagation eigenstates. A new matrix U^m which diagonalize H_W^{eff} must be introduced, by defining a new *instantaneous mass eigenstates* basis $\vec{\nu}_W^m = U^m \vec{\nu}_M^m$ which in general is different from point to point along the neutrino path if the density and therefore V changes.

In the two flavor case (which will be interesting for supernova mantle oscillations described in section 3.1.3) the effective weak Hamiltonian H_W^{eff} is diagonalized by the in-matter mixing matrix

$$U = \begin{pmatrix} \cos \theta_m & \sin \theta_m \\ -\sin \theta_m & \cos \theta_m \end{pmatrix}, \quad (3.12)$$

where θ_m is the mixing angle in matter and reads:

$$\sin 2\theta_m = \frac{\sin 2\theta}{\sqrt{\sin^2 2\theta + (\cos 2\theta - 2EV/\Delta m^2)^2}}. \quad (3.13)$$

The eigenvalues of $U^m H_W^{\text{eff}} U^{m\dagger}$ give the squared effective neutrino masses $\mu_{1,2}^2$,

$$\mu_1^2 = \frac{m_1^2 + m_2^2}{2} + \frac{2EV}{2} - \frac{\Delta m^2}{2} \sqrt{\sin^2 2\theta + (\cos 2\theta - 2EV/\Delta m^2)^2}, \quad (3.14)$$

$$\mu_2^2 = \frac{m_1^2 + m_2^2}{2} + \frac{2EV}{2} + \frac{\Delta m^2}{2} \sqrt{\sin^2 2\theta + (\cos 2\theta - 2EV/\Delta m^2)^2}. \quad (3.15)$$

From this we get $\Delta\mu^2 = \Delta m^2 \sqrt{\sin^2 2\theta + (\cos 2\theta - 2EV/\Delta m^2)^2}$ and $\ell_{\text{osc}}^m = 4\pi E / \Delta\mu_{ij}^2$.

In summary, the effect of the different neutrino interaction with the surrounding medium is that of producing a change in the mixing angle and therefore in the oscillation rate ℓ_{osc}^m . This change is maximal when the *resonant condition* is fulfilled:

$$2EV = \Delta m^2 \cos 2\theta. \quad (3.16)$$

When the medium density changes another “degree of freedom” is added to the oscillation dynamics of neutrinos. Starting from the equation of motion for flavor eigenstates in matter (3.11) we can obtain the instantaneous mass eigenstates $\vec{\nu}_M^m$ by solving:

$$i \frac{dU^{m\dagger} \vec{\nu}_M^m}{dt} = H_W^{\text{eff}} U^{m\dagger} \vec{\nu}_M^m, \quad (3.17)$$

$$i \frac{d\vec{\nu}_M^m}{dt} = \left(\frac{1}{2E} \text{diag}(\mu_1, \mu_2, \mu_3) - iU^m \frac{dU^{m\dagger}}{dt} \right) \vec{\nu}_M^m \quad (3.18)$$

The variation of U^m along the neutrino path makes the Hamiltonian in the last equation not diagonal and therefore $\vec{\nu}_M^m$ are not longer propagation eigenstates. As a result not only neutrino flavor change due to differences in the phase evolution of the propagation eigenstates as in vacuum, also the states mix among themselves.

The mixing of instantaneous mass eigenstates is governed by the ratio between the diagonal and off-diagonal terms of the Hamiltonian in eq. (3.18). The off-diagonal terms which are provided by $dU^{m\dagger}/dt$ depend on the rate of variation of the in-matter mixing angle $d\theta_m/dt$ which is determined by the density gradient.

Near the resonance region (3.16) the diagonal terms of the effective mass Hamiltonian are almost equal and cancel out by a phase redefinition of the fields. Therefore it is in that region where the instantaneous mass eigenstate are more important. If density varies slowly inside the resonance region (and the off-diagonal terms are close to zero) the instantaneous mass eigenstates are almost propagation eigenstates and do not oscillate. It is said that neutrinos perform an *adiabatic transition*. But, if the density gradient is steep enough, the instantaneous mass eigenstates strongly oscillates and neutrinos could emerge from the resonance layer as a different instantaneous mass *eigenstate*. It is said that the neutrino state *jumps*.

Quantitatively, the adiabaticity condition can be expressed in terms of the mixing parameters and the medium properties as [74]:

$$\gamma \equiv \frac{\Delta m^2 \sin^2 2\theta}{2E \cos 2\theta} \left| \frac{d \log n_e}{dt} \right|_{\text{res}}^{-1}, \quad (3.19)$$

where γ is called the *adiabaticity* parameter.

The jumping probability of instantaneous mass eigenstates near the resonance region is approximately given by the *Landau-Zener Formula*¹:

$$P_j = \exp(-\pi\gamma/2). \quad (3.20)$$

The resonant conversion of neutrinos in matter through the above process is conventionally called the *Mikheev-Smirnov-Wolfenstein effect (MSW)* [76, 77].

3.1.2 Neutrino mixing parameters - experimental values and limits

As we saw in the previous section the dynamics of *active* neutrino oscillation depends on 3 pairs of parameters: $(\Delta m_{12}^2, \theta_{12})$, $(\Delta m_{23}^2, \theta_{23})$, $(\Delta m_{13}^2, \theta_{13})$.

The study of neutrino oscillations in solar, atmospheric, reactor and accelerator experiments has allowed us to measure accurately some of these parameters, and to put limits on other ones. In the following, we present the most recent values and limits obtained from a global analysis of all the available experimental results [78]:

- $[\Delta m_{12}^2 = 7.4 - 9.2 \times 10^{-5} \text{ eV}^2, \theta_{12} = 28^\circ - 37^\circ]$ (99.7% CL).
This is the so-called *LMA solution* to the solar neutrino problem.
It is common to identify this pair of parameters as $(\Delta m_{\odot}^2, \theta_{\odot})$
- $[\Delta m_{23}^2 = 1.5 - 3.9 \times 10^{-3} \text{ eV}^2, \theta_{23} = 34^\circ - 45^\circ]$ (99.7% CL).
The sign of Δm_{23}^2 is still unknown and will depend on what is the mass hierarchy: **normal hierarchy** (NH) $\Delta m_{23}^2 > 0$ or **inverted hierarchy** (IH) $\Delta m_{23}^2 < 0$.
It is common to identify this pair of parameters as $(\Delta m_{\text{atm}}^2, \theta_{\text{atm}})$.
- $[\Delta m_{13}^2 \simeq \Delta m_{23}^2, \theta_{13} < 12.9^\circ]$ (99.7% CL).

3.1.3 Neutrino Oscillations in the Supernova Mantle

In the following sections we will apply these basic results to study neutrino oscillations in the supernova mantle.

¹In principle the Landau-Zener formula is accurate under the assumption of a small value of the adiabaticity parameter and a linear variation of the density *inside* the resonance region. We have verified that for typical supernova density profiles and mixing parameters this formula works as well as the double exponential formula used in other works [75].

3.1.4 Initial conditions

Inside the supernova core where neutrinos are produced, the effective neutrino potential felt by the electron (anti)neutrinos overwhelms the off-diagonal terms of the effective weak Hamiltonian H_W^{eff} (3.11) and flavor eigenstates are approximately local mass eigenstate. The correspondence between flavor and mass eigenstates in the production region will depend on the mass hierarchy [67]:

- with **normal hierarchy** we will have:

$$\begin{aligned} \nu_e &= \nu_{3m}, & \nu'_\tau &= \nu_{2m}, & \nu'_\mu &= \nu_{1m}, \\ \bar{\nu}_e &= \nu_{1m}, & \bar{\nu}'_\mu &= \nu_{2m}, & \bar{\nu}'_\tau &= \nu_{3m}. \end{aligned} \quad (3.21)$$

- for **inverted hierarchy**:

$$\begin{aligned} \nu_e &= \nu_{3m}, & \nu'_\mu &= \nu_{2m}, & \nu'_\tau &= \nu_{1m}, \\ \bar{\nu}_e &= \nu_{1m}, & \bar{\nu}'_\tau &= \nu_{2m}, & \bar{\nu}'_\mu &= \nu_{3m}. \end{aligned} \quad (3.22)$$

Where ν'_μ , ν'_τ , $\bar{\nu}'_\mu$ and $\bar{\nu}'_\tau$ are redefined states which diagonalize the (ν_μ, ν_τ) submatrix of H_W^{eff} [67]. It must be noticed that such redefinition does not change the supernova physics since for all practical purposes ν_μ and ν_τ are phenomenological identical in supernova conditions.

3.1.4.1 Resonance regions

Neutrinos emerging from the supernova core traverse matter with densities ranging from 10^9 g/cm³ to almost 0. In the process they will find the required conditions for resonant conversion. Two possible resonances are allowed by the mixing parameters:

- a high density **H-Resonance** corresponding to enhanced conversion into the heaviest mass eigenstate ν_3 and determined by the condition:

$$2E V(\rho_H^{\text{res}}) = \Delta m_{23}^2 \cos 2\theta_{13}. \quad (3.23)$$

- and a low density **L-Resonance** associated to transitions between the lightest eigenstates:

$$2E V(\rho_L^{\text{res}}) = \Delta m_{12}^2 \cos 2\theta_{12}. \quad (3.24)$$

Since $\Delta m_{12}^2 > 0$ the *L-Resonance will be only in the neutrino channel*.

On the other hand the *H-Resonance* will affect neutrinos and antineutrinos according to the mass hierarchy:

- for **normal hierarchy** ($\Delta m_{23}^2 > 0$) *H-Resonance will just affect neutrinos*,
- while in the case of an **inverted hierarchy** ($\Delta m_{23}^2 < 0$) *H-Resonance will occur in the antineutrino channel*.

3.1.4.2 Factorization of Dynamics

The hierarchical nature of the squared-mass differences $\Delta m_{23}^2 : \Delta m_{12}^2 \simeq 100 : 1$ will produce a natural decoupling of the conversion dynamics in the two resonance layers inside the supernova mantle.

At high densities (H-Resonance) the in-matter mixing of the lightest eigenstates U_{e2}^m will be suppressed. Transitions will affect just the heaviest eigenstate and the conversion description is reduced to the two flavor case (ν_1, ν_3). At low densities (L-Resonance) the mixing of the third eigenstate is near to its value in vacuum $U_{e3}^m \simeq U_{e3} \lesssim 10^{-2}$ and almost constant. Only the first and second eigenstate will mix and again the problem is reduced to a two flavor case (ν_1, ν_2).

Additionally as U_{e3} is very small the total survival probabilities for ν_e and $\bar{\nu}_e$ can be factorized [79, 80]:

$$P \approx P_H \times P_L. \quad (3.25)$$

Factorization of dynamics is a property which simplifies considerably the computation of the total conversion probabilities in the supernova mantle without a detailed numerical study of the neutrino propagation equation.

3.1.4.3 Jumping probabilities

We have computed generic jump probabilities using the Landau-Zener formula (3.20) for typical conditions found in the supernova mantle and generic mixing parameters. Contours of equal probability in the $(\Delta m^2, \sin^2 \theta)$ plane for different neutrino energies, are depicted in figure 3.1.

Observing the contours, we see that the neutrino transitions in the L-Resonance, which are governed by the solar mixing parameters $(\Delta m_{12}^2, \theta_{12})$ (LMA), is completely adiabatic, i.e. $P_L = 0$.

The case for the H-Resonance is not as simple. Since the neutrino transition through that layer is governed by the unknown mixing angle θ_{13} , the adiabaticity will be also uncertain.

We can recognize two extreme cases [67]:

- $\sin^2 \theta_{13} \gtrsim 10^{-4}$ ($\theta_{13} \gtrsim 1^\circ$). In this case for all the interesting neutrino energies the adiabaticity condition is fulfilled, i.e. $P_H \simeq 0$.
- $\sin^2 \theta_{13} \lesssim 10^{-6}$ ($\theta_{13} \lesssim 0.06^\circ$). In this case adiabaticity is strongly violated implying $P_H \sim 1$ for almost the entire range of supernova neutrino energies.

For $10^{-6} \lesssim \sin^2 \theta_{13} \lesssim 10^{-4}$ we will have an intermediate behavior with jump probabilities ranging between 0.1 and 0.9.

The energy dependency of the jump probability in the resonance region is another matter of concern. We have plotted in figure 3.2 P_H as a function of neutrino energy for different values of the mixing parameter $\sin^2 \theta_{13}$. It can be seen that for the range of interesting neutrino energies the jump probability in the extreme cases is almost constant. In the intermediate range of values of the mixing parameter, P_H will have only a mild variation in the energy range where most of the neutrino events will be expected.

The above conclusions apply also to antineutrinos in the inverted mass hierarchy case where the jumping probability \bar{P}_H becomes identical to P_H .

3.1.4.4 Conversion probabilities

Using the jumping probabilities and the fact that the dynamics in the resonance region decouple we can compute the *transition probability* $(\bar{p}_{\alpha i})p_{\alpha i}$, i.e. the probability that a given (anti)neutrino flavor α emerges from the supernova in the i^{th} mass eigenstate. Figure 3.3 illustrates schematically the way these probabilities are computed following the evolution of the neutrino state from the emission region to the star surface.

In table 3.1 we summarize the results of applying rules as those presented in fig. 3.3 to compute transition probabilities for neutrinos and antineutrinos, assuming normal and inverted hierarchies.

Transition probabilities allow for a straightforward computation of the final conversion probabilities, i.e. the probability that a given neutrino flavor α is detected as flavor β . In terms of $p_{\alpha i}$ the conversion probabilities are simply given by

Table 3.1: *Transition probabilities*
Normal mass hierarchy

Neutrinos			Antineutrinos		
ν_e	ν_1	ν_2	ν_3	$\bar{\nu}_e$	$\bar{\nu}_1$
ν'_μ	$P_H P_L$	$P_H(1 - P_L)$	$(1 - P_H)$	$\bar{\nu}_e$	1
	$(1 - P_L)$	P_L	0	$\bar{\nu}_\mu$	0
	$(1 - P_H)P_L$	$(1 - P_H)(1 - P_L)$	P_H	$\bar{\nu}_\tau$	0
Inverted mass hierarchy					
Neutrinos			Antineutrinos		
ν_e	ν_1	ν_2	ν_3	$\bar{\nu}_e$	$\bar{\nu}_1$
ν'_μ	0	P_L	$(1 - P_L)$	$\bar{\nu}_e$	P_H
	0	$(1 - P_L)$	P_L	$\bar{\nu}_\mu$	0
	1	0	0	$\bar{\nu}_\tau$	$(1 - P_H)$
					$\bar{\nu}_3$
					$(1 - P_H)$
					P_H

$$P_{\alpha\beta} = \sum_i p_{\alpha i} p_{i\beta}. \quad (3.26)$$

Where $p_{i\beta}$ is the probability that the mass eigenstate i^{th} be detected as the neutrino of flavor β .

In the absence of any other mixing effect neutrinos emitted from the supernova arrive to the Earth surface as incoherent mass eigenstates and $p_{i\beta}$ is the amplitude of the projection on the flavor basis in vacuum:

$$p_{i\beta} = |U_{\beta i}|^2. \quad (3.27)$$

We will focus on electron antineutrinos for reasons that we will give later.

As an example, the electron antineutrino conversion probabilities for normal and inverted hierarchy read:

$$\begin{pmatrix} P_{\overline{e}e} \\ P_{\overline{\mu}e} \\ P_{\overline{\tau}e} \end{pmatrix} = \begin{cases} \begin{pmatrix} |U_{e1}|^2 \\ |U_{e2}|^2 \\ |U_{e3}|^2 \end{pmatrix}, & \text{NH} \\ \begin{pmatrix} \overline{P}_H |U_{e1}|^2 + (1 - \overline{P}_H) |U_{e3}|^2 \\ |U_{e2}|^2 \\ (1 - \overline{P}_H) |U_{e1}|^2 + \overline{P}_H |U_{e3}|^2 \end{pmatrix}, & \text{IH} \end{cases} \quad (3.28)$$

We can see that in the case of a normal hierarchy the observed $\bar{\nu}_e$ will be an admixture of neutrinos emitted originally as $\bar{\nu}_e$ ($P_{\bar{\nu}e} = \cos^2 \theta_{12} \simeq 0.26$) and $\bar{\nu}'_\mu$ ($P_{\bar{\nu}e} = \cos^2 \theta_{12} \simeq 0.74$). On the other hand in the inverted hierarchy case the mixing will mainly depend on the adiabaticity of antineutrino transitions in the H-Resonance. If transitions are adiabatic, $\bar{P}_H \simeq 0$, the survival probability for $\bar{\nu}_e$ will be suppressed $P_{\bar{\nu}e} \simeq |U_{e3}|^2 \lesssim 10^{-2}$ and the observed $\bar{\nu}_e$ events will be $\bar{\nu}_\mu$ and $\bar{\nu}_\tau$ neutrinos converted in the supernova mantle into $\bar{\nu}_e$ ($P_{\bar{\nu}e} + P_{\bar{\nu}e} \simeq 1$).

Similar considerations can be done for electron neutrinos (see ref.[67]).

3.1.5 Neutrino oscillations in the Earth

If neutrinos travel inside the Earth oscillations will mix the arriving mass eigenstates and the probabilities $p_{i\beta}$ will be more complex.

Due to the hierarchical nature of the mass spectrum, antineutrino oscillations in the Earth could be also reduced to a 2 flavor oscillation problem [67]. In this case the probability that an arriving antineutrino mass eigenstate be detected as an electron antineutrino after crossing the Earth interior could be written as [75]:

$$\begin{aligned}\bar{p}_{1e} &\simeq \cos^2 \theta_{13} (1 - \bar{p}_\oplus), \\ \bar{p}_{2e} &\simeq \cos^2 \theta_{13} \bar{p}_\oplus, \\ \bar{p}_{3e} &\simeq \sin^2 \theta_{13},\end{aligned}\tag{3.29}$$

where \bar{p}_\oplus is the two-flavor oscillation probability after crossing the Earth. \bar{p}_\oplus can be computed under simple assumptions about the Earth interior. For example, if neutrinos travel only through the Earth mantle and we assume a constant density, the oscillation probability is given by [75]:

$$\bar{p}_\oplus = \sin^2 \theta_{12} + \sin^2 2\theta_m \sin(2\theta_m - 2\theta_{12}) \sin^2 \left(\frac{\sin 2\theta_{12} \Delta m_{12}^2 d}{\sin 2\theta_m 4E} \right),\tag{3.30}$$

where the in-matter mixing angle θ_m satisfies 3.13.

Figure 3.4 depicts the oscillation probability \bar{p}_\oplus for antineutrinos as a function of the neutrino energy assuming different distances d traveled inside the Earth mantle. We have assumed standard values for $\bar{\rho}_\oplus^{\text{mantle}} \simeq 4.5 \text{ g/cm}^3$ and $Y_e = 0.5$, and the mixing parameter values of sect. 3.1.2

A more complex problem is to describe neutrino oscillations when neutrinos traverse the mantle and the Earth core. In a dedicated study Akhmedov [81] obtained analytical relations assuming two layers of constant density. In that case the oscil-

lation probability p_{\oplus} for a neutrino which travel distances $d_M + d_C + d_M$ could be parameterized in the following way [75]:

$$p_{\oplus} = \sin^2 \theta_{12} + O_1^2 \cos 2\theta_{12} + O_1 O_3 \sin 2\theta_{12}, \quad (3.31)$$

where the “oscillating” coefficients O_1 and O_3 are the components of the vector

$$\vec{O} = 2 \sin \phi_M Y \vec{t}_M + \sin \phi_C \vec{t}_C \quad (3.32)$$

having defined Y, \vec{t} and ϕ as

$$Y \equiv \cos \phi_M \cos \phi_C - (\vec{t}_M \cdot \vec{t}_C) \sin \phi_M \sin \phi_C, \quad (3.33)$$

$$\vec{t} \rightarrow (\sin 2\theta_m, 0, -\cos 2\theta_m), \quad (3.34)$$

$$\phi \equiv \frac{\sin 2\theta_{12} \Delta m_{12}^2 d}{\sin 2\theta_m 4E}. \quad (3.35)$$

The subindices M and C for ϕ and \vec{t} in (3.32) and (3.33) refer to the mantle and core values of θ_m and d .

The distances traveled by neutrinos inside the mantle and core are given in terms of the Earth radius $R_{\oplus} = 6371$ km, the core radius $r_C = 3486$ km and the zenith angle z :

$$d_M = R \left(-\cos z - \sqrt{r_C^2/R_{\oplus}^2 - \sin^2 z} \right) \quad (3.36)$$

$$d_C = 2R \sqrt{r_C^2/R_{\oplus}^2 - \sin^2 z} \quad (3.37)$$

In figure 3.5 we show the probability p_{\oplus} for different energies and zenith angles.

3.2 The neutrino signal formalism

The theoretical relation between neutrino emission in a supernova and the detected signal involves three elements: i) the neutrino emission, ii) neutrino oscillations and iii) the detection process.

With the conversion probabilities we can proceed to determine the way neutrino oscillations mix the fluxes and spectra of the different neutrino flavors.

At the source, the total flux of neutrinos α , $S_\alpha(E, t)$ can be written in terms of the luminosity $L_\alpha(t)$, the neutrino average energy $\overline{E}_\alpha(t)$ and the spectral distribution $F_\alpha^{\text{em}}(E; t)$ as

$$S_\alpha(E, t) = \frac{L_\alpha(t)}{\overline{E}_\alpha(t)} F_\alpha^{\text{em}}(E; t). \quad (3.38)$$

At the detector these fluxes are mixed to construct the observed antineutrino flux according to the conversion probabilities (3.28):

$$L^2 S_{\overline{e}}^{\text{det}}(E, t) = P_{\overline{e}e} S_{\overline{\alpha}}(E, t) + (P_{\overline{\mu}e} + P_{\overline{\tau}e}) S_{\overline{x}}, \quad (3.39)$$

where L is the supernova distance and we have used the fact that for all purposes the $\overline{\nu}_\mu$ and $\overline{\nu}_\tau$ fluxes are identical $S_{\overline{x}} \equiv S_{\overline{\mu}} \simeq S_{\overline{\tau}}$ (see sect. 2.1).

Using the unitarity property of the conversion probabilities $\sum_\alpha P_{\overline{\alpha}e} = 1$ we can express the detected flux (3.39) in terms of just one probability, namely the electron antineutrino survival probability $\overline{p} \equiv P_{\overline{\nu}_e \overline{\nu}_e}$:

$$L^2 S_{\overline{e}}^{\text{det}}(E, t) = \overline{p} S_{\overline{e}} + (1 - \overline{p}) S_{\overline{x}}. \quad (3.40)$$

From the detected flux of electron antineutrinos we can straightforwardly compute the rate of events at a given neutrino detector:

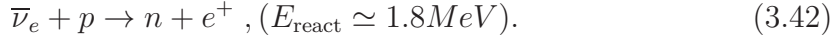
$$\frac{d^2 n_{\overline{\nu}_e}(E, t)}{dE dt} = N_T \int dE' S_{\overline{e}}^{\text{det}}(E', t) \sigma(E') \epsilon(E') \mathcal{R}(E, E'), \quad (3.41)$$

where $\sigma(E)$ is the detection cross-section, N_T is the number of target particles in the fiducial volume, $\epsilon(E)$ is the detection efficiency and $\mathcal{R}(E, E')$ is the energy resolution function that accounts for the uncertainties in the measurement of the neutrino energies.

3.2.1 Neutrino Detection

The statistical procedure that will be introduced in the next chapter is based on two assumptions about the neutrino signal: it must have a large number of events (several thousands) and both the energy and time measurements must be available. Both conditions are fulfilled for electron antineutrino events in water Čerenkov detectors and in scintillator detectors. This is the main reason why we concentrate our attention on $\overline{\nu}_e$.

Electron antineutrinos are detected in water and scintillator detectors through the inverse β process:

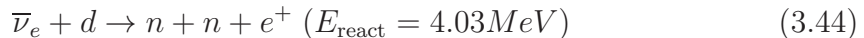


An accurate parameterization of the cross-section for this process has been recently provided by Strumia and Vissani[82]:

$$\frac{\sigma_{\bar{\nu}}(\bar{\nu}_e p \rightarrow e^+ n)}{10^{-43} \text{ cm}^2} = p_e E_e E_{\bar{\nu}}^{-0.07056 + 0.02018 \ln E_{\bar{\nu}} - 0.001953 \ln^3 E_{\bar{\nu}}}, \quad (3.43)$$

where $E_e = E_{\bar{\nu}} - Q_{np}$ with $Q_{np} = m_n - m_p \approx 1.293 \text{ MeV}$ and all the energies are in MeV. This parameterization is accurate on a wide range of neutrino energies. In figure 3.6 we compare this cross-section with the approximation $\sigma_{\bar{\nu}}(\bar{\nu}_e p \rightarrow e^+ n) \simeq 9.52 \times 10^{-43} \text{ cm}^2 p_e E_e$ and the corresponding time-integrated spectrum. We see that using an accurate cross-section the neutrino flux is reduced as much as 20%.

In heavy water (D_2O), $\bar{\nu}_e$ can be detected through the charged current reaction off deuterium:



SNO is the only operational heavy water detector and therefore, with fiducial volume much smaller than Super Kamiokande, the number of neutrino events detected through this process will not be enough large to apply efficiently our method.

Other reactions (as described in details in ref. [56]), including $\bar{\nu}_e$ absorption in oxygen (water detectors) and carbon (scintillator detectors), will produce typical number of events below 10% of the statistics from $\bar{\nu}_e$ β process. Additionally, some of these reactions have large energy thresholds or cannot provide energy and/or time informations, a central condition for the application of any method.

In our simulations we have assumed 100% detection efficiency above the energy threshold for all the detectors. This idealized situation will not change much the signal characteristics.

The uncertainty in the energy measurement is an important aspect in our simulations and their analysis. We have approximated the resolution function $\mathcal{R}(E, E')$ with a Gaussian distribution with mean E equal to the measured energy, and as standard deviation ΔE equal to the energy resolution, that can be parameterized as[66]:

$$\frac{\Delta E}{\text{MeV}} = a_E \sqrt{\frac{E}{\text{MeV}}} + b_E \frac{E}{\text{MeV}}. \quad (3.45)$$

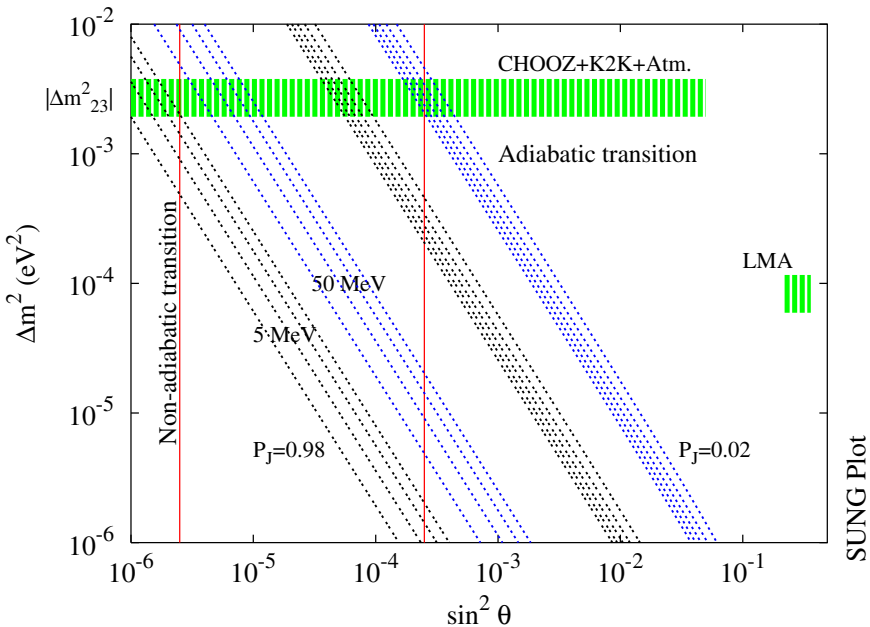


Figure 3.1: *Contours of equal neutrino jumping probability across a resonance region with different mixing parameters ($\Delta m^2, \theta$). Dotted lines correspond to a 50 Mev neutrino while dashed lines are for 5 MeV. Contours at the left range from $P_J = 0.02$ to $P_J = 0.1$ and at right from $P_J = 0.9$ to $P_J = 0.98$. It is possible to recognize three regions where jumping probabilities have different values: one were adiabatic transitions ($P_J \simeq 0$) take place (upper-right), a second one for which there are non-adiabatic transitions ($P_J \simeq 1$) (lower-left) and an intermediate one where P_J has intermediate values for almost all neutrino energies. Jump probabilities are computed assuming the simple density profile $\rho(r)Y_e = 2 \times 10^4 \text{ g/cm}^3 (r/10^9 \text{ cm})^3$ [67]*

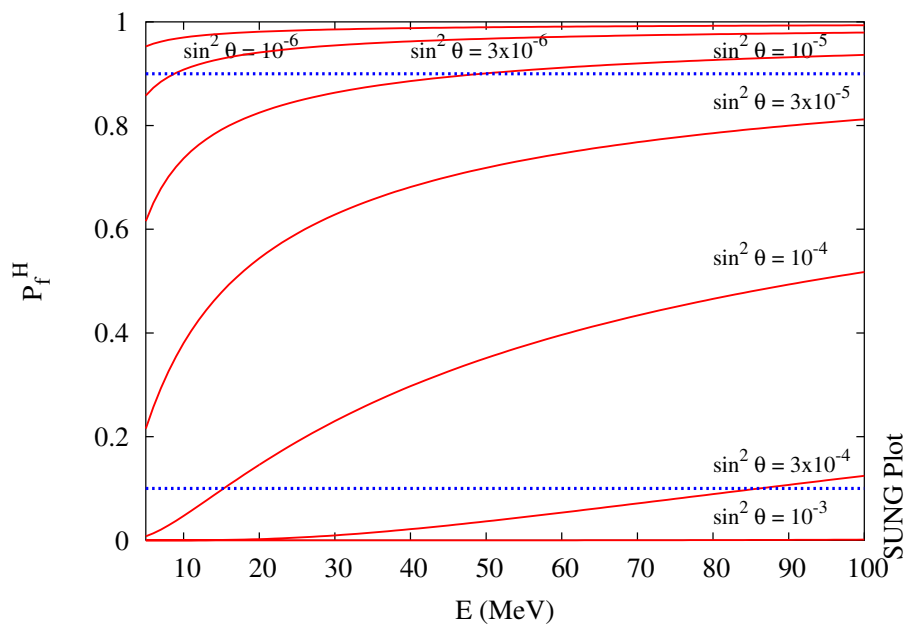


Figure 3.2: *Jumping probability P_H (\bar{P}_H for inverted hierarchy) as a function of energy for different values of the mixing parameter $\sin^2 \theta_{13}$.*

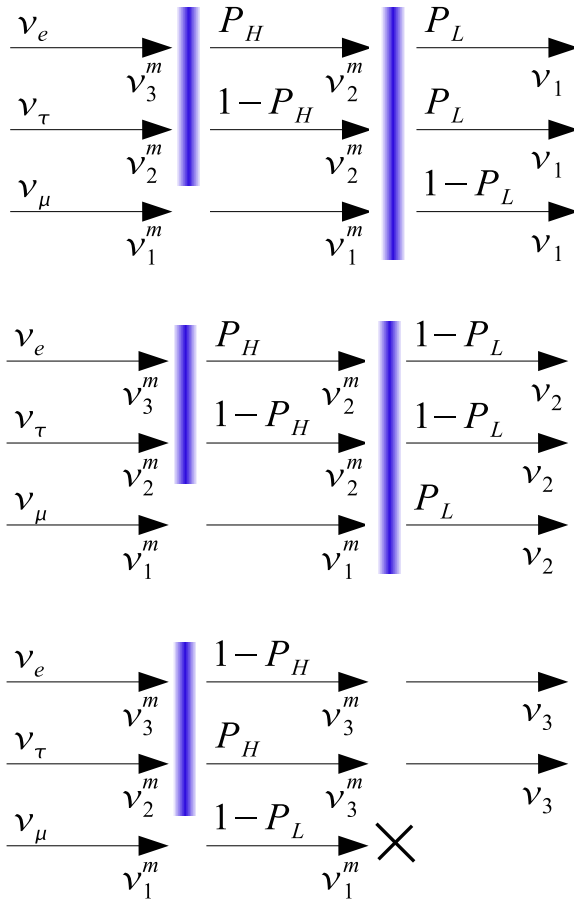


Figure 3.3: Schematic illustration of how transition probabilities are computed using jumping probabilities and following the evolution of neutrino state along the resonance regions. The example illustrated is for ν_e transitions and normal hierarchy.

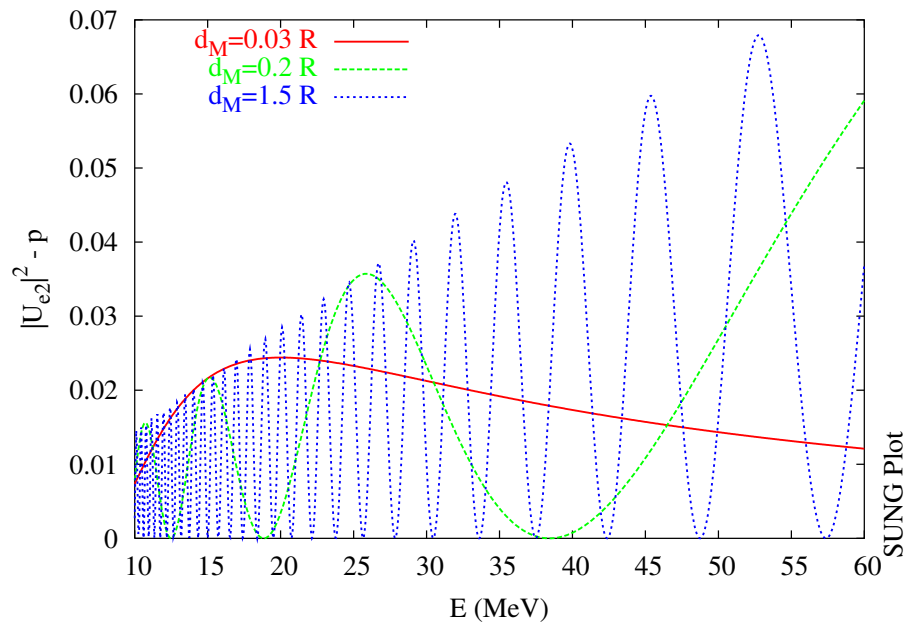


Figure 3.4: Oscillation probability p_+ in the Earth mantle for different distances d_M traveled. We used $\Delta m_{12}^2 = 8 \times 10^{-5}$, $\theta_{12} = 30^\circ$, $\bar{\rho}_\oplus^{\text{mantle}} = 4.5 \text{ g/cm}^3$ and $Y_e = 0.5$.

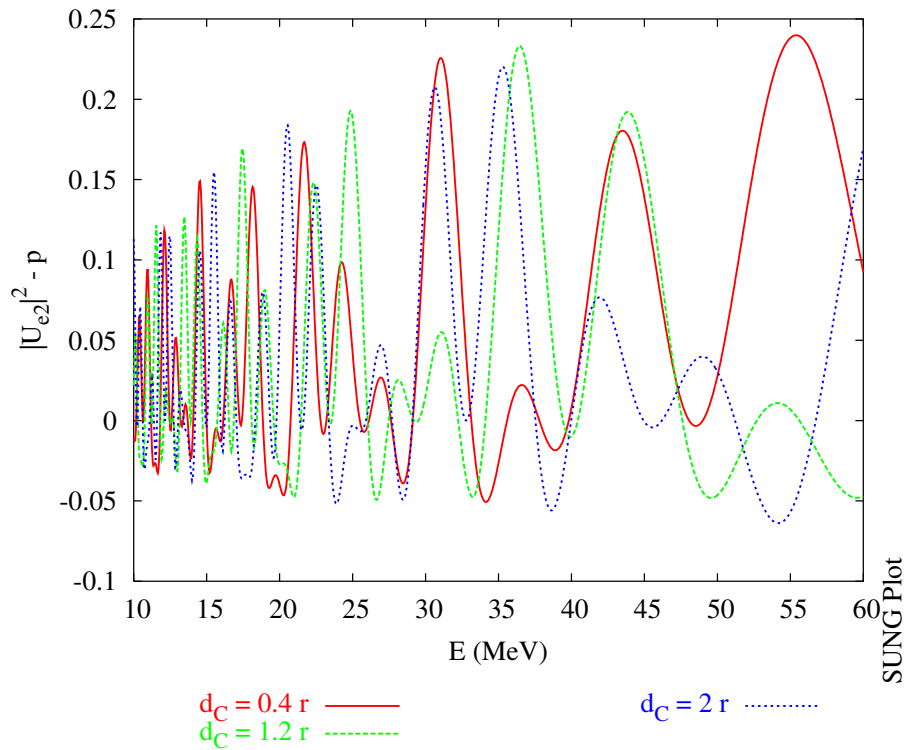


Figure 3.5: *Oscillation probability p_+ when neutrino traverse the mantle and core. We used $\Delta m_{12}^2 = 8 \times 10^{-5}$, $\theta_{12} = 30^\circ$, $\bar{\rho}_\oplus^{\text{mantle}} = 4.5 \text{ g/cm}^3$, $\bar{\rho}_\oplus^{\text{core}} = 12 \text{ g/cm}^3$ and $Y_e = 0.5$.*

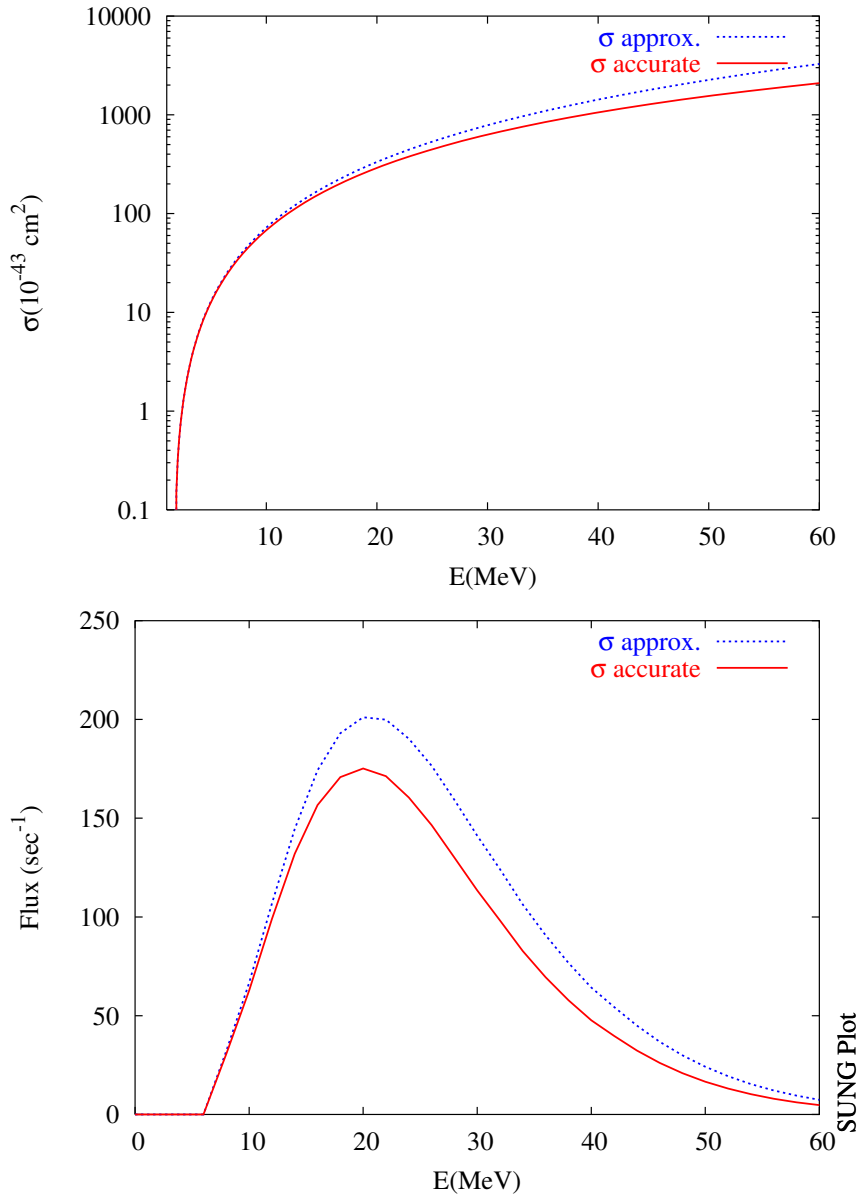


Figure 3.6: *Upper panel:* comparison between the approximate (dashed line) and the accurate cross-section (3.43). *Lower panel:* time integrated spectrum obtained when the approximate (dashed) and the accurate cross-section are used.

Detector	E_{th} (MeV)	(a_E, b_E)	Fiducial	$N_{\bar{\nu}_e}^{\text{det}}$
			mass kton	$(D = 10 \text{ kpc})$
Čerenkov	SK[0] (H ₂ O)	5	(0.47, 0)	32
	SNO[0] H ₂ O	4	(0.35, 0)	1.4
	D ₂ O			1.0
	KamLAND [0] (N12+PC+PPO)	2.6	(0, 0.075)	1.0
Scintillator	HK[0] (H ₂ O)	5	(0.5, 0)	540
	UNO [0] (H ₂ O)	5	(0.5, 0)	650
	LENA [0] (PXE)	2.6	(0.1, 0)	30
				100,000 - 170,000
Scintillator				120,000 - 203,000
				7,500 - 12,600

Table 3.2: *The relevant $\bar{\nu}_e$ detection parameters for present and proposed large volume detectors. In the last column we give a range for the total number of expected $\bar{\nu}_e$ events from a Galactic SN at 10 kpc. The larger and smaller numbers correspond respectively to a supernova model with large spectral differences between $\bar{\nu}_e$ and $\bar{\nu}_x$ (Supernova model I in chapter 5) and of a model where smaller spectral differences are obtained (Supernova model II). As regards to neutrino oscillations, we have assumed NH and $\sin^2 \theta_{12} = 0.26$ which give a mixing $\bar{\nu}_e : \bar{\nu}_x \approx 4 : 3$. Only charged current reactions, that provide good energy and time informations, have been considered.*

The value of the adimensional coefficients a_E and b_E and other characteristics of several operational detectors as well as of a few planned detectors are presented in table 3.2.

3.3 Characteristics expected for the signal

Starting from the detected neutrino rate (3.50) we can compute the properties of the detected signal. The most important informations are: i) the number of events, ii) the time-integrated spectrum and iii) the energy-integrated time-profile.

Normally the analysis performed on a neutrino signal focus on one of these properties. In this section we will evaluate these quantities under different conditions, in the attempt of understanding the interplay between the different effects for the determination of the signal characteristics.

3.3.1 Number of events

The number of events expected in a given energy and time interval is computed integrating the total rate in the desired region:

$$N(\Delta E_{12}, \Delta t_{12}) = \int_{E_1}^{E_2} dE \int_{t_1}^{t_2} dt \frac{d^2 n(E, t)}{dE dt}. \quad (3.46)$$

The counting of neutrino events provides very important global information on the signal. The total number of events, for example, is directly related to the total energy released in the supernova. In table 3.2 we present the total number of $\bar{\nu}_e$ events for a future Galactic Supernova in present and future detectors.

In our analysis the number of neutrino events in certain energy and time intervals are clue properties of a signal. For example, we are particularly interested in low energy events because they are very sensitive to a neutrino mass, and how many neutrinos of this type could be present in a signal becomes a very important piece of information.

In figure 3.7 we present the distribution of neutrinos inside several interesting E-t regions. To compute these numbers we used two very different supernova emission models and two extreme cases for the neutrino oscillation patterns.

We can see that almost in all cases the majority of events will have intermediate energies and will arrive at late times ($t \gtrsim 1$). Only few percent of the neutrinos will have energies below 10 MeV, this means that in a signal with 10^4 events, hundreds of neutrinos of low energy will be available, enough to provide a good sensitivity to the neutrino mass. This suggests that it may be appropriate for the purposes of mass related analysis to have energy thresholds below the 10 MeV level. Just few neutrinos with energies smaller than 5 MeV are observed in almost all cases implying that an improvement in the energy threshold below this level will not change too much the potential to neutrino mass measurements.

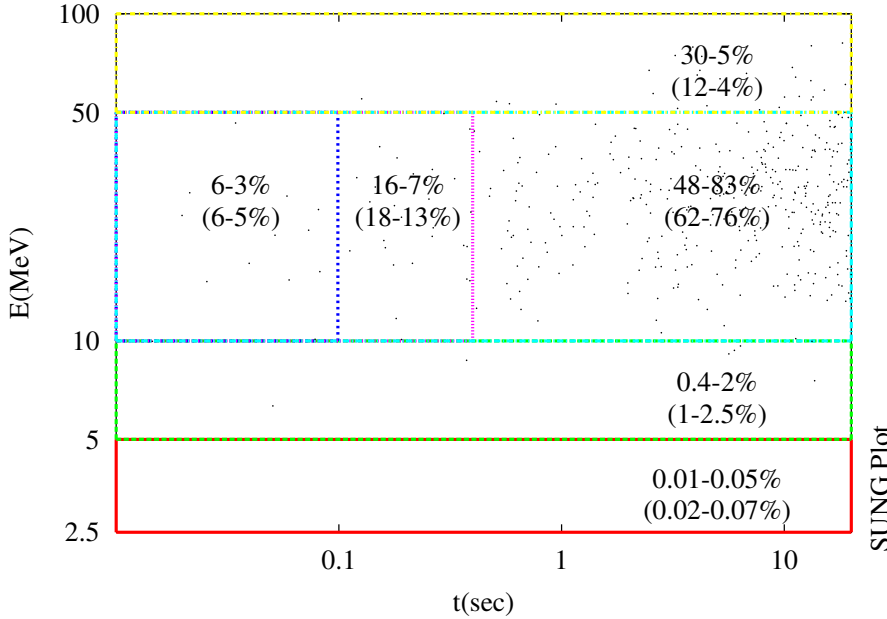


Figure 3.7: *Distribution of events in a supernova signal. Fractions are computed using (3.46). The ranges refer to results obtained with two different supernova emission models. The first figure correspond to Supernova model I (see chapter 5) with large spectral differences; the second one to Supernova model II with small spectral differences. Two different extreme mixing schemes were considered: a moderate mixing obtained when NH is assumed (numbers in parenthesis), and a complete spectral swap that can be produced with IH and $\sin^2 \theta_{13} \gtrsim 10^{-3}$.*

3.3.2 Time-integrated spectrum

One of the most interesting properties of a supernova signal is the distribution of neutrino energies. The energy spectrum of neutrinos could bring us clues about the neutrino emission process and will allow us to study the effects that oscillations in the supernova mantle and Earth interior will have on the signal.

The time-integrated energy spectrum computed from the total detected rate (3.41) is given by:

$$f_E^{\text{det}}(E) = \int dt \frac{d^2 n(E, t)}{dE dt}. \quad (3.47)$$

Substituting the detected flux S^{det} (3.39) in $d^2n/dt dE$ we can rewrite f_E in the following way

$$\begin{aligned} f_E^{\text{det}}(E) &= \bar{p}F_{\bar{e}}(E) + (1 - \bar{p})F_{\bar{x}}(E) \\ &= F_{\bar{e}}(E) - (1 - \bar{p})[F_{\bar{e}}(E) - F_{\bar{x}}(E)], \end{aligned} \quad (3.48)$$

where $F_{\bar{e}}(E)$ and $F_{\bar{x}}(E)$ are the independent time-integrated energy fluxes of $\bar{\nu}_e$ and $\bar{\nu}_x$ respectively. In the last equation we can see that neutrino mixing have a “modulation” effect on the neutrino spectrum distortion.

In figure 3.8 we depict f_E for two different emission models, and assuming different neutrino oscillations schemes. There are two interesting facts in the spectral distortion observed in the figures. The first one is that in the absence of Earth oscillations the distorting effects introduced in the case of normal hierarchy can be mimicked with an inverted hierarchy, if the mixing parameter $\sin^2 \theta_{13}$ has a value in the intermediate region of fig. 3.1. The other observation is that Earth matter effects will produce only a mild distortion.

3.3.3 Energy-integrated time profile

The energy-integrated time profile is computed from the detected rate (3.41) as:

$$f_t^{\text{det}}(t) = \int dE \frac{d^2n(E, t)}{dE dt}. \quad (3.49)$$

f_t provides global informations on how the neutrino flux changes in time, regardless of the neutrino energies.

Figure 3.9 depicts typical time-profiles obtained for different oscillation schemes.

We notice that besides a global modulation effect, the oscillatory distortion of the flux that was clearly observed in the spectrum can not be discerned in the time profile. In particular, Earth matter effects become almost undetectable. This is easy to understand since being indeed small, Earth effects are averaged out when the integration in the energy is performed.

3.4 Generation of full statistics signals

Many of the techniques that have been considered to analyze a signal from a future Galactic supernova use one or more of the properties described in the previous section. To obtain the number of events or the integrated signal profiles it is not

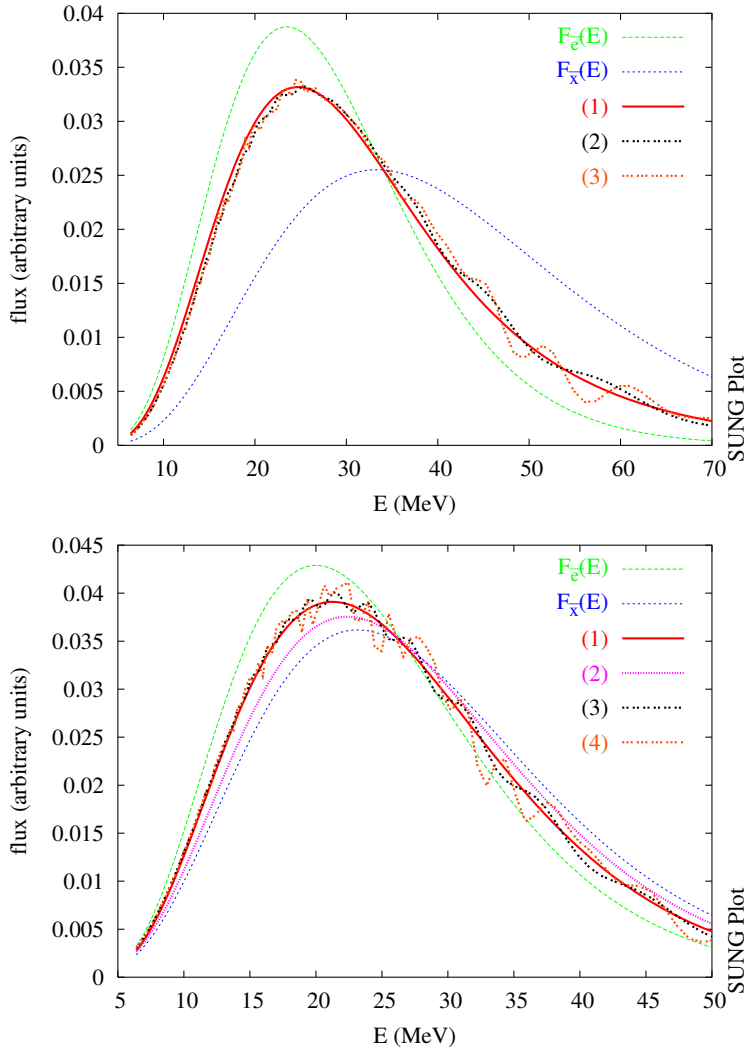


Figure 3.8: *Time integrated spectrum for two different supernova model and oscillations schemes. Upper panel: supernova model I: (1) NH, (2) IH, $\sin^2 \theta_{13} = 10^{-2}$, (3) IH, $\sin^2 \theta_{13} = 10^{-2}$, Earth matter effects, zenith angle $z = 100$ (path just into the mantle) (4) same as (3) but with $z = 180^\circ$ (mantle+core+mantle). Lower panel: supernova model II: (1) NH, (2) IH, $\sin^2 \theta_{13} = 10^{-2}$, Earth matter effects, $z = 100$ (path just into the mantle) (3) same as (2) but with $z = 180^\circ$ (mantle+core+mantle)*

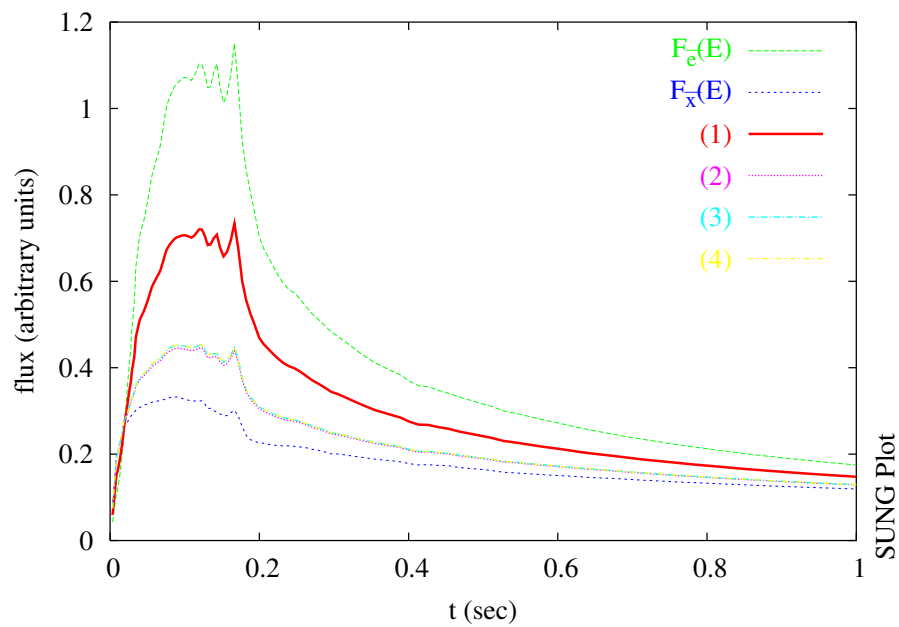


Figure 3.9:

necessary to generate a complete signal, and then testing these techniques is rather straightforward. On the other hand, if we want to perform a statistical analysis of the whole statistics in the signal, as is done in only a few of the proposed techniques, it becomes necessary to generate a complete realization of the signal in all its details.

There are two different ways to generate a detailed synthetic supernova neutrino signal. The first one is an intuitive procedure where the various physical processes are simulated. Neutrinos of different flavors are generated using the emitted fluxes $S_{\bar{\nu}}(E, t)$. Then the “seed” sample is filtered first according to the conversion probabilities, where neutrinos change flavor depending on their energy, and after with the cross section and efficiency of detection. The final signal is obtained joining all the resulting events.

Despite the apparent naturalness, this method has several defects. Firstly, although sampling the emitted fluxes seems to be rather simple, because they are not affected by the distorting effects of oscillations, designing reliable filters using the conversion probabilities, particularly in presence of an energy dependence or a strong oscillatory behavior, is a non trivial matter. On the other hand since the seed sample to which the filters are applied has a finite number of neutrinos, statistical fluctuations could be amplified by filtering, producing artificial enhancements or depletions of given parts of the signal.

The second method consists in sampling directly the detected rate $d^2n/dtdE$ (3.41):

$$\frac{d^2n_{\bar{\nu}_e}(E, t)}{dE dt} = N_T S_{\bar{\nu}}^{\text{det}}(E, t) \sigma(E) \epsilon(E). \quad (3.50)$$

The signal is constructed generating N pairs of energies and arrival times (E, t) (with N as given by eq. (3.46)). If a non zero neutrino mass is assumed, the time coordinate of each event is shifted according to the time-of-flight delay (1.4). To account for measurement uncertainties (which affect mainly the measured energies) the energy of each event is reshuffled according to a Gaussian distribution with mean equal to the generated value E , and dispersion equal to the resolution of the detector (3.45).

The synthetic signals used in the MC analysis performed to test our method were generated through this procedure.

Although the detected rate (3.41) could be in principle a complex multivariate function (see fig. 3.10), this method is free of the statistical flaws that could arise when the first procedure is used.

In figure 3.10 we have summarized all the characteristics of a synthetic signal. We have plotted the surface defined by the total rate in the most general case when

Earth matter effects are present, in the E-t plane we show a scatter plot of the events generated with such rate and on the E-rate and t-rate planes we show the time-integrated spectrum and the energy-integrated time profile.

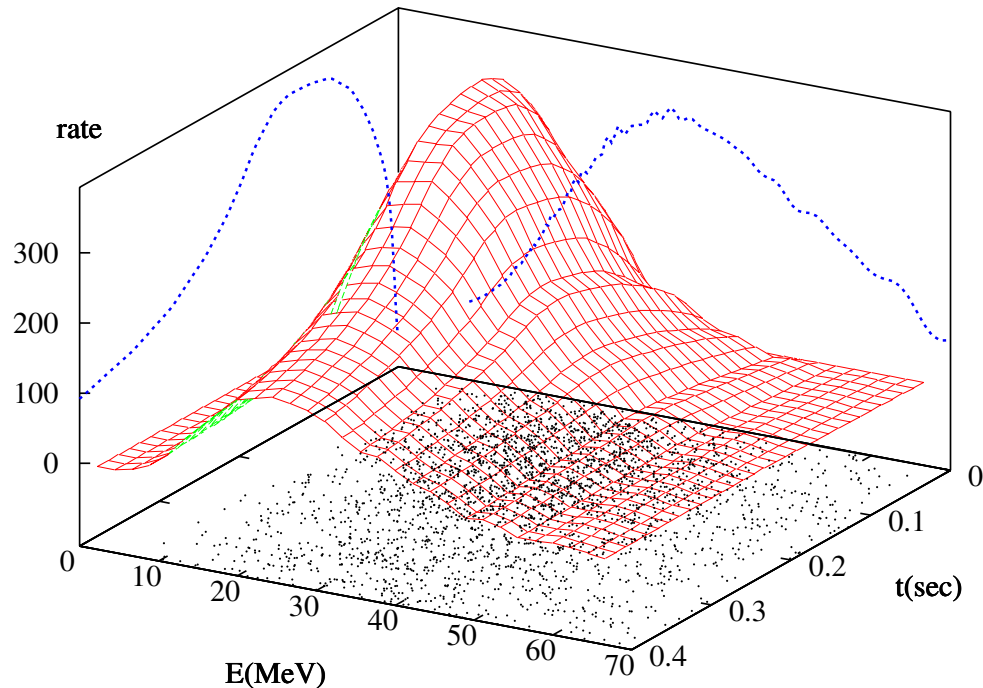


Figure 3.10: *Neutrino detected rate (surface), time-integrated energy spectrum (curve on E-rate plane), energy-integrated flux (plane t-rate) and scatter plot (dots on plane E-t) for a signal generated with Supernova model I assuming IH, $\sin^2 \theta_{13} = 10^{-5}$ and $z = 180^\circ$ (mantle-core-mantle). The profiles have been normalized properly to fit into the plot area.*

Other details of supernova signal synthesis are presented in Appendix B where we describe the computer tool that we have developed to generate and analyze supernova neutrino signals.



CHAPTER **4**

Mass limits with Supernova Neutrinos

In this chapter we will describe a new statistical method to constraint neutrino masses using a high statistics supernova neutrino signal. The method was described by the first time in a intuitive form in ref. [83].

We have organized this chapter as follows. The first two sections are devoted to present the main idea underlying almost all methods to measure or constraint neutrino mass using supernova neutrinos. Then we describe synthetically several of the recently proposed methods including those that were used to constraint the neutrino mass using the SN1987A signal. An outline of the new method and the main assumptions behind it is presented in section 4.3. Section 4.4 presents a rigorous description of the method and several of its mathematical and numerical properties. Details about the numerical computation of the statistics and other quantities related to the method are presented in sections 4.5 and 4.6.

4.1 Time-of-flight delay of supernova neutrinos

It was realized long time ago that valuable informations on the neutrino masses could be provided by the detection of neutrinos from a Supernova explosion [37, 38, 39, 40]. The basic idea relies on the estimation or measurement of the time-of-flight (TOF) delay Δt_{tof} that a relativistic neutrino of mass m_ν and energy E_ν traveling a distance L would suffer with respect to a massless particle:

$$\begin{aligned}
\frac{\Delta t_{\text{tof}}}{L} &= \frac{1}{v} - 1 \\
&= \frac{E}{\sqrt{E^2 - m^2}} - 1 = \frac{1}{2} \frac{m^2}{E^2} + \mathcal{O}\left(\frac{m^3}{E^3}\right) \\
\Delta t_{\text{tof}} &\simeq 5.1 \text{ msec} \left(\frac{L}{10 \text{ kpc}}\right) \left(\frac{10 \text{ MeV}}{E_\nu}\right)^2 \left(\frac{m_\nu}{1 \text{ eV}}\right)^2.
\end{aligned} \tag{4.1}$$

Figure 4.1 shows typical values of the TOF delay and its dependence on neutrino mass and energy.

A natural question arises: what could be a “benchmark” in the signal that could play the role of a “massless particle” to estimate the neutrino delays? Alternative answers to this question are at the root of different approaches used to exploit this basic idea. We will summarize several of them in the next section.

4.2 Neutrino mass and the TOF delay

In order to measure or constrain a neutrino mass using the TOF delay is necessary to identify some kind of “timing” information in the signal. Many different ideas have been proposed since the seminal work by Zatsepin [37]. Some of them have been even already used to obtain information on neutrino mass from SN1987A signal [44, 45, 46, 47, 48].

We could classify all the methods in three general classes:

- Methods that use the change in the time spread of the signal due to delays between the arrival time of high and low energy neutrinos.
- Methods that rely on the occurrence of specific timing events in coincidence with neutrino emission.
- Methods that make use of a detailed statistical description of the signal.

4.2.1 Time spread of the signal

A supernova neutrino signal has a relatively short duration. Most of the neutrinos are emitted in just few seconds and although the detailed evolution of the neutrino flux depends on the supernova model, the total duration of the signal, which is

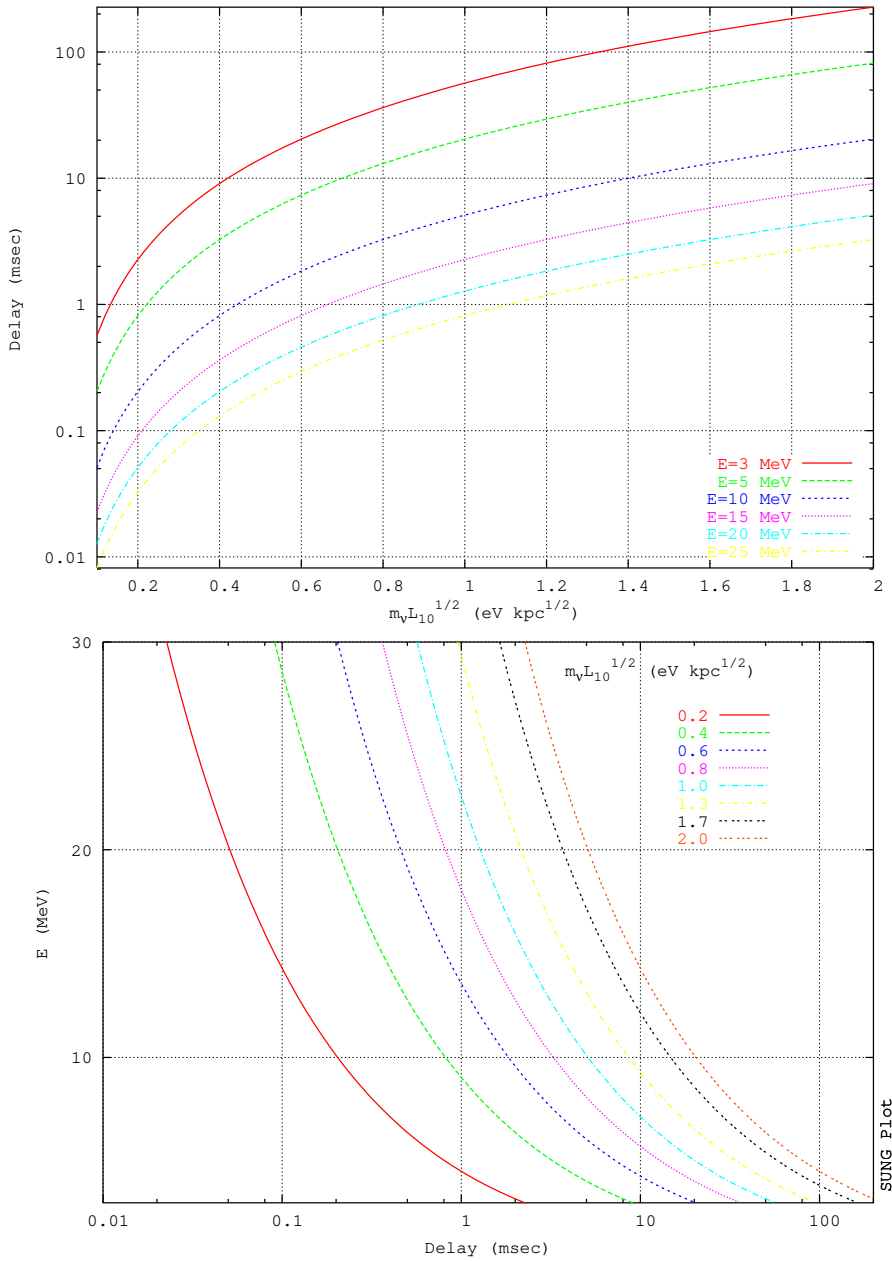


Figure 4.1: *TOF delay as a function of the neutrino mass and the supernova distance (upper panel) for different neutrino energies. Lower panel depicts the continuous dependence on the energy of the TOF delay for different values of the neutrino mass.*

determined by the time scale of neutrino diffusion in the supernova core, can be predicted from basic physical principles.

Neutrinos of different energies emitted simultaneously from the supernova core will arrive at different times. This effect will increase the time spread of the signal in an amount directly related to the value of neutrino mass and supernova distance according to (4.1). Therefore, knowing the expected duration of the supernova neutrino burst and measuring the observed time spread it is possible to constraint or measure the neutrino mass.

Using this kind of approach the total duration of the signal from SN1987A was used to estimate model independent limits on the electron neutrino mass in the range $20 - 30$ eV [44]. More stringent limits were obtained using specific assumptions about the signal time structure [45, 46, 47, 48].

More recently a method to measure the time spread of neutrinos emitted during the shock breakout in a future Galactic supernova has been proposed [52]. The short duration emission of neutrinos in this phase, determined by the time scale of the shock wave emergence in the supernova core, could allow to set limits at the level of 3 eV without make any additional assumption about the time structure of the neutrino emission.

4.2.2 Timing events

Another way to estimate a neutrino mass with a supernova signal is based on “timing” events that take place simultaneously with the supernova explosion, and used as benchmarks to measure the neutrino delays.

Gravitational waves are expected to be emitted almost in coincidence with the neutrino burst [50, 51]. If the supernova is close enough to allow a clear detection of gravitational waves, the peak in the emission of this radiation could be used to measure the delayed arrival of neutrinos in the early phases of the explosion, and constrain neutrino masses at the level of 1 eV [51].

Another possibility is the early formation of a Black hole in the supernova core that will abruptly truncate the neutrino emission. With a non zero neutrino mass the cutoff in the observed flux will not be turn off sharply, and a measurement of the time spread of the neutrino signal could allow to put limits on neutrino mass at the level of 1.8 eV [53, 54].

4.2.3 Detailed analysis of a signal

A non-zero neutrino mass will produce a global distortion in a supernova signal that would be very difficult to be mimicked by astrophysical effects at the source. Using a detailed model of neutrino emission and performing a complete statistical analysis, values of the neutrino mass could be constrained by subtracting the effect of the masses and measuring the agreement between the emission model and the signal.

A very accurate statistical analysis performed under these lines of reasoning was done recently by Loredo and Lamb [49]. They used a Maximum Likelihood analysis to fit several types of neutrino emission models with the SN1987A data, and Bayesian reasoning to account for prior information about those models and to perform statistical comparisons between them. They obtained the limit $m_{\bar{\nu}_e} < 5.7\text{eV}$ which is more stringent than any other limit coming from the analysis of SN1987A signal, and close to laboratory upper bounds on the electron neutrino mass.

The method proposed here belongs to this kind of approaches. In the following sections we present a detailed description of the method and its properties.

In table 4.1 we summarize the neutrino mass limits from a supernova signal, for SN1987A and for a future Galactic supernova.

4.3 Basic description of method

The method proposed has three basic characteristics:

1. It is based on a neutrino-by-neutrino kind of analysis and requires the determination of the time and energy of each event in the signal¹
2. The method uses the full statistics of the signal, i.e. every neutrino event in the signal is used to construct the statistical estimator.
3. It can be applied independently of particular astrophysical assumptions about the characteristics of the neutrino emission (time evolution of the neutrino luminosity and spectral parameters) and does not rely on additional benchmarks events for timing the neutrinos TOF delays.

The method relies on two basic assumptions:

¹ $\bar{\nu}_e$ events on scintillator and Čerenkov detectors are particularly well suited for this kind of analysis. Additionally, since $\bar{\nu}_e$ will provide the largest number of events on present and future detectors, we will focus on these events in the description of our method and in the tests performed to measure its sensitivity.

Table 4.1: *Limits on the neutrino mass from supernova neutrinos, SN1987A and from a future Galactic supernova neutrino signal.*

Limit	Description	References
SN1987A		
$m_{\bar{\nu}_e} \lesssim 20 - 30$ eV	Model independent mass limits using the total duration of the signal.	[44]
$m_{\bar{\nu}_e} \lesssim 10 - 26$ eV	Model dependent mass limits with assumptions on the time structure of signal.	[45, 46, 47, 48]
$m_{\bar{\nu}_e} \lesssim 5.7$ eV	Complete statistical analysis using different neutrino emission models and Bayesian techniques.	[49]
Potential		
$m_{\bar{\nu}_e} \lesssim 3$ eV	Model independent limit using time spread after shock breakout	[52]
$m_{\bar{\nu}_e} \lesssim 1.0$ eV	Gravitational waves as benchmark to measure neutrino delays in the early phase of the emission	[51]
$m_{\bar{\nu}_e} \lesssim 1.8$ eV	Time spread of the residual neutrino emission after the abrupt cutoff of the flux by the formation of a Black hole	[54, 53]

1. The first and most important one is that inside the collapsing core neutrinos are kept in thermal equilibrium, by means of continuous interactions with the surrounding medium, and therefore are emitted with a quasi-thermal spectrum. As was explained in chapter 2 this is a solid prediction of almost all supernova models and simulations and has also been confirmed by the duration of the SN1987A signal that constitutes an evidence for efficient neutrino trapping within the high density core.
2. The second hypothesis is that the time scale for the variation of the characteristics of the neutrino spectrum is much larger than the time lags induced by a non-vanishing mass (say, much larger than 5 msec., see (4.1)). Also this assumption is quite reasonable, since it is a robust prediction of all SN simulations [56, 60, 84, 3] that sizeable changes in the spectral parameters occur on a time scale much larger than 5 msec (see fig. 2.8).

According to the first assumption, a high statistics neutrino signal can be considered as a ‘self timing’ quantity, since the high energy part of the signal, that suffers only

negligible delays, could determine with a good approximation the characteristics of the low energy tail, where the mass induced lags are much larger. The second assumption implies that the time evolution of the spectral parameters as inferred from the detected sample will reproduce with a good approximation the time evolution of the neutrino spectrum at the source. No additional timing events are needed, and each neutrino, according to its specific energy, provides a piece of information partly for fixing the correct timing and partly for measuring the time delays.

Figure 4.2 illustrates schematically the basic strategy of the method.

4.4 Formalism for the signal analysis

In real time detectors, supernova electron antineutrinos are revealed through the positrons they produce via charged current interactions, that provides good energy informations as well. Each $\bar{\nu}_e$ event corresponds to a pair of energy and time measurements (E_i, t_i) together with their associated errors. In order to extract the maximum of information from a high statistics SN neutrino signal, all the neutrino events have to be used in constructing a suitable statistical distribution. The *Likelihood Function* is probably the best option to perform the analysis of the whole statistics of a supernova signal.

To compute a LF we need to specify a probability for each event in the signal and therefore we need to construct or select a suitable analytical model to describe the neutrino emission from supernova. However, we are interested in evaluating how much information about the neutrino mass is possible to extract from a signal irrespective of our detailed knowledge on the neutrino emission process. Therefore we will need to *marginalize* the extra information about the astrophysical description of the signal from the effect of a mass. We have constructed our statistical method on the basis of Bayesian principles of inference. In Appendix A we present a simple introduction to Bayesian reasoning. The definitions, results and terminology used in this section to describe our method is presented there, and therefore a first reading of that Appendix is recommended.

The power of Bayesian statistics to perform an analysis of supernova neutrino data has been demonstrated with the analysis of the SN1987A signal by Loredo and Lamb in ref. [49]. Our method is similar in several aspects to the Loredo's analysis but the fact that we will analyze signals with thousands of events will require a somewhat different mathematical and numerical approach.

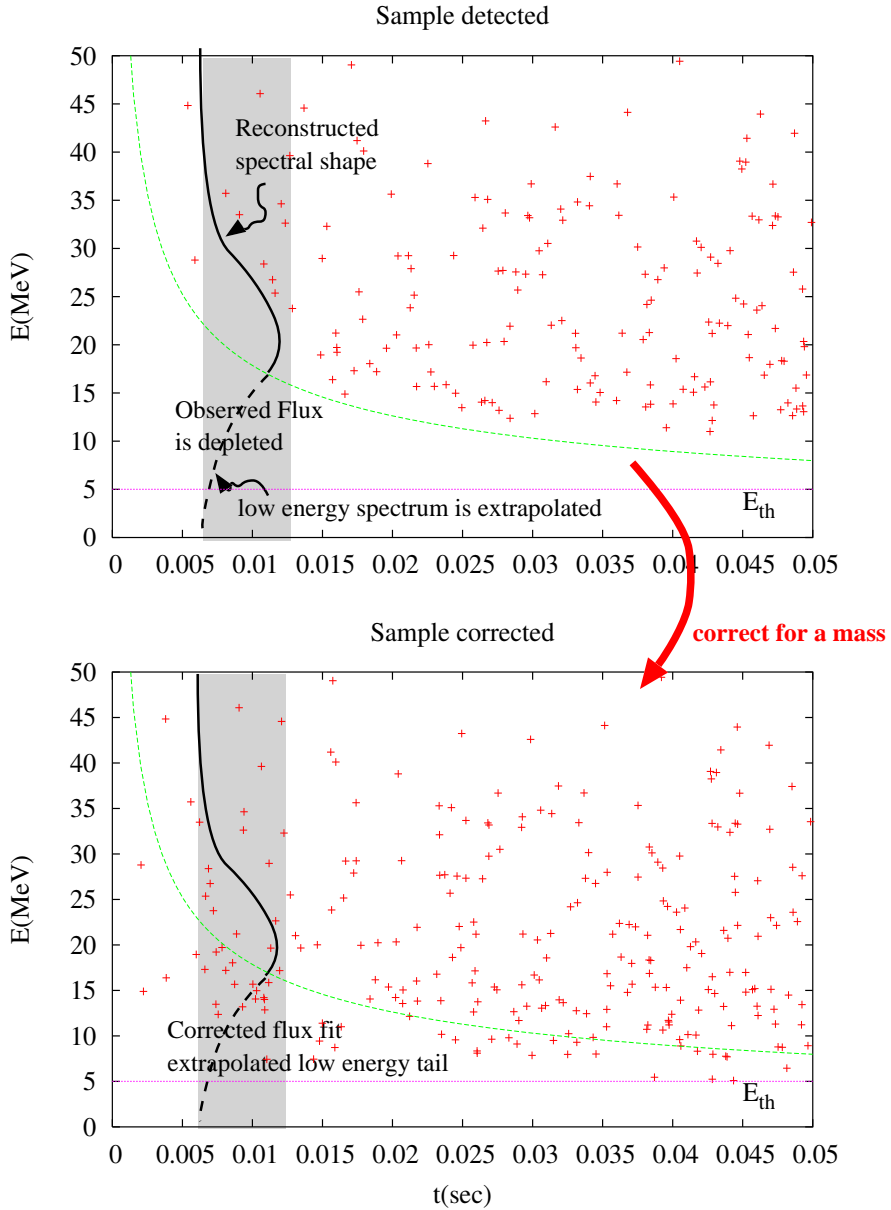


Figure 4.2: *Schematic explanation of the method strategy. Using the observed neutrino energy distribution at high energy the best-fit spectrum at a given time is found (upper panel). The neutrino mass can be measured by shifting the events with a time delay according to the test mass and event energy, until the corrected flux reproduces what is expected from the extrapolation to low energies of the fitted spectra at each time (lower panel).*

4.4.1 The Likelihood Function

We identify a signal as a set of pairs of energy and time measurements $\mathcal{D} \equiv \{E_i, t_i\}$. The Likelihood Function (LF) \mathcal{L} , associated to a particular parametric model of the emission $\mathcal{M} \equiv \mathcal{M}(\{\theta\})$ and a given neutrino mass m_ν^2 , could be *schematically* written as:

$$p(\mathcal{D}|m^2, \mathcal{M}) \equiv \mathcal{L}(m^2, \{\theta\}; \mathcal{D}) = \prod_i f(E_i, t_i), \quad (4.2)$$

where the index i runs over the entire set of events in the signal. Here, $f(E, t)$ represents a *probability distribution function* (pdf) used to evaluate the contribution to the likelihood of a single event.

Using the emission rate expression in eq. (3.38) and the total detected rate in eq. (3.41), f can be written as:

$$f(t, E; m^2, \{\theta\}) = N^{-1} \phi(t) \times F(E; t) \times \sigma(E), \quad (4.3)$$

where the normalization constant is $N = \int dt \int dE \phi(t) F(E; t) \sigma(E)$. In the above definition we identify three components: the neutrino time profile flux $\phi(t)$, the energy spectrum $F(E; t)$ which in general evolves in time, and the detection cross-section $\sigma(E)$ which is a well known function of the neutrino energy.

4.4.2 Posterior probabilities

In Bayesian inference the likelihood of a given model in the presence of some experimental evidence must be always weighted with the prior probability that we could give to the model itself and to the measurement process (see Appendix A). Therefore, when using Bayesian principles the LF is just the first step to obtain the *posterior* probability for the theoretical model.

Using Bayes theorem (A.4) the *posterior probability* of a signal model is given by:

$$\begin{aligned} p(m^2, \{\theta\}|\mathcal{D}) &\equiv \frac{\mathcal{L}(m^2, \{\theta\}; \mathcal{D})p(m^2)p(\{\theta\})}{p(\mathcal{D})}, \\ p(m^2, \{\theta\}|\mathcal{D}) &= \mathcal{N}^{-1} \mathcal{L}(m^2, \{\theta\}; \mathcal{D})p(m^2). \end{aligned} \quad (4.4)$$

In the last equation the *evidence*, $p(\mathcal{D})$, which does not depend on the parameters of the model $\{\theta\}$, has been absorbed in a normalization constant \mathcal{N} . Flat prior

probabilities for the model parameters $p(\{\theta\}) = \text{const.}$ (as it is often the case) can also be absorbed in the normalization.

The choice of some suitable form for the prior probability for m_ν^2 is more subtle. We have used for simplicity a step function $p(m^2) = \Theta(m^2) = 1, (0)$ for $m^2 \geq 0, (< 0)$ to exclude unphysical values of the neutrino mass. It must be noticed however that this is not the better way to describe our present knowledge about neutrino mass, since a prior probability flat on m_ν^2 implies an uneven prior probability on m . We will discuss later in sect. 5.4 how the choice of other priors can affect the results of the analysis.

The posterior probability in eq. (4.4) corresponds to the joint probability of the emission model characterized by the set of parameters $\{\theta\}$ and a given neutrino mass. However, here we are just interested on what the signal could tell us about the mass and then we need the posterior probability just for this quantity. Bayesian statistics provides a natural way to *marginalize* the *nuisance parameters* (the emission model parameters $\{\theta\}$) by integrating them out

$$\begin{aligned} p(m_\nu^2|\mathcal{D}) &= \int d\{\theta\} p(m^2, \{\theta\}|\mathcal{D}), \\ p(m_\nu^2|\mathcal{D}) &= \mathcal{N}^{-1} \Theta(m^2) \int d\{\theta\} \mathcal{L}(m_\nu^2, \{\theta\}; \mathcal{D}). \end{aligned} \quad (4.5)$$

Our final goal will be to compute $p(m_\nu^2|\mathcal{D})$ and to derive from it all the possible probabilistic informations contained in the signal.

All methods to constrain the neutrino mass using a supernova signal are directly sensitive to m_ν^2 . However it is common to search for a way to express the limits on m_ν^2 as limits on m_ν . In our case that translation is natural since knowing the pdf for m_ν^2 , to write down the pdf for m_ν requires only a variable transformation. The posterior pdf for m_ν reads:

$$p(m|\mathcal{D}) = 2|m|p(m^2|\mathcal{D}) \quad (4.6)$$

4.4.3 Best-fit value and neutrino mass limits

Once the posterior pdf for m_ν^2 and m_ν are computed it is possible to derive probabilistic statements about the neutrino mass. There are three pieces of information which can be obtained.

Firstly the LF alone could provide the best-fit values for m_ν^2 and for the parameters

of the emission model (the ones that maximize the likelihood). This *Maximum Likelihood* (ML) analysis gives us the most probable value m_{fit}^2 and its error, compatible with the neutrino signal, but conditioned to the specific set of best-fit values $\{\theta_{\text{fit}}\}$ of the model parameters.

For practical reasons in the ML analysis the logarithm of the likelihood function, the *log-likelihood function* (log-LF) is used. Using eq. (4.2) the log-LF reads

$$\begin{aligned}\log \mathcal{L} &= \sum_i \log f(E_i, t_i; \{\theta\}) \\ &= \sum_i \log [\phi(t_i) \times F(E_i; t_i) \times \sigma(E_i)] - \log \mathcal{N}.\end{aligned}\quad (4.7)$$

It is the maximum of the posterior pdf $p(m_{\nu}^2 | \mathcal{D})$ which actually provide us with the most probable neutrino mass, irrespective of the value of the model parameters and taking into account all the prior information.

The most useful information about the mass is obtained computing the *credible regions* (CR) that are the range where the neutrino mass lies with a certain probability.

For our purposes we will use three CR that respectively give us the lower and upper limits in m_{ν}^2 , and an upperbound on m_{ν} .

Upper and lower limits for m_{ν}^2 . The upper and lower limit on m_{ν}^2 is obtained requiring that

$$\int_{-\infty}^{m_{\text{up}}^2} p(m_{\nu}^2 | D) \, dm_{\nu}^2 = CR, \quad (4.8)$$

and

$$\int_{m_{\text{low}}^2}^{\infty} p(m_{\nu}^2 | D) \, dm_{\nu}^2 = CR. \quad (4.9)$$

Figure 4.3 illustrate the definition of these limits.

Upper bound for m . If the neutrino mass is too small to be discerned an upperbound on m can be obtained from its posterior pdf (4.6) requiring

$$\int_0^{m_{\text{up}}} p(m_{\nu} | D) \, dm_{\nu} = CL, \quad (4.10)$$

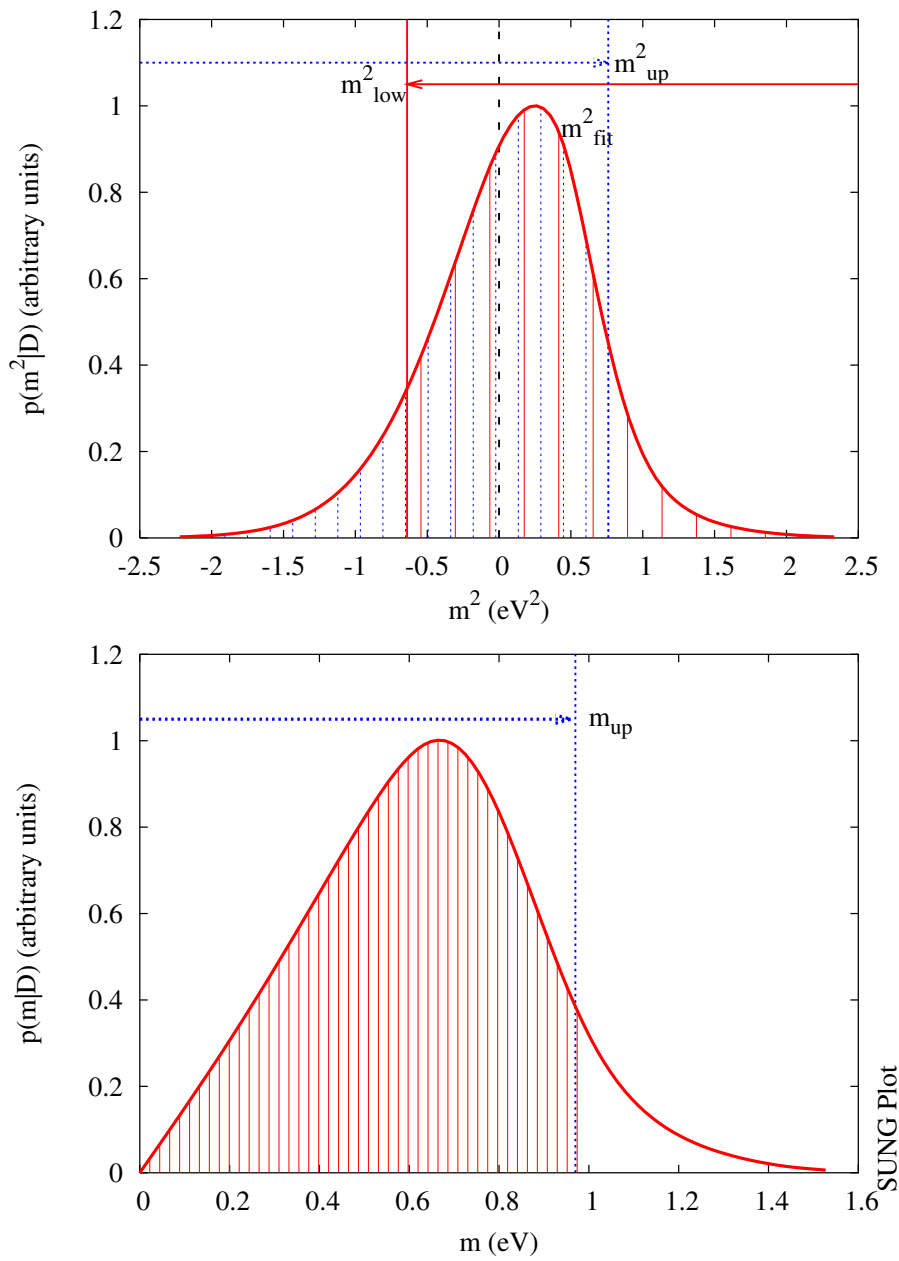


Figure 4.3: *Schematic illustration of the determination of mass limits from the posterior probabilities for m^2 (upper panel) and m_ν (lower panel).*

4.5 Construction of the Likelihood Function

To compute the LF (4.2) two basic elements are required. First, we need to deduce the time evolution of the spectral parameters from the sample in order to describe the neutrino energy spectrum at any time. Second, we have to find a suitable class of parametric analytical function $\phi(t)$ that could fit reasonably well the *detected* flux.

4.5.1 Neutrino spectrum

According to the first assumption in sect. 4.3 the spectrum can be reasonably described by a quasi-thermal (analytical) distribution. If for example a distorted Fermi-Dirac function $\sim [1 + \exp(E/T - \eta)]^{-1}$ is used, as was done in ref. [83], F can be parameterized in terms of a time dependent effective temperature T and degeneracy parameter η describing the spectral distortions. According to the second assumption, the time dependence of the relevant spectral parameters can be inferred directly from the data.

Here, we model the observed neutrino spectrum $F(E; t)$ by means of an α -distribution (2.7),

$$F(E, \bar{\epsilon}(t), \alpha(t)) = N(\bar{\epsilon}, \alpha) (E/\bar{\epsilon})^\alpha e^{-(\alpha+1)E/\bar{\epsilon}}, \quad (4.11)$$

where $\epsilon(t)$ and $\alpha(t)$ describe the evolution in time of the spectrum.

The choice of this distribution to fit the observed neutrino spectrum instead of the physically better motivated Fermi-Dirac, obeys similar reasons than those presented in sect. 2.2.3. Starting from a discrete sample of neutrinos, a Fermi-Dirac spectrum can be reconstructed only by carrying out numerical fits to the energy momenta until the correct values of T and η are determined through a minimization procedure. In contrast, the α -distribution can be straightforwardly determined through the simple analytical relations (2.8) connecting the spectral parameters and the two first momenta of the energy distribution.

Since the effect of the detection cross-section (see sec. 3.2.1) modifies the measured energy distribution, we need to find a way to reconstruct the energy momenta of the emitted distribution from the set of observed energies.

If we call $F_e(E)$ the energy spectrum at the source (where for simplicity we have dropped the temporal dependence) and $F_d(E)$ the (unknown) observed neutrino spectrum, $F_d(E) = F_e(E) \times \sigma(E)$, the $n^t h$ -momentum of F_e is given by:

$$\begin{aligned}\overline{E^n} &\equiv \frac{\int_0^\infty dE E^n F_e(E)}{\int_0^\infty dE F_e(E)} \\ &= \frac{\int_0^\infty dE E^n F_d(E)/\sigma(E)}{\int_0^\infty dE F_d(E)/\sigma(E)}.\end{aligned}$$

The last relation allows us to define the new *cross-section weighted* momenta:

$$\langle E^n \rangle \simeq \frac{\sum E_i^n / \sigma(E_i)}{\sum 1 / \sigma(E_i)}. \quad (4.12)$$

This weighted momenta provide us an estimate of the momenta of the emitted energy spectrum and allows us to find the spectral parameters around a given time. So, in order to obtain the spectral evolution, we slice the sample in many time windows and find the values of α and ϵ inside them.

A couple of words about the procedure of signal slicing procedure are necessary to explain in more details how the functions giving the spectral parameters evolution are constructed.

Any slicing procedure faces the effects of statistical fluctuations. In our case these fluctuations come from the limited statistics on each window and from the fact that neutrinos from different times and with different spectral temperatures at the source could be mixed up inside a single window.

To reduce statistical fluctuations in the spectral parameters estimation the construction of the time windows and the processing of the resulting information has been performed in the following way:

1. The width of each window is chosen large enough to contain a sufficient number of neutrinos (a few hundreds). This reduces the statistical uncertainties coming from finite statistics effects.
2. Time windows are overlapped: the central value of each new window is determined as $t_{n+1} = t_n + \delta t$, with $\delta t \ll \Delta t_{\text{t.of.}}$. Therefore many neutrinos of neighbor windows will be contained on each window and averaging the resulting fluctuations will produce smooth estimates for the spectral parameters (see fig. 4.4).
3. Once the spectral parameters in each window have been estimated their values are smoothed to wash-out the statistical fluctuations and the effect of neighbors.

4. The time variation of α and ϵ is finally fitted with a non-linear least-square analysis.

A schematic illustration of the above procedure is depicted in fig. 4.4.

In figure 4.5 we compare the estimation of the spectral parameters with the described procedure, for a set of synthetic supernova signals and the real values of those parameters used to generate the samples.

4.5.2 Detection cross-section

Also for the analysis we have used the accurate parameterization presented in sec. 3.2.1. This is the same cross-section used to generate the signals.

4.5.3 Flux model

Coming back to the problem of constructing the Likelihood function, and in particular of choosing a specific time profile for the neutrino flux (namely the model \mathcal{M}) we have proceeded according to the following requirements:

1. the analytical flux function must go to zero at the origin and at infinity
2. it must contain at least two time scales: the initial, fast rising phase of shock-wave breakout, and the later Kelvin-Helmholtz cooling phase. Another parameter could be required to describe the accretion phase, i.e. the transition point between these extreme phases.
3. it must contain the minimum possible number of free parameters to avoid degenerate directions in parameter space and to speed up the Maximum Likelihood analysis. Still, it must be sufficiently ‘adaptive’ to fit in a satisfactory way the numerical flux profiles resulting from different SN simulations, as well as flavor mixed profiles as would result from neutrino oscillations (see section 3.1).

In order to test how much our results on the neutrino mass will depend on the specific flux profile, we have performed several tests using two different flux models constructed following the above criteria (results are described in sect. 5.2.2).

In the following paragraphs we will describe some of the main properties of these two general fluxes.

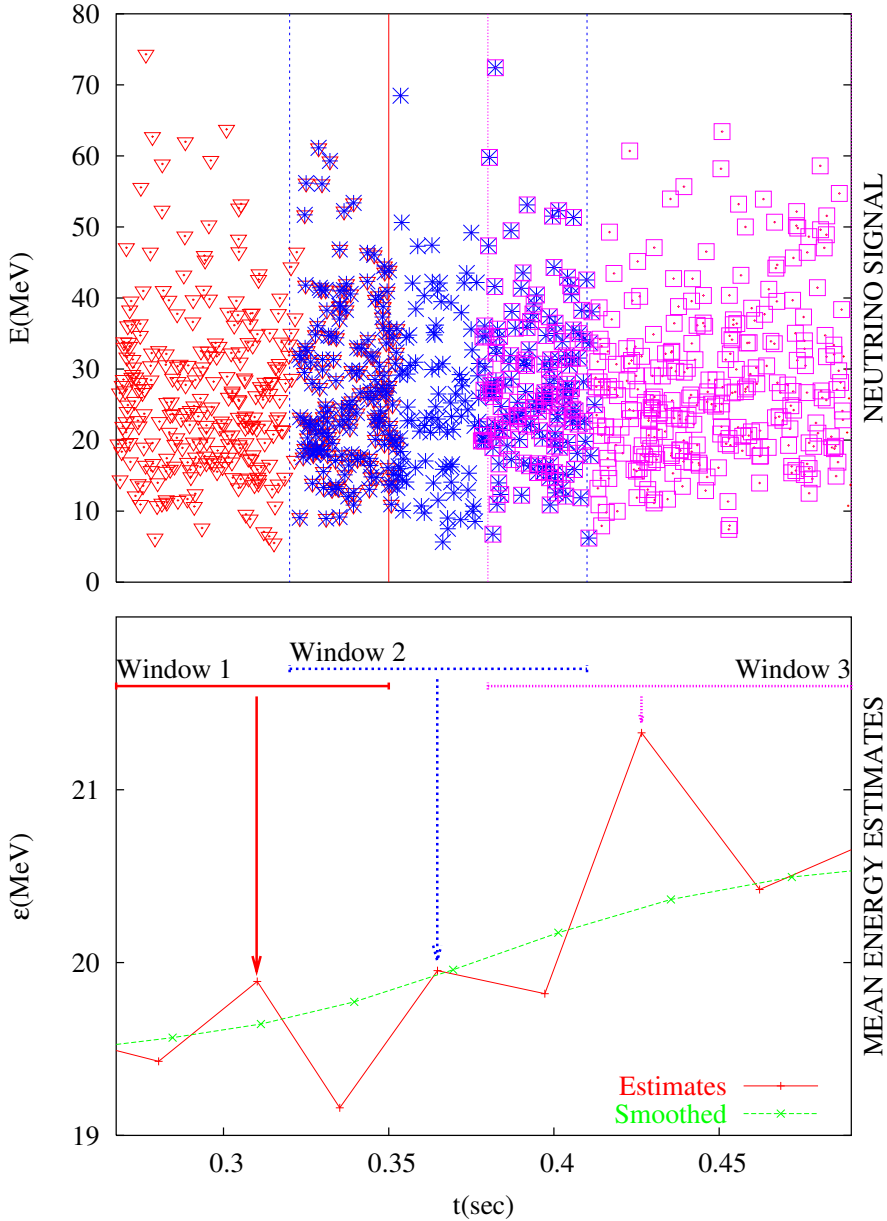


Figure 4.4: *Schematic illustration of the spectral parameter estimation using overlapped time windows. The signal (upper panel) is sliced in overlapped time windows with enough statistics (different points belong to three selected time windows). The emitted spectral mean energy ϵ is estimated using the cross-section weighted momenta of the events contained on each window. The result is the polygonal line in the lower panel. The final values used as parameter ϵ in the analysis are the smoothed values of the dotted line.*

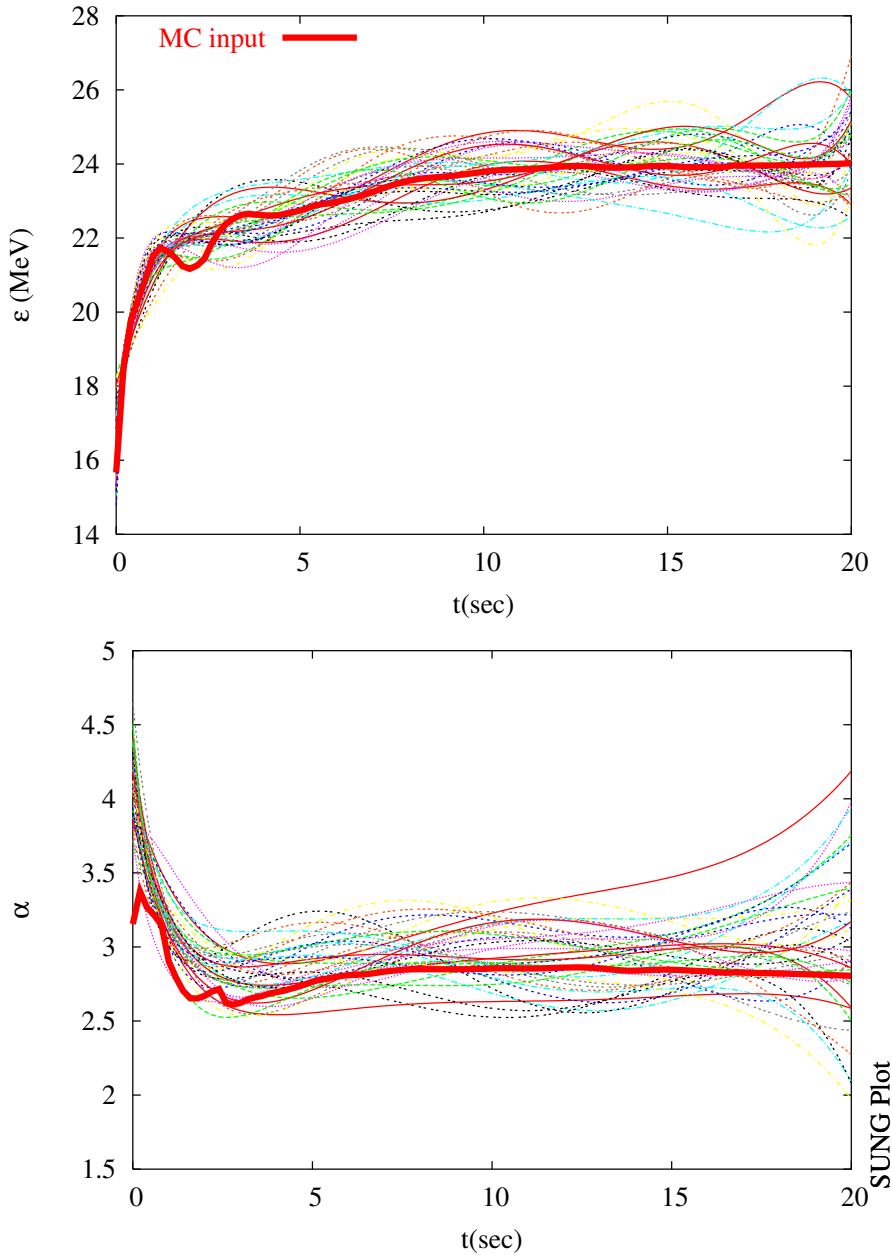


Figure 4.5: *Results of the spectral parameters estimation for 40 synthetic signals. Upper panel (lower panel): spectral mean energy ϵ (spectral pinching α), estimated from the sample with the procedure described in the text (oscillatory curves). Continuous line represent the expected value after the mixing of $\bar{\nu}_e$ and $\bar{\nu}_x$ fluxes due to oscillations in the SN mantle. The acceptable level of agreement confirms the validity of the procedure.*

Flux model I: exponential rising and power-law decay

The following model for the flux, in spite of being very simple, has all the required behaviors, and moreover it showed a remarkable level of smoothness and stability with respect to numerical “extremization” and multi-parameter integrations:

$$\phi(t; \{\theta\}) = \frac{e^{-(t_a/t)^{n_a}}}{[1 + (t/t_c)^{n_p}]^{n_c/n_p}} \sim \begin{cases} e^{-(t_a/t)^{n_a}} & (t \rightarrow 0). \\ (t_c/t)^{n_c} & (t \rightarrow \infty). \end{cases} \quad (4.13)$$

This model has five free parameters that on the l.h.s of (4.13) have been collectively denoted with $\{\theta\}$: a time scale t_a for the initial exponentially fast rising phase, a second one t_c for the power law cooling phase, two exponents n_a and n_c that control the detailed rates for these two phases, and one additional exponent n_p that mainly determines the width of the “plateau” between the two phases (see figure 4.6).

For the purposes of our numerical tests we have reduced the number of parameters to three by fixing the values of exponents $n_a = 1$ and $n_c = 8$ found with a fit of realistic time profiles. Although for each supernova model it is necessary to find the best values of these exponents, the election of these parameters will not affect too much the results of the analysis.

Flux model II: Truncated accretion and power-law decay

Here we describe a second analytical model for the evolution in time of the emitted neutrino flux that is based on the phenomenological analysis presented in sect. 2.1.4.

The analytical model in (2.4) does not fulfill all the requirements: for example, it does not include a description of the shock breakout phase and therefore, does not go to zero when $t \rightarrow 0$. To correct this we have included to (2.4) a multiplicative damping factor.

Our phenomenologically motivated flux model reads:

$$\begin{aligned} \phi(t; \{\theta\}) &= (1 - e^{-(t/t_d)^{n_d}}) \left[\frac{A e^{-(t/t_a)^{n_a}}}{(1 + t/t_b)^{n_b}} + \frac{C}{(1 + t/t_c)^{n_c}} \right], \\ &\sim \begin{cases} (t/t_d)^{n_d} & (t \rightarrow 0). \\ (t_c/t)^{n_c} & (t \rightarrow \infty). \end{cases} \end{aligned} \quad (4.14)$$

This model has 11 parameters: four time scales, t_d for the initial fast rising, t_a and t_b for the flux plateau and the early flux decay and t_c for the long term decay; four exponents, n_a to n_d which controls the rate of each component; and two amplitudes

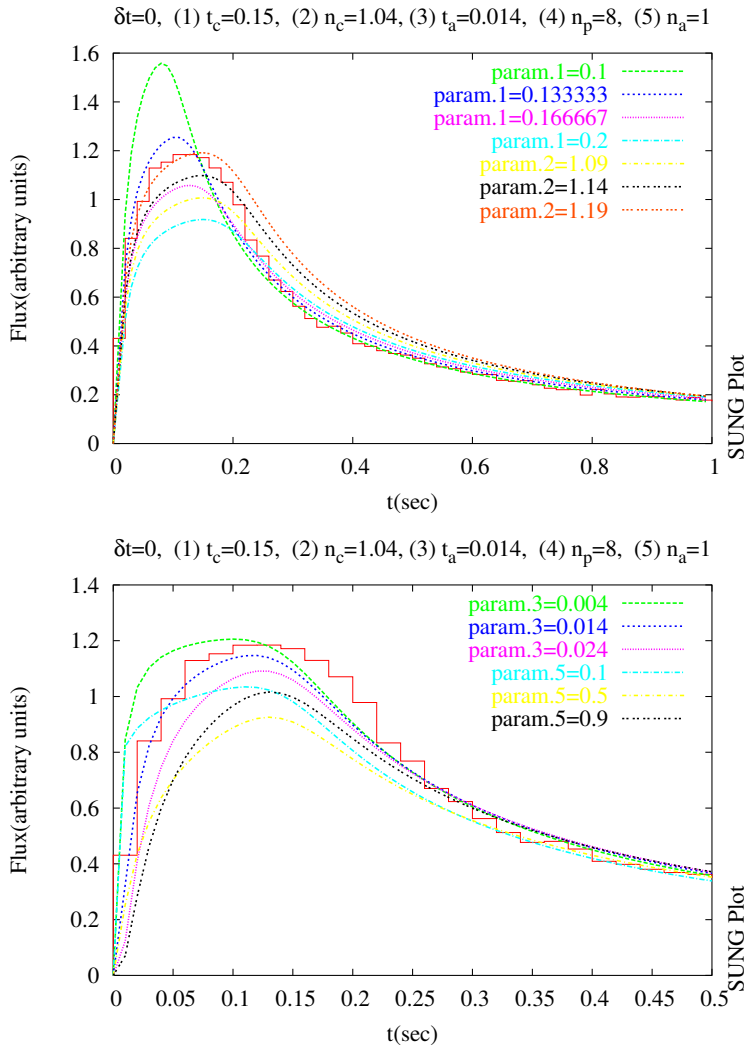


Figure 4.6: *Flux model I (4.13) and the effect of each parameter. Upper panel: the effects of parameters 1 (time scale t_c) and 2 (rate of decay n_c); as can be seen the effect of both parameters are very different and little correlation between them is expected. Lower panel: the effects of parameters 3 (time scale t_a) and 5 (rate of exponential rising n_a); also in this case little correlation is expected.*

A and C which determine the relative contribution of the accretion and cooling terms to the total flux.

As was done with the more simple flux model, we need to reduce the number of free parameters to simplify the extremization procedures. Studying the impact of each parameter (see fig. 4.7) we have determined that enough flexibility could be still obtained free just three relevant parameters: the cooling exponent n_c , and the time scales of fast rising t_d and early decay (truncated accretion) t_a . The rest of parameters could be fixed at the beginning performing a simple fit of the signal time profiles with the flux model.

In presence of neutrino oscillations the detected flux will be an admixture of $\bar{\nu}_e$ and ν_x fluxes. Since the mechanism responsible for the emission of the two species of neutrinos are different, a simple description of the resulting flux is not possible.

Given that in the Likelihood analysis we will set the origin of times in coincidence with the first neutrino detected, and this obviously cannot correspond to the origin of time of a flux function which must satisfy $\phi(0) = 0$, an additional parameter δt is needed to allow the function to shift freely along the time axis according to $\phi(t) \rightarrow \phi(t + \delta t)$.

4.5.4 LF regularization

Until now we have not discussed the role of the mass in the likelihood function.

The neutrino mass determines the value of the time shift $\Delta t = \Delta t(m_\nu^2, E, L)$ applied to the event probability (4.3) in the definition of the LF (4.2). In that sense we could think about the neutrino mass as another parameter of the pdf f .

However, in order to make more transparent the way the neutrino mass enters into the likelihood, we could treat the effect of this parameters in the following completely equivalent way. For each new value of the tested was we could think as if the sample were changed: all neutrinos are shifted to smaller times according to $\Delta t(m_\nu^2, E, L)$ and we define a new set of pairs of energies and times (E_i, t_i^{sh}) (see fig. 4.8). The LF of the emission model for this particular mass will be,

$$\mathcal{L} = \prod f(E_i, t_i^{\text{sh}}; \{\theta\}). \quad (4.15)$$

According this procedure, it is natural that some neutrinos can end up with negative values $t_i^{\text{sh}} < 0$. This effect would induce a compensation through a time shift of the flux model. The procedure is illustrated schematically in figure 4.8.

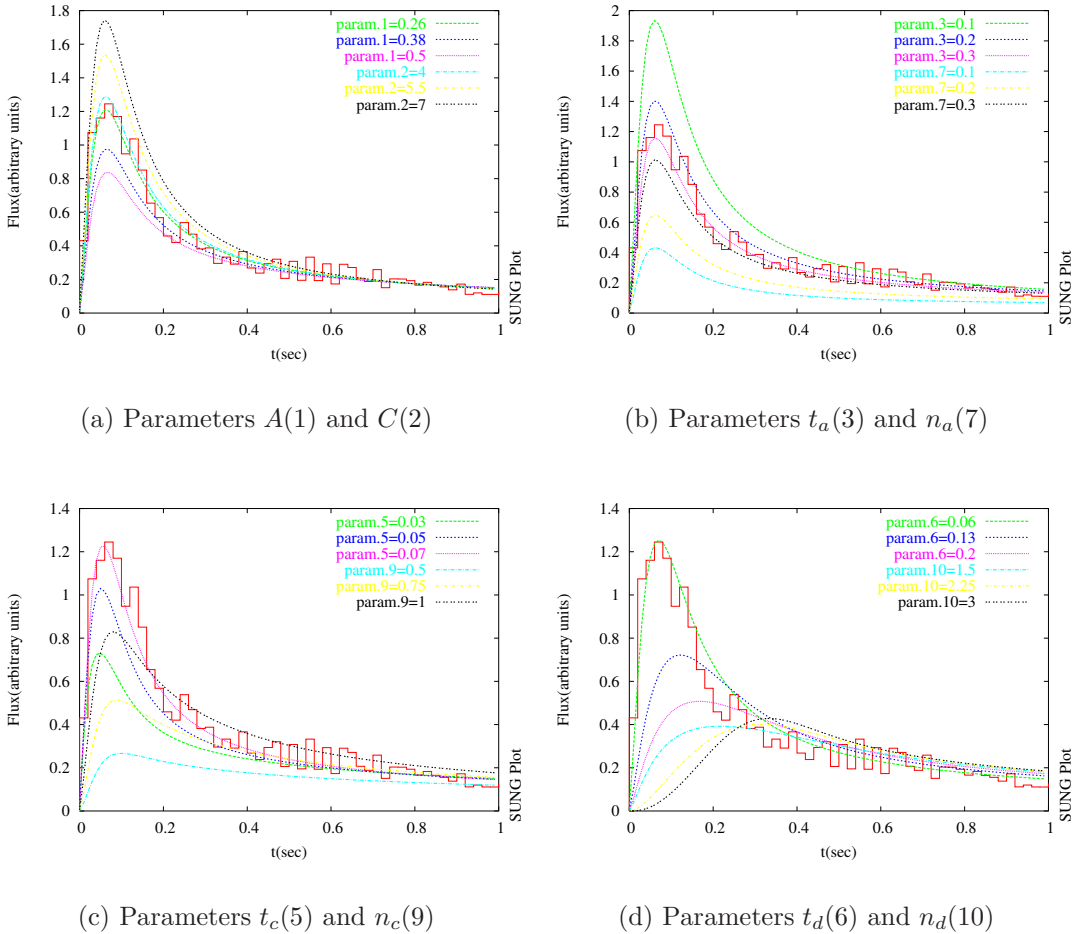


Figure 4.7: Behavior of the flux model II in eq. (4.15) under changes in its parameters. We start with the reference set of parameter values: (1) $A = 0.2$, (2) $C = 1.5$, (3) $t_a = 0.2$, (4) $t_b = 300$, (5) $t_c = 0.1$, (6) $t_d = 0.05$, (7) $n_a = 0.3$, (8) $n_b = 0.4$, (9) $n_c = 2.0$ and (10) $n_d = 1.5$. In each panel a pair of parameters are studied. As can be seen in panels 4.7a,b,c the parameters A , C , t_a , n_a and t_c have similar overall effect on the flux shape. To avoid correlations we have left free just one of them (t_a). On the other hand n_c , t_d and n_d determine different behaviors and therefore are all left free.

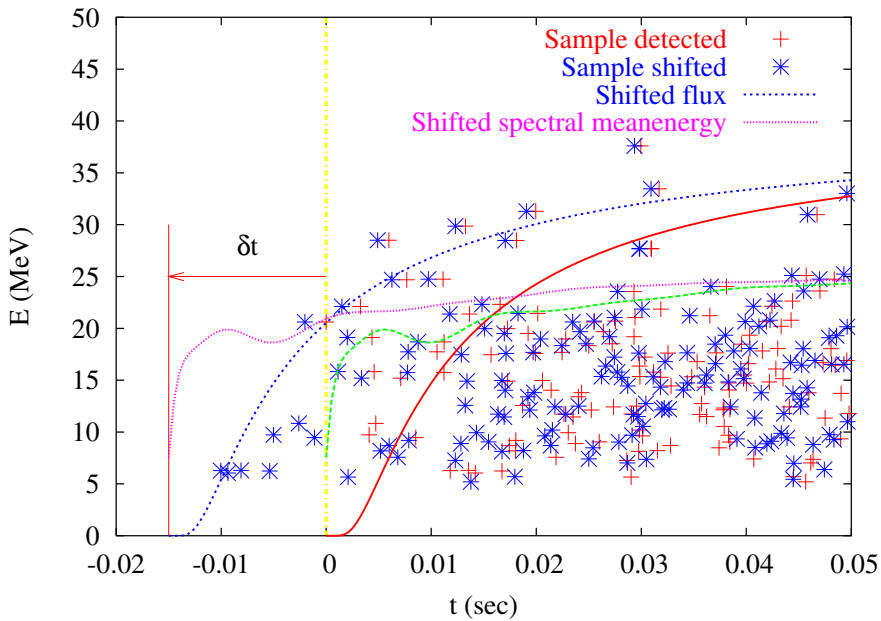


Figure 4.8: *Schematic illustration of the two-step process used to evaluate the likelihood function of a given model. Given a test neutrino mass a new sample (asterisks) is constructed shifting the times of all the events. The LF is computed by calculating the probability f of the events in the shifted sample, by applying a global shift to the flux model and spectral parameters (curves).*

Because of the finite energy resolution of any detector, the *measured* neutrino energies that are used to evaluate the time shifts for neutrinos in the sample do not correspond to the *true* energies that determine the real neutrino delays. Therefore, even when the correct value of the test mass is used, the time-shifted neutrino sample will not correspond exactly to the sample originally emitted. Although completely natural (as well as unavoidable), this behavior can produce a dangerous situation. When the energy measurement yields a value *smaller* than the true energy, a neutrino arrival time can be shifted to negative values where the flux function, even with a non-zero time shift, vanishes, implying that the log-Likelihood diverges. This would imply rejecting the particular neutrino mass value for which the divergence is produced, regardless of the fact that it could actually be close to the true value. Figure 4.9 illustrates this point.

To correct this problem we have adopted the following procedure. The contribution f to the Likelihood (4.15) of a neutrino event with measured energy $E_i \pm \Delta E_i$ for which, after subtracting the delay $\delta t_i = m_\nu^2 L / 2E_i^2$, we obtain a negative value $t_i^{\text{sh}} < 0$ (or a value close to the origin of the flux function $t_i \sim -\delta t$) is computed by convolving it with a Gaussian $\mathcal{G}(t; t_i^{\text{sh}}, \sigma_i)$ centered in t_i^{sh} and with standard deviation $\sigma_i = 2 \delta t_i \Delta E_i / E_i$:

$$\tilde{f}(E, t_i^{\text{sh}}; \{\theta\}) = \int dt f(E, t; \{\theta\}) \mathcal{G}(t; t_i^{\text{sh}}, \sigma_i). \quad (4.16)$$

Clearly this regularization of the divergent contributions to the Likelihood is physically motivated by the fact that the origin of the problem is the uncertainty in the energy measurements, that translates into an uncertainty in the precise location in time of the neutrino events after the energy-dependent shifts are applied.

The regularization procedure is one of the novel features of the method proposed. Although it is not free of numerical problems (e.g. the likelihood can have discontinuities that must be corrected as illustrated in fig. 4.10), the most interesting property of this procedure is that of allowing the inclusion in the likelihood of informations about the resolution of the detector: the same event in different neutrino detectors will have a different contribution to the LF, when shifted to the *forbidden region* $t^{\text{sh}} < -\delta t$, because the width of the resolution function \mathcal{G} in (4.16) will be also different. Therefore detectors with a better energy resolution will be more sensitive to changes in the position of the events and therefore in the tested neutrino mass.

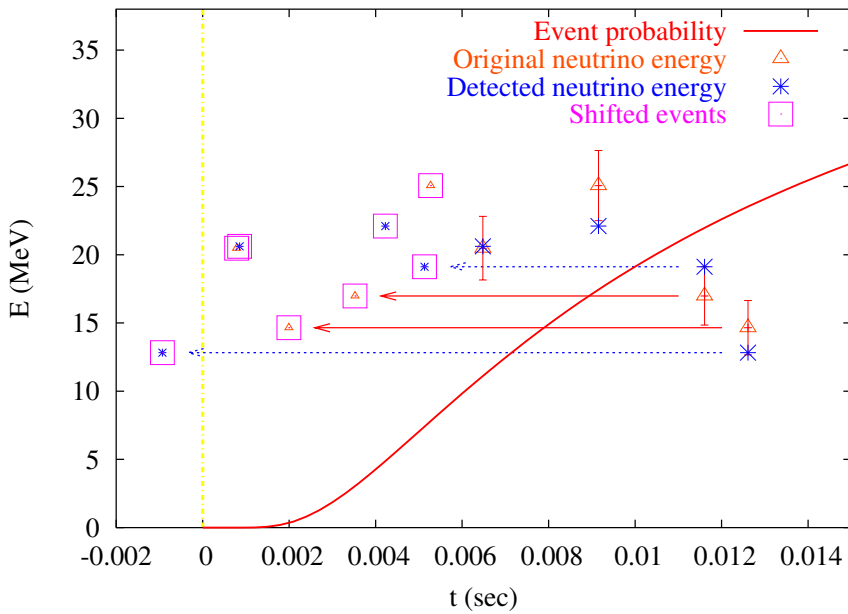


Figure 4.9: *Schematic illustration of the problem introduced because the detected neutrino energies are not the true energies, after shift according to a test mass. The asterisks represent the detected events. Triangles are at the original energy of the event. Bars indicate the size of the energy resolution of the detector (Super Kamiokande resolution is used). When shifted with a test mass the position of the detected events are different from the original positions. This is a natural result of the energy dependence of this shifts. However, when the measured energy is smaller than the original one, as in the lowest energy event, even if a mass equal to the real neutrino mass is used, the resulting time shift could bring the event to a region where the log-LF diverges.*

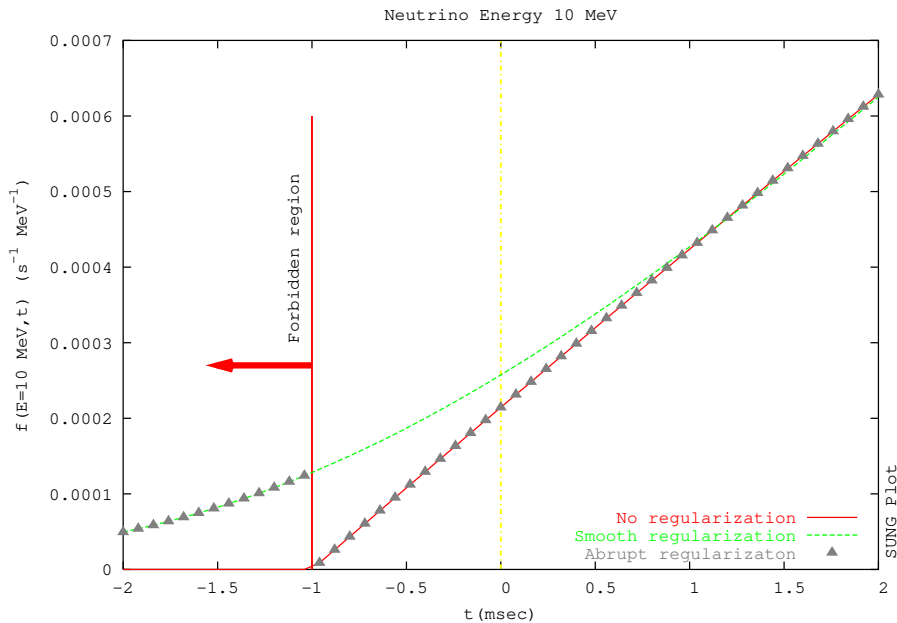


Figure 4.10: Time profile of \tilde{f} for a 10 MeV neutrino using three different schemes of regularization: no regularization at all (continuous line), regularization of events just into the forbidden region $t^{\text{sh}} < -\delta t$ (triangles) and regularization of events inside and outside (but close) the forbidden region (dashed line). The last strategy intends to avoid discontinuous changes in the likelihood produced when a single neutrino event leaves the region where f is regularized.

4.6 Likelihood marginalization

The LF alone cannot give us the information that we want about the neutrino mass without reference to the other parameters used to describe the signal. Independent probabilistic information on m_ν^2 is obtained by calculating the *posterior* pdf $p(m_\nu^2|\mathcal{D})$ that results from marginalizing the LF with respect to the nuisance (flux) parameters.

In practice, the marginalization procedure can be a very expensive numerical multidimensional integration of a particularly “heavy” function. Each evaluation of the LF for a typical signal from a future Galactic supernova could require several thousands of evaluations of relatively complex functions (flux model, spectrum and cross-section). With all these conditions it is clear that the CPU time required to carry out all the necessary operations would be exceedingly large, specially considering that to draw any statistical conclusion about the quality of our method, we need to analyze a large set of neutrino samples, corresponding to different SN models, SN-earth distances and also to different detectors.

A way to avoid this problem, is to approximate the marginal posterior probability with the *profile likelihood* (PL) $\hat{\mathcal{L}}(m_\nu^2; D)$, that corresponds to the trajectory in parameter space along which for each given value of m_ν^2 the Likelihood is maximized with respect to all the other parameters (see fig. 4.11).

It can be shown that for a multivariate Gaussian the PL coincides with the marginal posterior $p(m_\nu^2|D)$ (for details see appendix A), and therefore our results will be reliable to the extent the Likelihood approximates well enough a normal distribution. In fig. 4.12 we compare different contours in parameter space for $\log \mathcal{L}(m_\nu^2, \{\theta\}; D)$ with those of a corresponding multivariate normal distribution, with the same mean and covariances than the likelihood. We see that within the region where the contributions to the integrations are large, the behavior of the Likelihood is indeed approximately Gaussian.

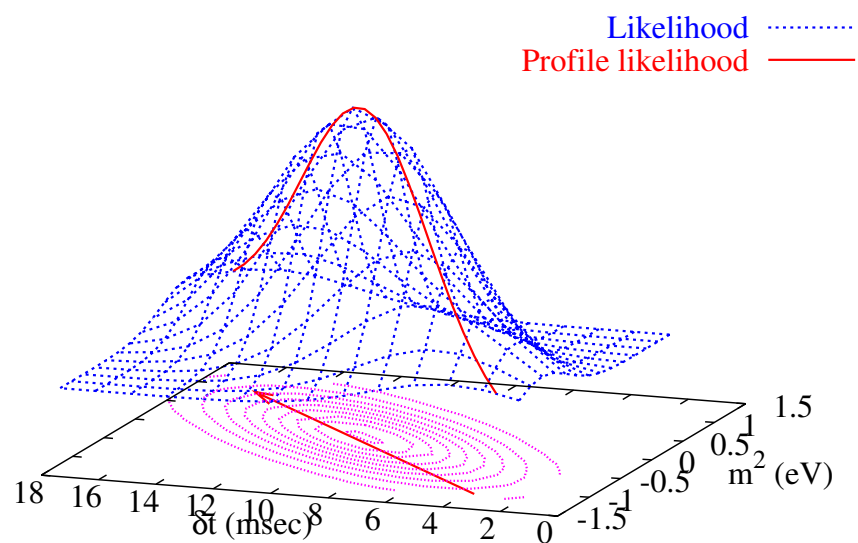


Figure 4.11: *Illustration of the profile likelihood computation for m_ν^2 .*

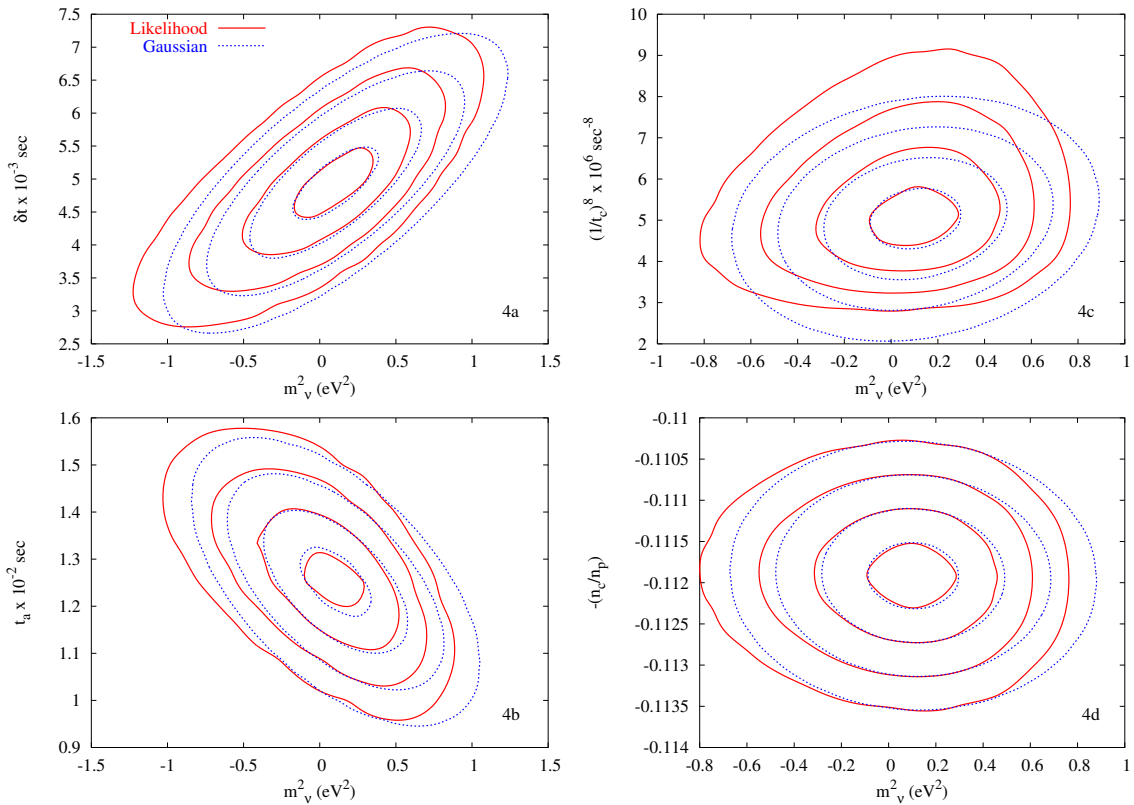


Figure 4.12: *Contours of the log-LF compared with the contours of a Gaussian distribution of the same mean and covariance in four different two parameters spaces: m_ν^2 versus 4.12a: the time shift δt of the flux function; 4.12b: the time scale of the fast initial rase t_a ($n_a = 1$); 4.12c: the time scale of the cooling phase t_c ($n_c = 8$); 4.12d: the ratio n_c/n_p (see eq. (4.13)). For the construction of this contours we have used a particular parameterization of the flux-model (4.13), the same used in ref. [83], in order to minimize correlations between parameters. The contours are plotted at 0.5, 1.0, 1.5 and 2.0 σ .*

CHAPTER **5**

Results and discussion

We present in this chapter the results of a series of tests performed to study the behavior of the method and to estimate its sensitivity to a neutrino mass.

The tests were performed with a wide range of emission (SN model), propagation (neutrino oscillations) and detection conditions, as described in sect. 5.1. The general results of the ML analysis are summarized in sect. 5.2. To quantify the sensitivity of the method we have measured two statistical properties for each set of analyses. The results of these measurements are presented and analyzed in sect. 5.3. Finally, we discuss in sect. 5.5 the implications of the results and its relevance in the context of current and future neutrino mass searches. A summary and the conclusions of this work are presented in this section.

Part of the material presented in this chapter were published in a similar form in the paper[85]

5.1 Description of tests

In the absence of a real high statistics supernova signal, we can only test our method applying it to realistic *synthetic* signals generated with the methods described in chapter 3. However of course we cannot derive any general and reliable conclusion from the analysis of a single signal and just one particular emission model and supernova set of properties.

In order to have an overall understanding of what to expect if our method could be applied to a real signal, we have carried out a Monte Carlo (MC) analysis using many synthetic signals, that were generated under a wide range of conditions for the

emission (SN fluxes and spectra, SN distance), propagation (oscillations and TOF delays) and neutrino detection (number of events, energy resolution and energy thresholds).

We divide our MC analysis in a set of different *tests*. For each test we applied the method to a sample of ~ 40 synthetic signals each one generated with the same set of input conditions (we can imagine the samples conforming one test, as a set of many realizations of the same supernova, detected with the same detector).

The input conditions considered to construct the whole set of tests were:

- **Neutrino emission.** Two different supernova models were used:

the first model (*supernova model I*) corresponds to the results of a simulation of the core collapse of a $20 M_{\odot}$ star which was performed with the code developed by the Lawrence Livermore Laboratory group [86]. These results were used to study supernova r-processes [60]. Figure 5.1a depicts the neutrino luminosity and mean energy evolution obtained in this simulation. This model is characterized by large spectral differences between electron and non-electron neutrino species, which, as explained in sect. 2.3, is a result of the approximate description of the ν_x transport in the SN core.

Neutrino spectra and their evolution were not published in the original paper by Woosley et al. [60]. We have therefore used the spectral shapes taken from the dedicated study of Janka and Hillebrandt [87] and we have assumed for simplicity that the α -parameter, which quantify the spectral distortions, remains constant during the emission. We have used the standard values $\alpha_{\bar{\nu}_e} = 3.5$ and $\alpha_{\nu_x} = 3.0$ for this quantity.

The second model (*supernova model II*) correspond to the recent state-of-the-art hydrodynamical simulation of the core collapse of $15 M_{\odot}$ progenitor star [3, 61] carried out by means of the Garching group code [88, 89, 90]. This simulation included a more complete treatment of neutrino opacities [91, 63, 3], that resulted in smaller spectral differences between $\bar{\nu}_e$, ν_e and ν_x (see fig. 5.1a).

The Garching group simulations were stopped after 750 msec, and the results were not completely reliable already after the firsts 300 msec [61]. Since our study assumes a signal time duration of 20 sec, after which the neutrino flux is assumed to become undetectable, we have done a conservative extrapolation of the signal to later times. For the luminosities we have assumed a power law decay in agreement with general results of SN simulations [56, 84, 60, 3] while for the mean energies we have assumed a mild decrease and a constant pinching after 750 msec.

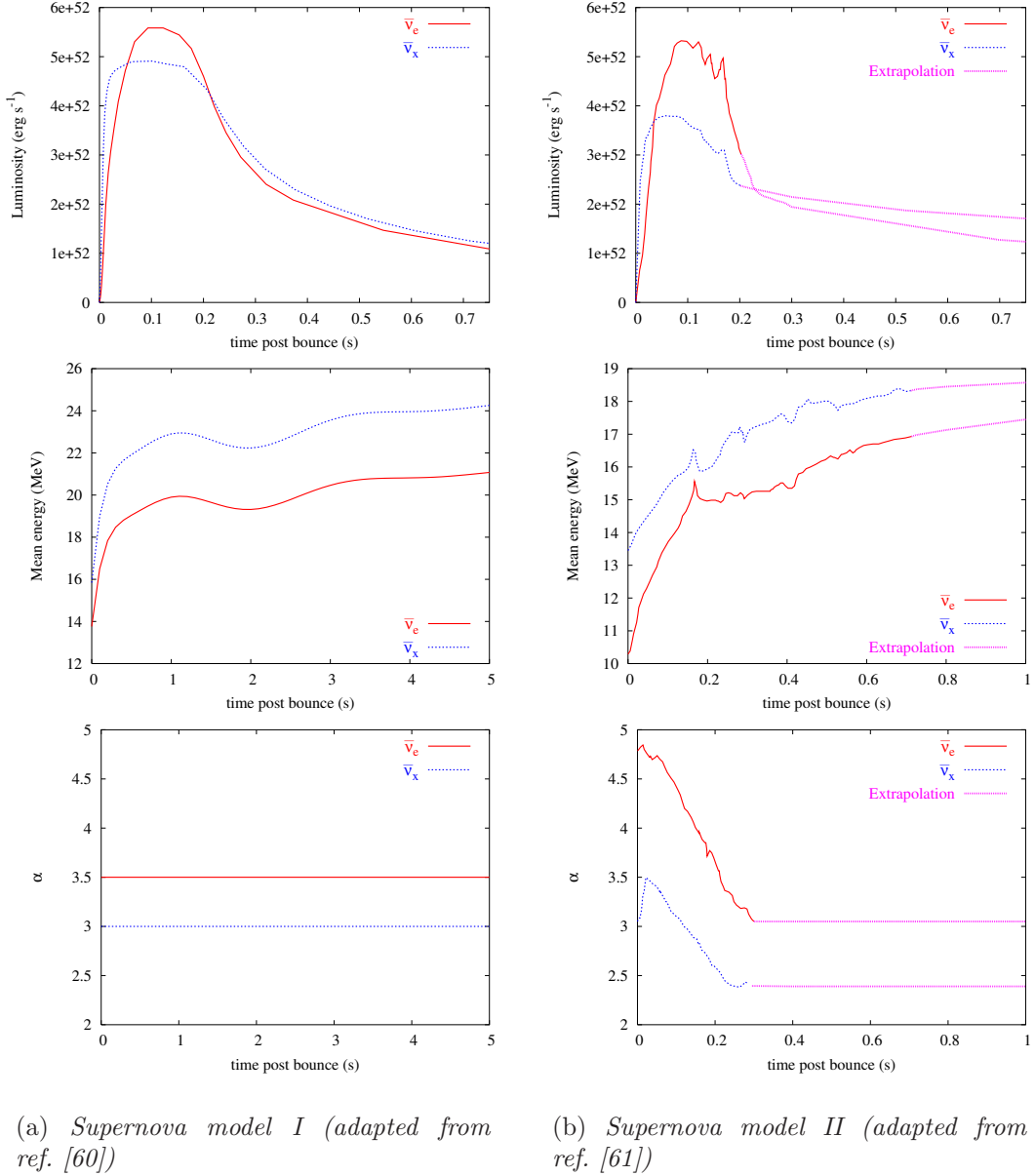


Figure 5.1: Luminosity, mean energy and α -parameter for $\bar{\nu}_e$ and $\bar{\nu}_x$ in the supernova models used in this work to generate the synthetic signals.

We have also varied SN-earth distance into the representative values 5, 10, and 15 Kpc.

- **Neutrino oscillations.** To perform the MC analyses we used an oscillation scheme with a normal mass hierarchy and the LMA mixing parameters set (see sect. 3.1.2). With this oscillation scheme the observed flux of $\bar{\nu}_e$ correspond to an admixture of $\approx 74\%$ $\bar{\nu}_e$ and $\approx 26\%$ $\bar{\nu}_x$.

The case of a complete swap $\bar{\nu}_x \leftrightarrow \bar{\nu}_e$ that can result from an inverted mass hierarchy and $|U_{e3}|^2 \gtrsim 10^{-3}$, can be considered equivalent to the non-oscillation case (studied in ref. [83]) with a larger average energy for $\bar{\nu}_e$. Indeed we can consider the results of the analysis performed with supernova model I as the harder spectrum version of that corresponding to supernova model II.

We do not include Earth matter effects, since they will depend on the specific position in the sky of the SN relative to the Earth, on the specific location of each detector and on the time of the day. However, given that even with a dedicated analysis it appears quite challenging to identify clearly these effects [71], we believe that this neglect is of no practical importance.

- **Detection.** As explained in the previous chapter the application of our method requires the knowledge of both energy and time of each neutrino event. On the other hand the spectral estimation procedure described in sect. 4.5 requires a large statistics of neutrinos. Electron antineutrino detection will provide by far the largest number of events from a future Galactic supernova, and therefore our analysis will be restricted to this kind of neutrinos and to detection processes capable to measure the energies and arrival times with good precision.

Today, the Super-Kamiokande (SK) detector, having the largest fiducial volume among all operative detectors, suited for the kind of analysis we propose. Operative scintillator detectors are characterized by a lower threshold and/or better energy resolution, which in principle represents an advantage in the analysis. However, their significantly smaller fiducial volume imply the possibility of detecting only a few hundred of $\bar{\nu}_e$ events (see tab. 3.2). Such a low statistics is not well suited for the application of our method. However, since KamLAND (KL) is located at the same site as SK (and equally affected by neutrino oscillations in the Earth) KL events can be the high statistics of SK, possibly yielding some sensitivity improvement. We have performed this kind of joint analysis to study the impact of the addition of KL events to the SK signal.

For the future large volume detectors we have chosen two of the most interesting proposals: Hyper-Kamiokande [92] (a megaton water Čerenkov detector) and the multi-kiloton scintillator detector LENA (Low Energy Neutrino Astrophysics) [93].

The properties of all the detectors used in the MC analysis are summarized in tab. 3.2 in sect. 3.3.

The following table defines the set of labels that will be used hereafter to identify the different tests of the method and their particular input conditions:

Label	Supernova model	Detector(s)	Distance (kpc)	Flux model
TSNI-1	model I	SK	10	model I
TSNI-2	—	—	—	model II
TSNI-3	—	—	5	model I
TSNI-4	—	—	15	—
TSNI-5	—	SK + KL	10	—
TSNI-6	—	LENA	—	—
TSNI-7	—	HK	—	—
TSNI-8	—	HK	—	model II
TSNII-1	model II	SK	10	model II
TSNII-2	—	—	—	model I
TSNII-3	—	—	5	model II
TSNII-4	—	—	15	—
TSNII-5	—	SK + KL	10	—
TSNII-6	—	LENA	—	—
TSNII-7	—	HK	—	—

In the last column of the table we have indicated what flux model (model I (4.13), model II (4.15) was used to compute the signal pdf (4.3).

For the signals generated with supernova model II we have mainly used the more flexible flux model II. The analysis with such a flux in the case of supernova model I does not show any relevant difference with respect to the simple flux model I.

5.2 Results of the maximum likelihood analysis

To illustrate some of the most interesting properties of the method and before proceeding with the estimation of its sensitivity, we performed a set of MC analyses

using an hypothetical MC neutrino mass $m_\nu = 1$ eV.

Several interesting facts about the behavior of the method could be observed when the output of the ML analysis, namely the best-fit values of mass and flux parameters, are studied. In the following two sections we describe these results.

5.2.1 Best-fit values and limits on m_ν^2

The best-fit values for m_ν^2 and its limits are summarized graphically in the *band-plots* presented in figs. 5.2-5.5.

All the signals on a band plot were generated under the same set of input conditions. The squares indicates the position of the best fit value m_{fit}^2 and the “error bars” correspond to the lower and upper limits computed from the posterior pdf $p(m_\nu^2 | \mathcal{D})$ using (4.9) and (4.8).

Some of the analysis have exceedingly large error bars when compared with the rest of analysis in the same set. In most of the cases they correspond to badly behaved analysis, where the extremization procedures used to compute the profile likelihood found peculiar directions in parameters space corresponding to large correlations between the mass and the flux parameters. In a few cases such “failures” can be caused by just one or two neutrinos that randomly get abnormal values of their energy. Exclusion of these neutrinos can generally rescue a well behaved analysis.

The first remarkable fact is that regardless of the wide range of input conditions (supernova emission model, particular detector, flux model used to analyze the samples) in almost all cases the average value of m_ν^2 is close to the MC mass used to generate the signals. This is a clear indication that the signal can act as a self timing observable and that no particular assumption on the signal time structure is needed to measure the value of the mass. This fact represents a confirmation of our original hypothesis.

The only feature of the analysis sensible to particular input conditions is the dispersion around the best-fit values of the mass. As expected, a lower statistics increase the dispersion and reduces the sensitivity to a neutrino mass. This can partially explain the slight difference between the results for the two supernova models. Since supernova model I signals have a larger number of events than supernova model II, the dispersion is smaller for the first model. We can conclude that a harder neutrino spectrum would increase slightly the sensitivity to a neutrino mass, by increasing the statistics of the signal.

Results obtained with just SK events (TSNI-II-1) and SK+KL events (TSNI-II-5) do not exhibit any appreciable difference, meaning that the better energy resolu-

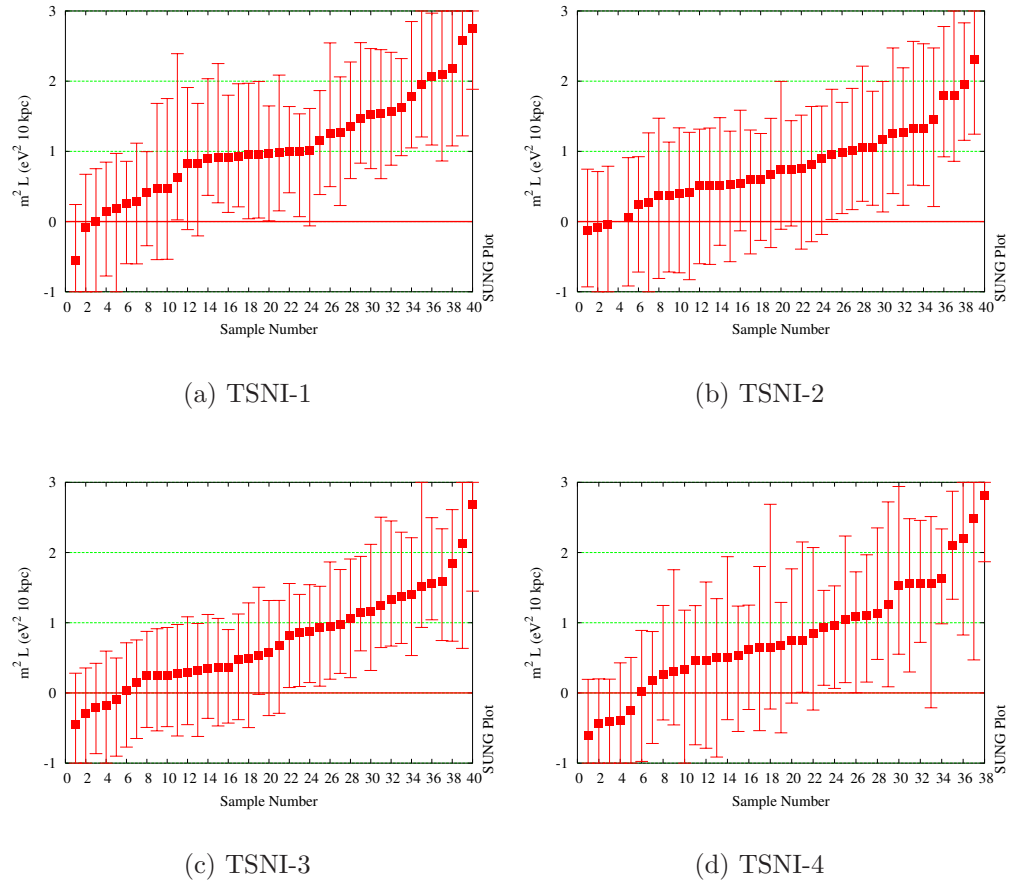


Figure 5.2: *First set of band plots for tests performed with supernova model I and $m_{\text{MC}}^2 = 1.0 \text{ eV}^2$. The best-fit values for m_ν^2 obtained from the ML analysis are represented by the filled squares. The error bars extend from m_{low}^2 to m_{up}^2 .*

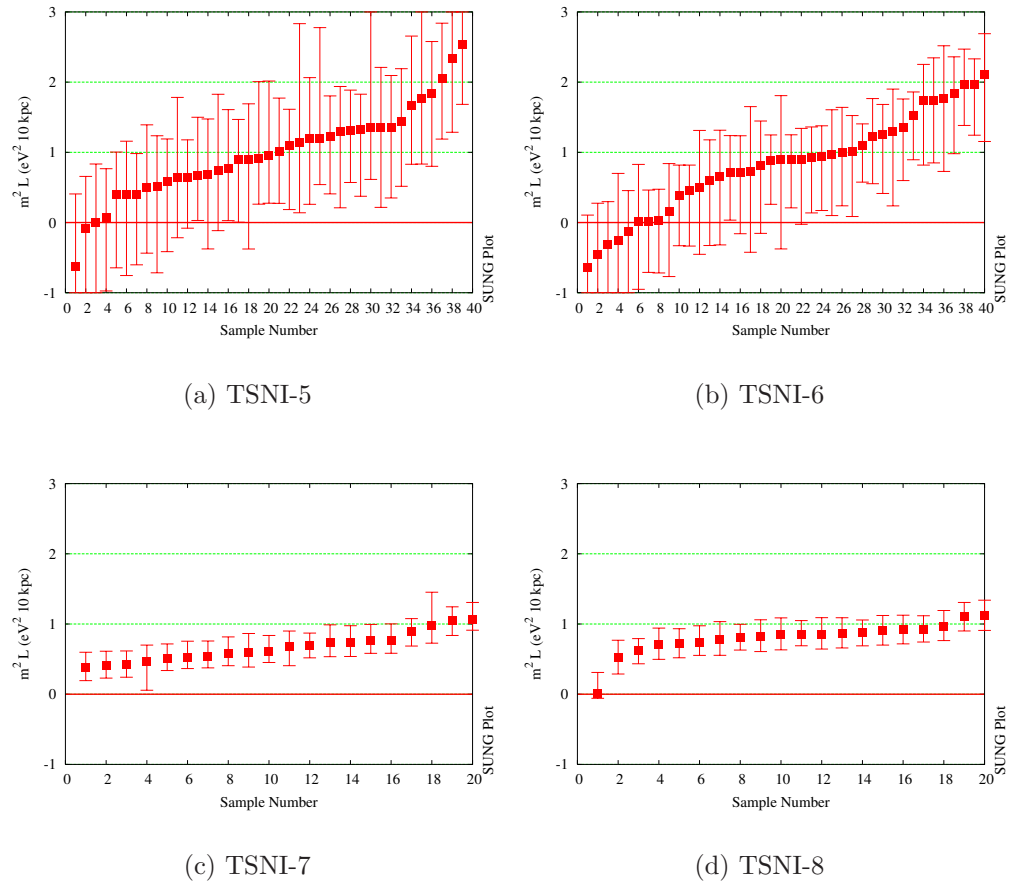


Figure 5.3: Second sets of band plots for tests performed with supernova model I.

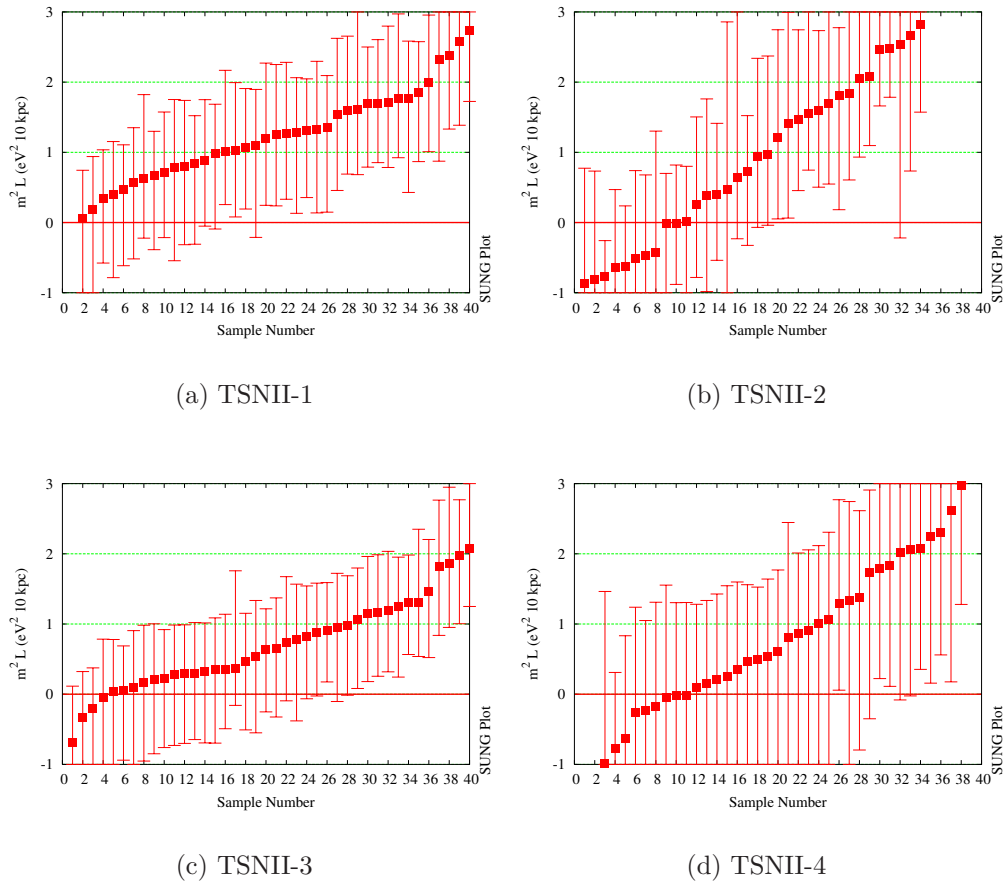


Figure 5.4: First set of band plots for tests performed with supernova model II.

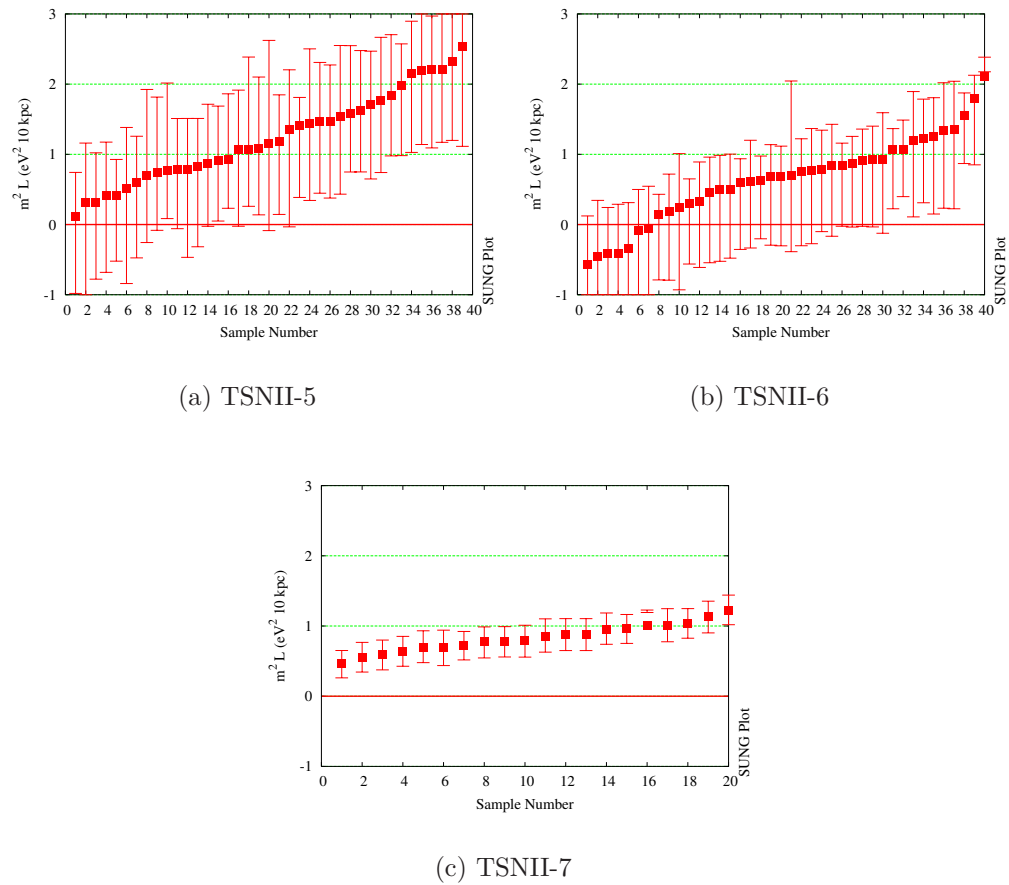


Figure 5.5: Second set of band plots for tests performed with supernova model II.

tion and lower threshold of KamLAND cannot compete with the SK much larger statistics.

A qualitative overall analysis of these results shows that sensitivities at the level of 1 eV level can be achieved with SK and future LENA detector, while the sensitivity will be improved by a factor of 2 with a future megaton water Čerenkov detector.

5.2.2 Fit to the flux model

The ML analysis of the signals described in the previous section provides in each case also a set of best-fit values of the flux model parameters. The fit to the flux model is actually of little interest for the purposes of our work, but a comparison between the results of such a fit with the input time profiles and with the histograms of the detected samples, reveals other interesting aspects of our method.

It must be realized that a direct comparison between the flux model $\phi(t)$ and the observed time profile $f_t^{\text{obs}}(t)$ cannot be performed directly. The energy-dependent detection cross-section depletes the flux at early times when the mean energy of the neutrinos is lower. The comparison must be done between the observed profile and the energy integrated time-profile given by

$$f_t^{\text{signal}}(t) \equiv \left[N^{-1} \int dE F(E; t) \sigma(E) \right] \phi(t). \quad (5.1)$$

In figures 5.6-5.7 we depict comparisons between $f_t^{\text{obs}}(t)$ and $f_t^{\text{signal}}(t)$ for several of the tests. Additionally we have included there the expected time-profile computed from the signal rate (3.41):

$$f_t^{MC}(t) \equiv n_{\text{tot}}^{-1} \int dE \frac{d^2 n_{\bar{\nu}_e}}{dt dE}, \quad (5.2)$$

The last comparison allows us to understand how well the original emitted flux can be guessed from the signal analysis.

As can be observed the analytical flux models do not fit perfectly the signal. Several fits seem actually rather poor (see for example TSNII-2). Nevertheless in almost all the cases in average the right value of the mass was obtained (see figs. 5.2-5.5). A bad fit to the flux model just increases the dispersion in the mass values, but does not change too much the best-fit point. Again, this is an indication that the right value of the neutrino mass can be measured even if the fit to the signal detailed shape is only approximate.

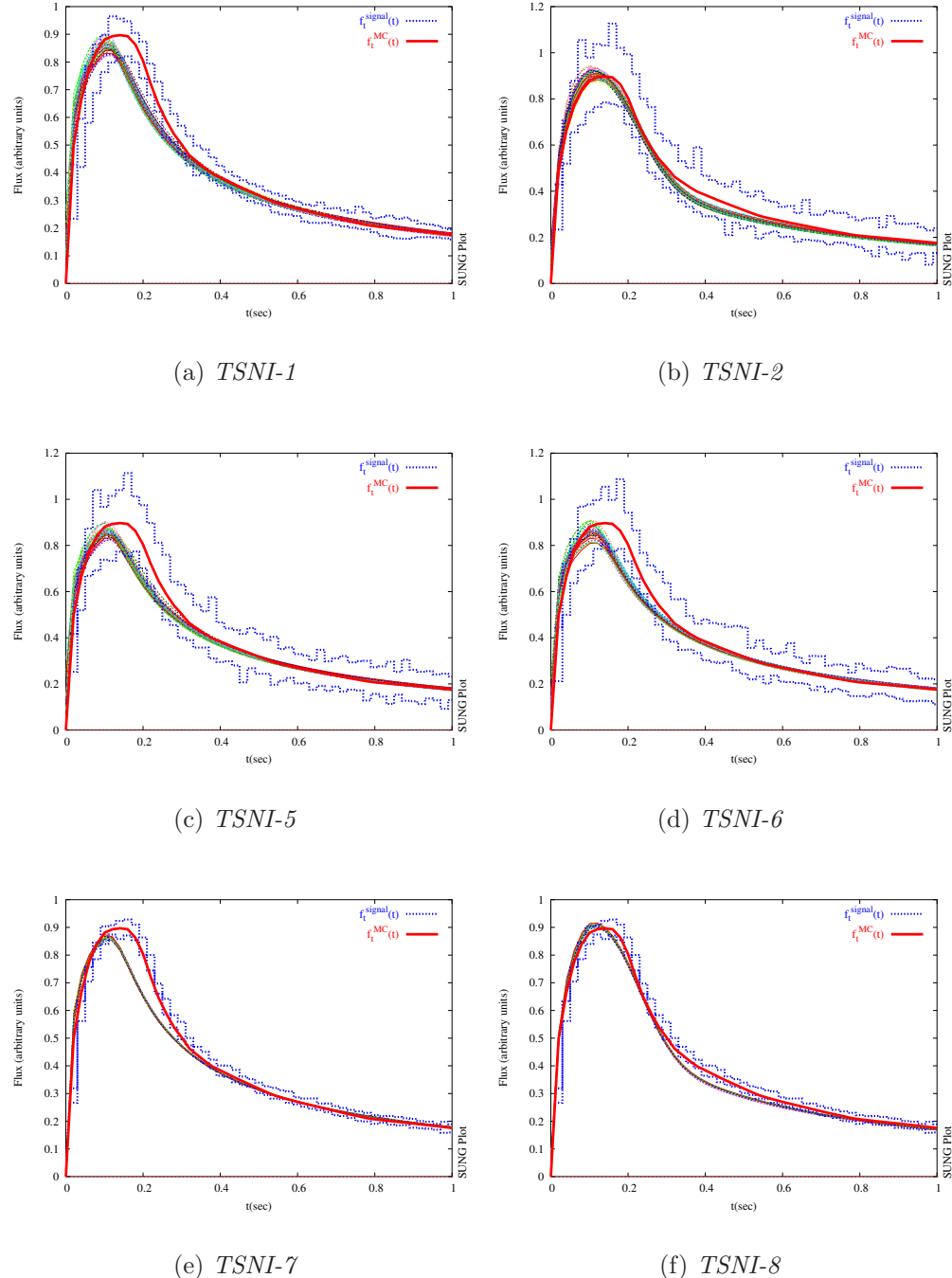


Figure 5.6: *Fits to the flux model for various sets of input conditions using supernova model I.* In each figure we compare the input time profile $f_t^{\text{MC}}(t)$ (5.2) (thick continuous line), the best-fit flux model $f_t^{\text{signal}}(t)$ for each signal (bunch of curves) and the observed time profile $f_t^{\text{obs}}(t)$ (the outer and inner histograms enclose the observed profiles for all the signals).

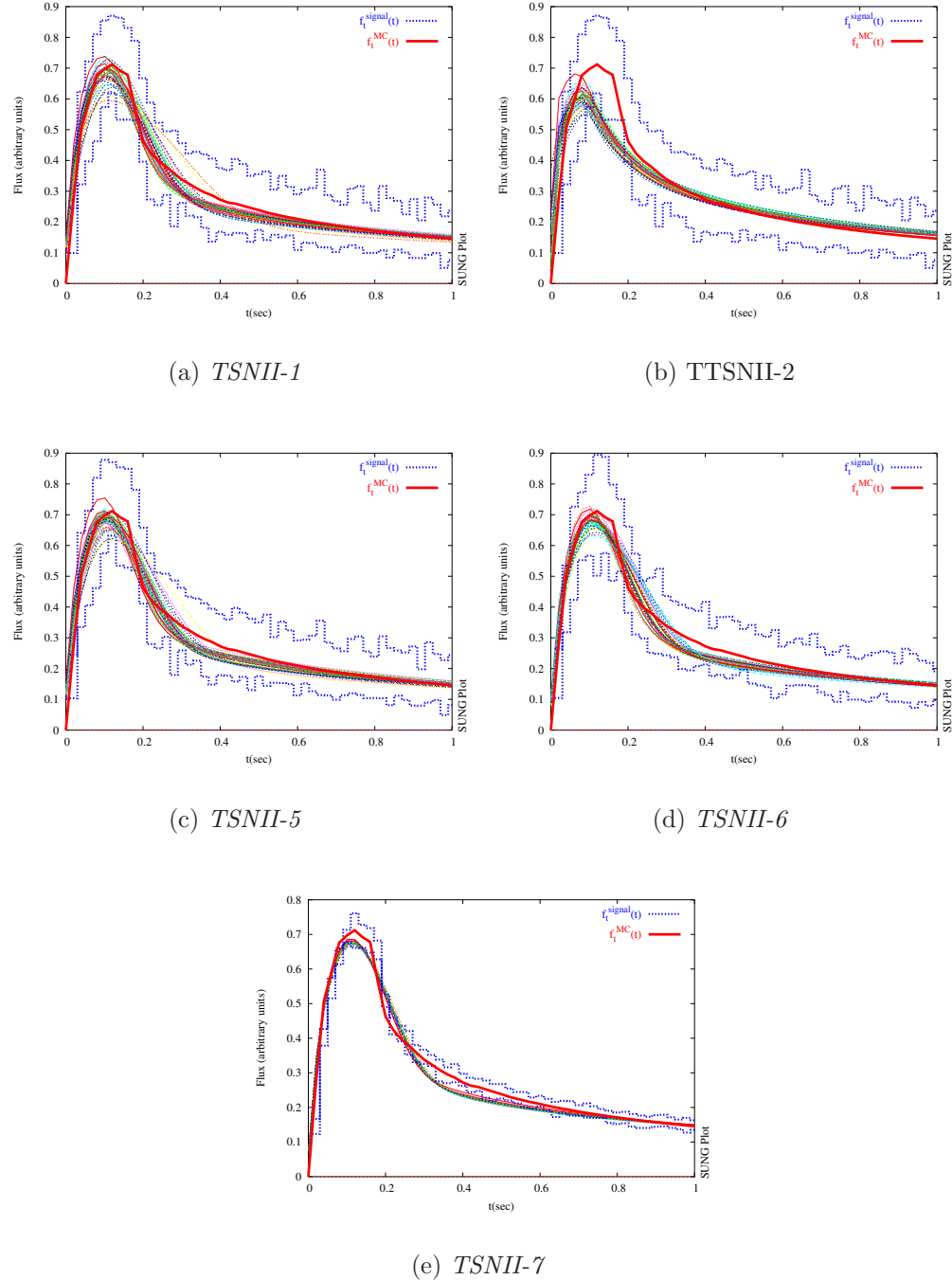


Figure 5.7: *Fits to the flux model for various sets of input conditions using supernova model II.*

The more flexible flux model II fits better the signals when supernova model II is used (compare TSNII-1 and TSNII-2). This flux model allows to describe more accurately the inflections of the flux for this model of supernova neutrino emission. The supernova model I signals are relatively well fitted by the simpler flux model I, and no significative difference in the best-fit mass can be observed with respect to flux model II.

The parts of the detected flux that are fitted better are the initial rising phase and the decay. In all cases, when the model fits properly these phases, the fit to the mass is successful.

Altogether, these evidences support the idea that the flux model fit is to a large extent uncorrelated with the neutrino mass measurement. Regardless of the availability of a good astrophysical description of the signal, the method could extract enough information on the neutrino mass from a high statistics signal under a wide range of conditions.

5.3 Quantifying the sensitivity of the method

The results presented in the previous section give us a general idea of the overall properties of our method. Now we want to put quantitative limits on how much information on the neutrino mass could be extracted from a future supernova signal.

In order to quantify the potential sensitivity of our method we have devised two different approaches:

Averaging the upper bounds. If the neutrino mass is small and the sensitivity of the method is not large enough to resolve it, the only information that we can obtain is what is the largest neutrino mass compatible with the signal. In terms of the profile likelihood $\hat{\mathcal{L}}$ the mass upperbound m_ν^{up} can be computed using the prescription (4.10):

$$\int_0^{m_\nu^{\text{up}}} p(m_\nu | \mathcal{D}) dm_\nu \simeq \int_{-\infty}^{m_\nu^{\text{up}}} 2m_\nu \hat{\mathcal{L}}(m_\nu^2 | \mathcal{D}) dm_\nu = CR. \quad (5.3)$$

We have performed a MC analysis generating ~ 40 synthetic signals per each set of input conditions and assuming a MC neutrino mass $m_\nu^{\text{MC}} \approx 0$. For each signal the mass upperbound with a 90% of probability was computed. We have used a flat prior probability for $m_\nu^2 \geq 0$ and vanishing probability for $m_\nu^2 \leq 0$.

Using these results we characterize the sensitivity of the method with two numbers: the average value \bar{m}_{up} of the upper bounds, and the dispersion Δm_{up} around this

value (see fig. 5.8). Clearly, the only meaning of these two numbers is that of identifying the possible range for the upper limits that could be obtained in a real case. In particular, Δm_{up} is given only to indicate to what extent \overline{m}_{up} is a good representative of the different results of the entire ensemble, and should *not* be understood as the error on the quoted upper limit.

Rejection of the massless neutrino hypothesis. If neutrino mass were large enough to be resolved, an alternative way to quantify the sensitivity of the method is to determine for which value of the input mass m_{ν}^{MC} the massless hypothesis can be rejected for a significative fraction of the analyzed signals.

We performed different MC analysis using several values of $m_{\nu}^{\text{MC}} > 0$. In each case for every signal we computed the lower limit using the prescription (4.9):

$$\int_{m_{\text{low}}^2}^{+\infty} p(m_{\nu}^2 | D, I) dm_{\nu}^2 \simeq \int_{m_{\text{low}}^2}^{+\infty} \hat{\mathcal{L}}(m_{\nu}^2 | D, I) dm_{\nu}^2 = CL \quad (5.4)$$

The minimum value of the input neutrino mass $m_{\nu}^{\text{MC}} = m_{\text{min}}$ for which m_{low}^2 was larger than 0 (90% CR) for more than 50% of the signals was used as a measure of the sensitivity (see fig. 5.8). In this case $\hat{\mathcal{L}}$ must be normalized over the whole interval $-\infty < m^2 < \infty$ to obtain a physically significant m_{low}^2 .

In table 5.1 we summarize the results of applying the previous procedures to quantify the sensitivity of the method.

The first thing we can deduce from the results is that the average number of events in the signals is the dominant factor. This is clearly illustrated in fig. 5.9 were we have plotted the values of \overline{m}_{up} against the average number of events. It must be noticed that the improvement in the sensitivity due to an increase in the statistics is not dramatic. Comparing the sensitivity of the method at HK with the analogous results of SK we see that an increase by a factor of 10 in the statistics improves the sensitivity only by a factor of 2.

Comparing the results of the combined analysis SK+KL (TSNI-5 and TSNII-5) with these performed on SK alone (TSNI-1 and TSNII-1) we see that sensitivity is determined by the larger statistics SK and the better energy resolution and lower threshold of KamLAND does not impact too much the result. A similar conclusion is obtained observing that the planned scintillator detector LENA presents only a minor improvement in the sensitivity with respect to SK. Even if the energy resolution is better, the comparable fiducial volumes that implies comparable number of events results in quite similar sensitivities for the two detectors.

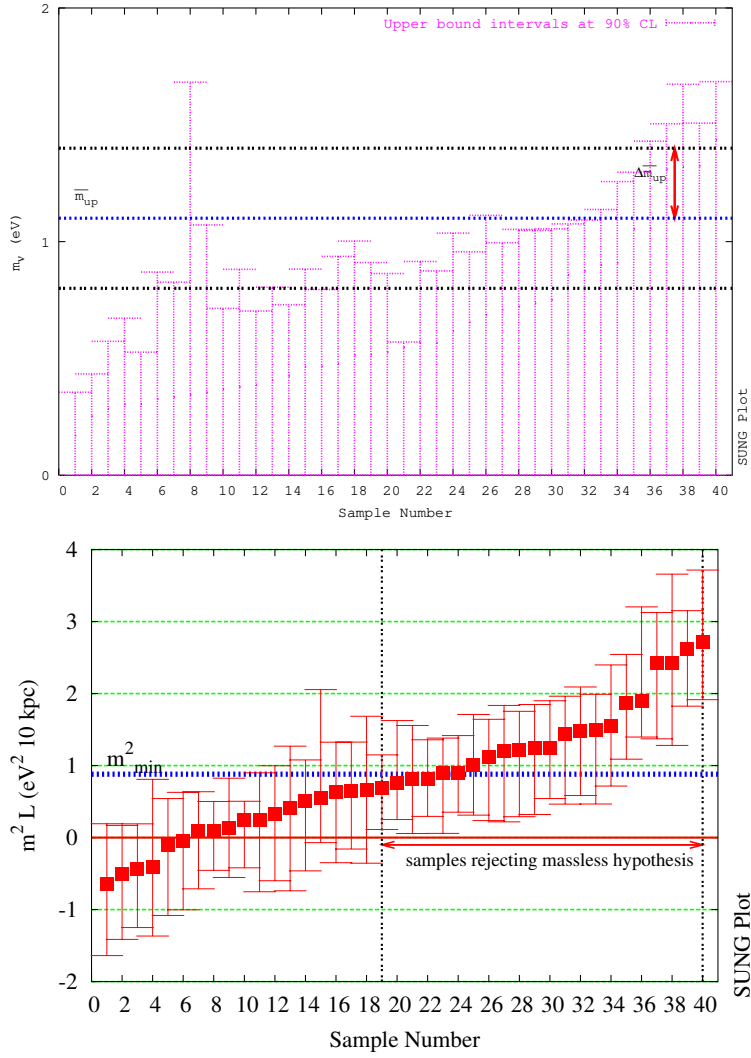


Figure 5.8: Two ways to quantify the sensitivity of the method. Upper panel: the average of the mass upper bounds and its dispersion $\Delta\bar{m}_{\text{up}}$. Lower panel: increasing the MC mass used to generate the samples we find the minimum value for which more than 50% of the analysis can reject the zero neutrino mass hypothesis.

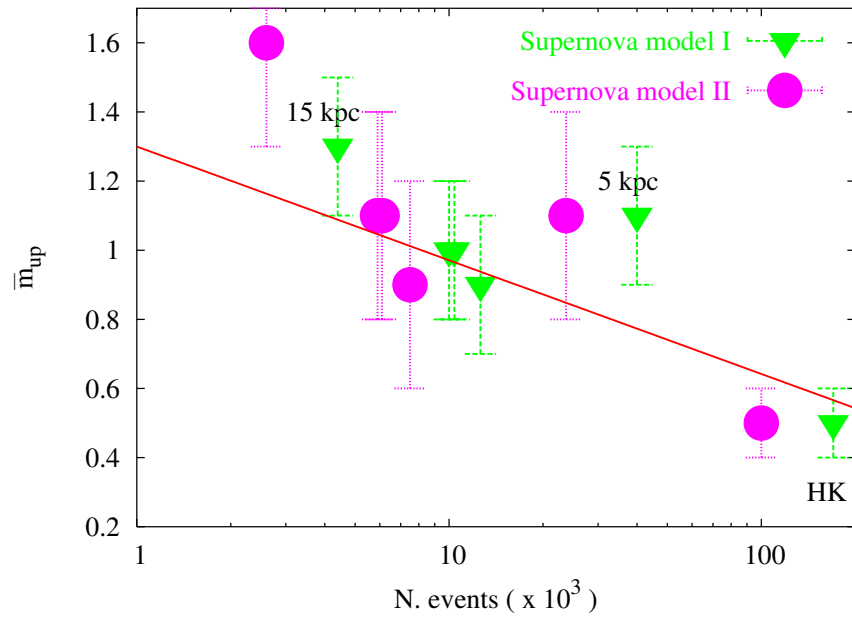


Figure 5.9: *Relation between the number of events in the signal and the sensitivity of the method. The continuous line highlights the empirical “logarithmic” relation between the sensitivity and the amount of events in the signal. For different distances also the different TOF is involved in the determination of the sensitivity, and the respective results deviate from the linear-log fit.*

Table 5.1: *Results for \bar{m}_{up} and $\sqrt{m_{\text{min}}^2}$ under different emission and detection conditions computed inside a 90% C.R. (95% C.R. values are in parenthesis). The average number of events of the signals for each set of conditions is included for reference in the fourth column. The values reported in columns 5 and 6 are affected by statistical uncertainties at the level of $\sim 5\%$. The typical number of signals per test is ~ 40 .*

supernova model I

Test	Detector	Distance	N. events ($\times 10^3$)	$\bar{m}_{\text{up}} \pm \Delta m_{\text{up}}$ (eV)	$\sqrt{m_{\text{min}}^2}$ (eV)
TSNI-1	SK	10 kpc	10.0	$1.0(1.1) \pm 0.2$	$1.0(1.1)$
TSNI-3	–	5 kpc	40.0	$1.1(1.2) \pm 0.2$	$1.1(1.2)$
TSNI-4	–	15 kpc	4.4	$1.3(1.4) \pm 0.3$	$1.4(1.5)$
TSNI-5	SK+KL	10 kpc	10.4	$1.0(1.1) \pm 0.2$	$0.9(1.0)$
TSNI-6	LENA	10 kpc	12.6	$0.9(1.0) \pm 0.2$	$0.9(1.0)$
TSNI-7	HK	10 kpc	170	$0.4(0.5) \pm 0.1$	$0.5(0.6)$

supernova model II

Test	Inputs	N. events ($\times 10^3$)	$\bar{m}_{\text{up}} \pm \Delta m_{\text{up}}$ (eV)	$\sqrt{m_{\text{min}}^2}$ (eV)
TSNII-1	SK	10 kpc	5.9	$1.1(1.2) \pm 0.3$
TSNII-3	–	5 kpc	23.7	$1.1(1.2) \pm 0.3$
TSNII-4	–	15 kpc	2.6	$1.6(1.7) \pm 0.6$
TSNII-5	SK+KL	10 kpc	6.1	$1.1(1.2) \pm 0.3$
TSNII-6	LENA	10 kpc	7.5	$0.9(1.0) \pm 0.3$
TSNII-7	HK	10 kpc	100	$0.5(0.6) \pm 0.1$
<hr/>				
Reference test:		10 kpc	9.6	$0.8(0.9) \pm 0.2$
<hr/>				

Changing the supernova distance two competitive effects arise. On one hand decreasing the distance increases the signal statistics, which in principle implies an increase of the sensitivity. However, at smaller distances the TOF delays induced by the mass are also smaller and become harder to identify. As can be learned with tests TSNI-3 and TSNII-3 these two effects tend to compensate each other.

It is natural to ask if anything better could be done to measure neutrino masses from a supernova neutrino signal. In the attempt to answer this question, we have performed the following test: we have produced a sample of synthetic signals assuming no mixing in the spectrum (no oscillations) and using as inputs to our MC flux model I (4.13) with a suitable choice of the relevant parameters, together with an analytical α -distribution spectrum corresponding to the average energy profile given in fig. 5.1a. We have then performed our usual set of fits to the neutrino mass (we assume the SK detector) but fixing the value of the flux parameters to the ones used in the MC, and we also adopt the same time varying spectrum used to generate the sample. This simulates the ideal (and unrealistic) situation where the time-energy dependence of the signal at the source is known, and the only free parameter is the neutrino mass. The results of this test are given in the last row in table 5.1 and should be compared with the results for tests TSNI-1 and TSNII-1. We see that only a mild improvement is achieved with respect to the realistic situation. This allows us to conclude that the sensitivity to neutrino masses of the detectors presently in operation is very likely bounded to values not much below 1 eV.

5.4 Additional remarks on the method

To arrive to the results we have just presented, some specific choices about the overall procedure that was followed had to be made. Here we will briefly discuss the impact of some of these choices on the final results.

Different priors. As was stated in sect. 4.4.2 the choice of the prior probability for m_ν^2 is a subtle issue. For all the analysis presented in this work we have used a Θ function as the prior probability on m_ν^2 . In order to understand the impact that a different prior could have on the results we have compared the mass limits with the ones obtained with a flat prior on m_ν .

In figure 5.10 we present the mass upper bounds obtained with both priors. We observe that the differences are not large. In the context of Bayesian reasoning this means that the signal contains enough “evidence” about the mass and therefore a change in the prior does not affect the results.

Estimation of the energy spectrum. The choice of the spectral function used

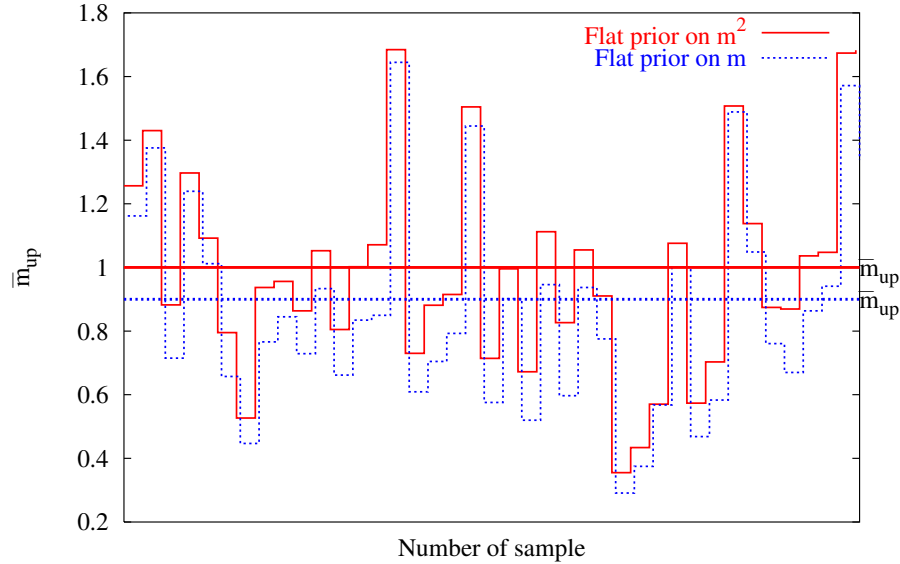


Figure 5.10: *Upper bounds obtained when two different prior probability on neutrino mass are used. Continuous line correspond a flat prior on m_ν^2 as used for all the analysis reported in this work. Dashed line are the upperbounds for the same signals obtained with a flat prior on m_ν .*

to fit the energy distribution of the events represent an interesting issue in our analysis. In ref. [83] we used a Fermi-Dirac distribution. Comparing these results with the ones presented here, where the α -function was used, it is evident that the particular spectral shape parametrization has no big impact on the final results. The main difference is the more direct way the parameters of the α -distribution can be estimated. In the Fermi-Dirac case the estimation of the spectral temperature and effective degeneracy parameter η involves a numerical procedure which mainly slows down the numerical analysis.

Energy threshold. As was observed in sect. 5.3 an increase in the energy resolution of the detector does not affect too much its sensitivity. However a too large energy threshold could affect considerably the method resolution.

In ref. [83] we compared the results for analysis performed on signals detected in SK assuming two different energy thresholds: 5 MeV, the threshold used here, and a more conservative threshold of 10 MeV. In that work the sensitivity dropped down by a factor of two making apparent that the low energy neutrinos play a central role in the determination of the sensitivity.

A new question arises: why the analysis of scintillator detector signals with a significantly lower threshold does not produce a similar improvement in sensitivity? The answer is that the increase in number of events is about 1-2% (see fig. 3.7) when we go from the 10 MeV threshold to 5 MeV (and this represents 100-200 additional low energy events in the SK signal) while lowering the threshold down to $\sim 3\text{MeV}$ implies only a $\sim 0.05 - 0.1\%$ increase (5-10 events).

5.5 Summary and Conclusions

We have described in this work a new method to measure and constrain the absolute scale of the neutrino mass using a high statistics signal from a future Galactic supernova.

The method relies on three basic conditions:

- An almost thermal neutrino spectra at the source (see sect. 2.2).
- The distribution of the high energy neutrino events, less affected by the TOF delay induced by a non-zero neutrino mass, can be used to extrapolate the signal profiles at low energies, since the time scale of the spectral evolution is larger than the typical mass induced time delay (fig. 2.8).
- A theoretical description based on general characteristics of the neutrino flux time evolution (an early fast rise followed by a steady decay on time scales of several seconds) is sufficiently accurate to construct a likelihood for studying the neutrino mass more probable values.

We combined a ML estimator and Bayesian techniques to construct the statistical procedure designed to constrain a neutrino mass, irrespectively of the particular flux model parameters used to describe the signal.

Different tests corresponding to two different supernova models, different oscillation schemes and detector were carried out. For each particular set of conditions, about 40 complete analysis were performed.

The general results of these tests have been described in detail in sects. 5.2. In particular, it was shown that regardless of the fine details of the signal, the measured value of the neutrino mass can be nailed around the correct value. The spread in the uncertainty depends however, on the quality and the amount of details used to describe the signal.

The two analytical models introduced to describe the flux behaved relatively well when applied to very different numerical neutrino fluxes. Satisfactory results were obtained with the first more simple flux model (4.13) especially when fitting supernova model I signals. The more flexible flux model II (4.15) required a tuning of various parameter that had to be fixed to suitable value to leave just a reasonable number of free variables in the likelihood multiparameter extremization.

The sensitivity of our method was estimated in two different ways, first, by determining the typical upper bound on m_ν that could be obtained in case the neutrino

mass is too small to be resolved. Secondly, by evaluating the minimum mass that could be distinguished from zero.

We believe that the method that we have proposed represents an improvement with respect to previous techniques, both in sensitivity and in the independence from particular astrophysical assumptions.

The sensitivity to neutrino masses of the detectors presently in operation can reach a level down to 1 eV. This is sizable better than present results from tritium β -decay experiments [27, 28], is competitive with the most conservative limits from neutrinoless double β -decay [29, 31, 26, 30], and although less precise than cosmological measurements [33, 34, 35], is also remarkably less dependent from prior assumptions. Future megaton water Čerencov detectors as Hyper-Kamiokande will allow for about a factor of two improvement in the sensitivity. However, they will not be competitive with the next generation of tritium β -decay [94, 95] and neutrinoless double β -decay experiments (see [96] and references therein).

In figure 5.11 we compare the limits that could be obtained with the present method, with other available and foreseen limits from laboratory, astrophysical and cosmological data.

We conclude that the occurrence of a Galactic supernova explosion within the next few years might still provide valuable informations on neutrino masses that however will not be able to explore a region much below 1 eV. Therefore as new laboratory experiments and cosmological observations will push the neutrino mass limits sensibly below 1 eV, the corresponding effects of the neutrino time of flight delays on a supernova signal will become unmeasurable.

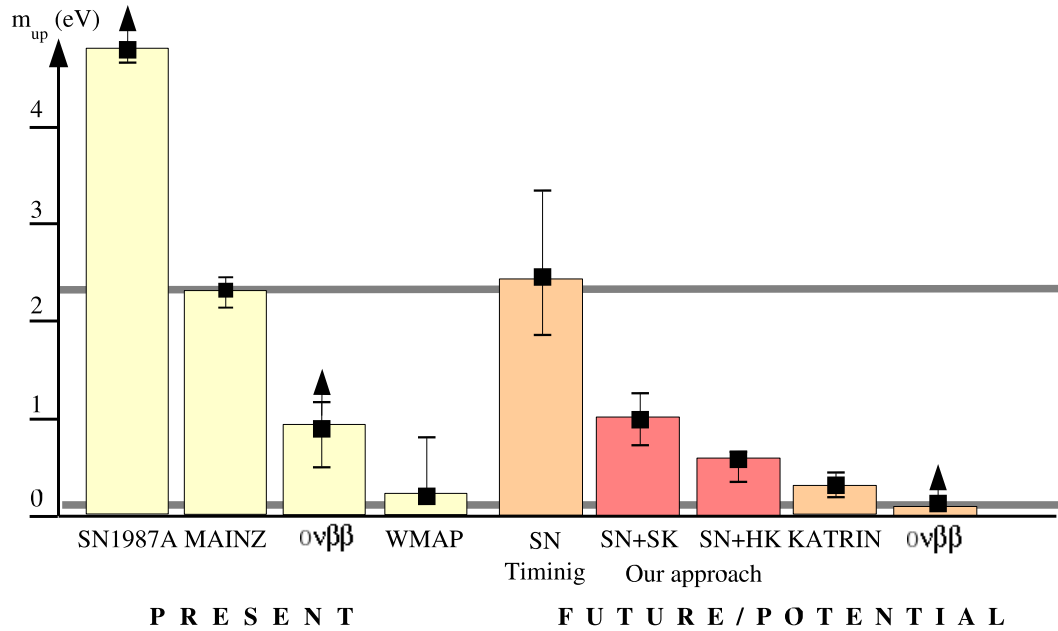


Figure 5.11: *Mass limits from present and future laboratory (MAINZ[27], KATRIN[95], $0\nu\beta\beta$ [96]), astrophysical (SN[52, 51, 54]) and cosmological studies (WMAP[32]). The thick gray lines in the background indicates the absolute upper limit from Tritium decay $m_\nu < 2.3$ eV [27] and the lower limit from oscillation evidences $m_\nu > \sqrt{\Delta m_{\text{atm}}^2} \simeq 0.05$ eV [78].*

Appendix A

Bayesian Inference: basic definitions

The method and techniques used in this work to obtain informations about a neutrino mass from a synthetic supernova signal are based on Bayesian principles of inference. Bayesian reasoning in data analysis has recently gained more and more relevance in a wide range of scientific disciplines, including frontier physics [97]. This appendix is aimed to introduce the main definitions and results of Bayesian inference in data analysis on which the method proposed in this work is based. A self contained and physics oriented introduction to Bayesian reasoning can be found in [49] while a more complete review of Bayesian techniques and their applications in physics data analysis is given in [97].

A.1 Basic principles

Bayesian inference is founded on two basic ideas. The first is the conception of probability as the *degree of belief* that a given proposition is true as opposite to the *conventional statistical* definition of probability as the long-run relative frequency with which the event defined by the proposition occurred on many repeated experiments [98]. Curiously (or indeed not) the Bayesian idea of probability correspond to the original concept by Laplace (as the father of inference reasoning in science) two centuries ago[98]. The second idea is that every probabilistic statement that we can make on any proposition must be a *conditional probability*, i.e. it must be conditioned to the available relevant information related with the proposition.

Formally, Bayesian inference is based on two central rules that can be derived from

the requirement of logical consistency of the probability theory[99]. By denoting with $p(A|B)$ the probability that A is true, given that B is true, it is straightforward to write down the *product rule*:

$$\begin{aligned} p(M, D|I) &= p(M|D, I) \times p(D|I) \\ &= p(D|M, I) \times p(M|I). \end{aligned} \quad (\text{A.1})$$

which states that the probability that propositions M and D are true *given* the background information I is equal to the probability of M , given D and I , times the probability of D given I . On the other hand we have the *sum rule*:

$$\sum_i p(M_i|I) = 1, \quad (\text{A.2})$$

where M_i is a set of mutually *exclusive* and *exhaustive* set of propositions and 1 refers to the convention to assign this value to the probability of a *tautological* proposition.

A.2 Bayes theorem

Starting from the two rules introduced in the previous section two central results can be obtained: the Bayes theorem and the marginalization procedure.

Let us suppose that in a given measurement we obtain the data D . Based on some background information I we assume that model M can describe the data. Using the previous knowledge (product of our expertise) on the phenomenon we assign to model M a *prior probability* $p(M|I)$ which measure the *plausibility* of that model given the background information I . The *posterior probability* of M given the data and the background information can be computed from $p(M|I)$ using the product rule (A.1):

$$p(M|D, I) = p(M|I) \frac{p(D|M, I)}{p(D|I)} \quad (\text{A.3})$$

This result is called the Bayes theorem. Here $p(D|M, I)$ is the probability that the data D be described by model M , and it is called the *sampling probability* for D or the *Likelihood* for model M . $p(D|I)$ is called the *evidence* for D and represents the probability that the measurement produce the data D for the entire class of hypotheses (models).

When M is described by a (continuous) set of parameters collectively denoted as $\{\theta\}$, posterior $p(\{\theta\}|D, I)$ becomes multivariate *probability distribution functions*

(pdf) of the parameters, while the Likelihood $p(D|\{\theta\}, I)$, that we will denote by the symbol $\mathcal{L}(D; \{\theta\})$ in spite of its explicit dependence is not by itself a pdf for the parameters. The evidence $p(D|I)$ is independent of $\{\theta\}$ and plays simply the role of the posterior pdf normalization constant $N \equiv p(D|I)$. Bayes theorem now reads:

$$p(\{\theta\}|D) = N^{-1} p(\{\theta\}|I) \mathcal{L}(D; \{\theta\}), \quad (\text{A.4})$$

where for simplicity we have dropped out the reference to the background information I .

An interesting way to see what Bayes theorem establishes is to think that our knowledge on how a model describes a given phenomenon grows when new evidence is accumulated. In this sense we could think at Bayes theorem as a recipe for learning [100].

A.3 The marginalization procedure

Often some of the parameters that are used to describe a model, thought important for the computation of the Likelihood, are uninteresting for the final conclusions that one wants to extract from the experimental evidence. The principles of Bayesian reasoning provide a natural way to *marginalize* these *nuisance parameters*. Using the continuous limit of the sum rule (A.2):

$$\int p(\theta|D) d\theta = 1, \quad (\text{A.5})$$

the *marginal posterior probability* for parameter θ_0 can be written as:

$$\begin{aligned} p(\theta_0|D) &= \int d\{\theta\} p(\theta_0, \{\theta\}|D) \\ &= N^{-1} p(\theta_0) \int d\{\theta\} \mathcal{L}(D; \theta_0, \{\theta\}) p(\{\theta\}) \end{aligned} \quad (\text{A.6})$$

Marginalization is one of the most important features of Bayesian inference when compared with conventional approaches. However, performing the multidimensional integrals required for finding the marginal distribution can be a computational challenge in terms of the large times necessary to carry out such integrations. Several solutions have been devised and are used in the most complicated problems where Bayesian inference is applied (see section 2 of ref.[100]). As was described in sect. 4.6,

we have used the simple approximation of taking the *profile likelihood* (PL) as the marginal distribution, under the assumption that the likelihood can be approximated by a multivariate Gaussian (normal) pdf. In the following section we will prove that the profile of a normal likelihood coincides with its marginal distribution.

A.3.1 Marginalization of a normal pdf

The general form of a multivariate normal pdf for parameters $\vec{\theta} \equiv (\theta_0 \dots \theta_{n-1})^T$ is:

$$\mathcal{G}_n(\vec{\theta}; \vec{\mu}, \mathbf{C}) = \frac{1}{(2\pi)^{n/2} \sqrt{\det(\mathbf{C})}} \exp \left[-\frac{1}{2} (\vec{\theta} - \vec{\mu})^T \mathbf{C}^{-1} (\vec{\theta} - \vec{\mu}) \right], \quad (\text{A.7})$$

where $\vec{\mu} \equiv (\mu_0 \dots \mu_{n-1})^T$ are the mean values of the parameters (here for simplicity we will assume $\mu_i = 0$) and \mathbf{C} is the covariance matrix:

$$\mathbf{C} = \begin{pmatrix} \sigma_0^2 & \rho_{01}\sigma_0\sigma_1 & \dots \\ \rho_{01}\sigma_0\sigma_1 & \sigma_1^2 & \dots \\ \dots & \dots & \dots \end{pmatrix} \quad (\text{A.8})$$

with ρ_{ij} the correlation coefficient between parameters i and j .

To simplify let's take the particular case of a bivariate normal pdf. In this situation eq. (A.7) is given by:

$$\begin{aligned} \mathcal{G}_2(\theta_0, \theta_1; \sigma_0, \sigma_1) &= \frac{1}{2\pi\sigma_0\sigma_1\sqrt{1-\rho^2}} \exp \left[-\frac{1}{2(1-\rho^2)} \left(\frac{\theta_0^2}{\sigma_0^2} + \frac{\theta_1^2}{\sigma_1^2} - \frac{2\rho\theta_0\theta_1}{\sigma_0\sigma_1} \right) \right] \\ &= Z^{-1} \exp \left[-\frac{1}{2} (a\theta_0^2 + b\theta_1^2 - 2c\theta_0\theta_1) \right], \end{aligned} \quad (\text{A.9})$$

with $\rho \equiv \rho_{12}$ and in the last equation we have defined $Z \equiv 2\pi\sqrt{1-\rho^2}\sigma_0\sigma_1$, $a \equiv 1/\sigma_0^2(1-\rho^2)$, $b \equiv 1/\sigma_1^2(1-\rho^2)$ and $c \equiv \rho/\sigma_0\sigma_1(1-\rho^2)$.

Using (A.9) the marginal pdf on θ_0 , $p(\theta_0)$ reads,

$$\begin{aligned} p(\theta_0) &= \int d\theta_1 \mathcal{G}_2(\theta_0, \theta_1; \sigma_0, \sigma_1) \\ &= Z^{-1} \exp \left(-\frac{a\theta_0^2}{2} + \frac{c^2\theta_0^2}{2b} \right) \int d\theta_1 \exp \left[-\frac{1}{2} b(\theta_1 + d)^2 \right] \end{aligned}$$

$$\begin{aligned}
&= Z^{-1} \sqrt{2\pi/b} \exp\left(-\frac{1}{2\sigma_0^2}\theta_0^2\right) \\
&= \frac{1}{\sqrt{2\pi}\sigma_0} \exp\left(-\frac{1}{2\sigma_0^2}\theta_0^2\right),
\end{aligned}$$

where after completing the square in the exponential of the second equation ($d = c\theta_0/\sqrt{b}$) the resulting integration is performed using $\int \exp(-x^2/2\sigma) = \sqrt{2\pi}\sigma$. As can be seen from the last equation, the marginal distribution in θ_0 is simply a normal distribution with dispersion σ_0 .

Now we will proceed to compute the *profile likelihood* (PL) $\hat{p}(\theta_0)$ which is defined by:

$$\hat{p}(\theta_0) \propto \mathcal{G}(\theta_0, \theta_{1\max}; \sigma_0, \sigma_1) \quad (\text{A.10})$$

where $\theta_{1\max}$ refers to the value of θ_1 for which \mathcal{G} is maximum at the given value of θ_0 (see figure 4.11). The proportional symbol ' \propto ' means that $\hat{p}(\theta_0)$ is not necessarily normalized.

The value of $\theta_{1\max}$ is found maximizing the denominator in the exponential of (A.9) which gives $\theta_{1\max} = c\theta_0/b$. This results in,

$$\hat{p}(\theta_0) \sim \exp\left[-\frac{1}{2}\left(a\theta_0^2 + \frac{bc^2}{b^2}\theta_0^2 - 2\frac{c^2}{b}\theta_0^2\right)\right] \quad (\text{A.11})$$

$$\sim \exp\left(-\frac{1}{2\sigma_0^2}\theta_0^2\right) \quad (\text{A.12})$$

Therefore the profile likelihood is also a normal distribution in θ_0 with dispersion equal to σ_0 and coincides with the marginal distribution $p(\theta_0)$.

This result can be generalized to more than two variables. *When the likelihood is a multivariate normal distribution in the parameters the profile likelihood for a given parameter coincides with the marginal distribution.*

A.4 Credible regions

(Marginal) posterior pdf are the general outcome of inference analysis based on Bayesian reasoning. It is common to summarize the properties of these distributions using for example the *mode* (the values of parameters where the pdf is maximum)

or the mean value and dispersion of the parameters as obtained from the posterior using the classical prescriptions.

It is also common to construct *credible regions* (CR), defined as the interval(region) where the parameter value(s) is found with a probability CR ,

$$\int_{CR} d\theta p(\theta|D) \equiv CR \quad (\text{A.13})$$

The credible regions are the analog of the *confidence intervals* in *frequentist* statistics that however are computed and interpreted in a very different way.

Appendix **B**

SUNG: SUpernova Neutrino Generation tool

In chapter 3 we describe how the properties of a supernova signal are computed starting with the characteristics of the emitted neutrino signal as provided by self-consistent simulation of the core collapse and using the proper description of neutrinos oscillations in the supernova mantle and the Earth interior and simulating the neutrino detection process. Numerically this procedure involves a particular manipulation of the supernova simulation results that are used as the inputs of the general description of the signal and the development of specially designed routines to model neutrino oscillations under general circumstances in the supernova mantle and the Earth interior.

Other numerical challenges arise when the purpose is to generate full statistics signals. In this case it is necessary on one hand to use especialized algorithms and techniques to sample the complex observed rate but in the other hand to design mechanisms to perform a cross-checking to the generated signal to ensure that its events already follows the original distribution.

Using the experience and the computer codes created in the frame of this project we have created a computer package, SUNG (SUpernova Neutrino Generation tool) intended to offer a simple and acsequible computer solution to reproduce the results published in this work and to perform similar aproaches to the analysis of supernova neutrino signals.

For new or experienced researchers in the field SUNG is a solution to fastly obtain results that can require non-trivial programming efforts. Certainly it is not an ultimate solution for the computation and generation of supernova neutrino signals

under rather arbitrary conditions. The main philosophy behind this effort is that of promote the creation of computational solutions in the field of neutrino astrophysics as has been done in other fields (e.g. CMBFAST for CMBR simulation and analysis [101]).

In this appendix we describe the general features of SUNG and some of the methods and algorithms used to perform the most important tasks that the package can perform.

For a more complete description of the package including simple reference manuals for the final user and the programmer please refer to the web site <http://www.sungweb.tk>.

B.1 Package structure

SUNG is more than a simple single program to generate supernova neutrino signals. It is also a specialized programming framework that can be used for a wide variety of different applications.

SUNG has three main components:

- A library of (ANSI C) routines for data analysis originally designed or adapted from other libraries, and other routines created to simulate neutrino oscillations in the Supernova mantle and inside the Earth.

The routines has been designed and organized to offer a coherent programming framework. Even the specialized numerical routines of other scientific libraries are inserted into routines especially formated for this library [102].

In the core of the numerical integration, special functions, interpolation and random number generation routines SUNG uses routines of the GNU scientific library (GSL)[103]. Function minimization routines used in fit procedures use the MINUIT package routines from the CERN library [104].

The SUNG library also includes a series of routines to generate data plots in eps and ps format using the plotting package GNUPLOT [105].

In this sense the SUNG library can be seen as a special purpose common interface to those scientific libraries and packages.

- A set of C programs, written down using the routines in the SUNG library and perl/tcl scripts designed to perform mainly four tasks: manipulate supernova simulation results, compute the properties of supernova neutrino signals under different input conditions, generate full-statistics realizations of those

signals and analyze high-statistics supernova neutrino signals using a suitable analytical model.

All the programs are designed to be ran from the command-line. That programs are the best example on how complex tasks can be programmed using the routines of the package library.

- The package have a special Graphical User Interface (GUI) which has been designed to run on a web browser. This *webGUI* consist of an elaborated set of php scripts and works almost as a regular off-line GUI but with the advantage of not depend on any particular GUI library. Once installed in a server (with an Apache and Php server) it can be run locally or remotely on a platform independent basis.

A running version of the SUNG web interface can be found in the web site of the project <http://www.sungweb.tk>.

B.2 Methods and Algorithms

In the following paragraphs we describe the methods and algorithms used by the package to perform the most important general tasks for which it was designed.

It is important to recall that this work was performed using the same computer codes of the package and therefore the algorithms described below are the same ones involved in the production of the results presented here.

B.2.1 Manipulation of Supernova simulations

In order to describe the properties of an observed supernova neutrino signal it is necessary to know the properties of the emitted neutrinos.

There are three main pieces of information that describe almost completely the neutrino emission from a supernova at a given time: the luminosity, the average energy and the non-thermal distortion (quantified with an α -parameter for example). In the ideal case the non-thermal distortions information is replaced by the detailed knowledge of the spectral shape at each time.

Most of the supernova simulations results produce as an output that informations and in our case they are the input of the computation of the observed signal properties.

In the manipulations of results from supernova simulations several problems must be faced. One of the most common problems arise when a given simulation result

is limited to a shorter interval than the total assumed duration of the signal (20 sec in this work). This is the case for Supernova model II [61] where neutrino emission properties are just reliable for times less than 300 msec.

The routines included in the package are not prepared to face this kind of limitations and an external extrapolation of the results is required (see sec. 5.1).

All the data files describing the evolution and the luminosity of the spectral properties are treated by the SUNG library as continuous functions using linear interpolation.

B.2.2 Expected signal properties

The signal properties computed by SUNG are the same described in sec. 3.3:

- **Number of events.** This property is computed using the definition (3.46):

$$N(\Delta E_{12}, \Delta t_{12}) = \int_{E_1}^{E_2} dE \int_{t_1}^{t_2} dt \frac{d^2 n(E, t)}{dE dt}. \quad (\text{B.1})$$

Where the detected signal rate is given by (3.41) and (3.40):

$$\begin{aligned} \frac{d^2 n_{\bar{\nu}_e}(E, t)}{dE dt} &= N_T \int dE' S_{\bar{e}}^{\text{det}}(E', t) \sigma(E') \epsilon(E') \mathcal{R}(E, E'), \\ L^2 S_{\bar{e}}^{\text{det}}(E, t) &= \bar{p} S_{\bar{e}} + (1 - \bar{p}) S_{\bar{x}}. \end{aligned}$$

The three dimensional integration involved in the computation of N is performed using a recursive procedure [106] supported by one-dimensional adaptive Gaussian-Kronrod integrations.

- **Time-profiles.** There are two kind of time-profiles computed by SUNG. The energy integrated time-profile as defined in sec. 3.3.3 also called in the package context the *marginal time-profile* (3.49):

$$f_t^{\text{det}}(t) = \int dE \frac{d^2 n(E, t)}{dE dt}. \quad (\text{B.2})$$

The other profile is given by the histogram that describes the number of events inside narrow time windows of regular width Δt . This histogram is given by:

$$h_i^t = \int_{t_i - \Delta t/2}^{t_i + \Delta t/2} dt \int dE \frac{d^2 n(E, t)}{dE dt}. \quad (\text{B.3})$$

- **Energy-profiles.** The energy-profiles (time integrated spectrum and energy-profile histogram) are computed similarly using the definitions given in sec. 3.3.2.

B.2.3 Signal generation

The generation of full statistics signals is the central problem solved by SUNG.

As explained in sec. 3.4 we can conceive several alternative algorithms to generate the events in a supernova neutrino signal including all the effects of the neutrino propagation, oscillation and detection.

SUNG uses the approach of generate the signal by sampling directly the detected rate.

The algorithm used by SUNG to perform this task is described in the following lines:

Signal generation Algorithm

1. Compute the number of events that different neutrinos emitted as a given flavor will produce in the detector:

$$\begin{aligned} N_{\bar{\nu}_e \rightarrow \bar{\nu}_e} &= \int dE \int dt N_T \bar{p} \frac{S_{\bar{e}}}{L^2} \\ N_{\bar{\nu}_x \rightarrow \bar{\nu}_e} &= \int dE \int dt N_T (1 - \bar{p}) \frac{S_{\bar{x}}}{L^2} \end{aligned}$$

where $N_{\bar{\nu}_e \rightarrow \bar{\nu}_e}$ ($N_{\bar{\nu}_x \rightarrow \bar{\nu}_e}$) are the number of $\bar{\nu}_e$ events produced by neutrinos emitted from the supernova core as $\bar{\nu}_e$ ($\bar{\nu}_x$).

2. Reshuffle the total number of neutrinos computed in the previous step according to a Poisson distribution with average equal to $N_{\text{tot}} = N_{\bar{\nu}_e \rightarrow \bar{\nu}_e} + N_{\bar{\nu}_x \rightarrow \bar{\nu}_e}$. According to the reshuffled value N'_{tot} compute the finally detected number of neutrinos of each flavor $N'_{\bar{\nu}_e, \bar{\nu}_x \rightarrow \bar{\nu}_e}$ obeying the original proportions.
3. Generate $N'_{\bar{\nu}_e \rightarrow \bar{\nu}_e}$ ($N'_{\bar{\nu}_x \rightarrow \bar{\nu}_e}$) pairs of neutrino energies and times $\{E_i, t_i\}$ according to the respective neutrino detected flux (3.38), $\bar{p} S_{\bar{e}}/L^2$ ($(1 - \bar{p}) S_{\bar{x}}/L^2$) with $S_{\bar{e}, \bar{x}}$ given by (3.38):

$$S_\alpha(E, t) = \frac{L_\alpha(t)}{\overline{E_\alpha}(t)} F_\alpha^{\text{em}}(E; t). \quad (\text{B.4})$$

4. Shift the neutrino time according to the mass induced delay (4.1):

$$t_i = t_i + \Delta t_{\text{tof}}(m_\nu^2, L, E_i) \quad (\text{B.5})$$

5. Reset the neutrino times in order to place the first neutrino detected at $t_1 = 0$.

6. Compute the energy of the secondary produced by the detection of each neutrino: $E_i^{\text{p}} = E_i - Q_{pn}$.

7. Reshuffle the positron energy according to the energy measurement uncertainty (3.45):

$$E_i^{\text{p}} \rightarrow \mathcal{G}(\bar{x} = E_i^{\text{p}}, \sigma = \Delta E) \quad (\text{B.6})$$

The result of this procedure is the set $\{E_i^{\text{p}}, t_i\}$ with $i = 1, \dots, N'_{\text{tot}}$.

List of symbols and abbreviations

C.1 List of symbols

Symbol	Definition
m_ν	Absolute scale of neutrino masses. In the case of non-degenerate masses it refers to the electron neutrino mass in the context of this work.
ν_x	Non-electron neutrinos and antineutrinos $\equiv \nu_{\mu,\tau}, \bar{\nu}_{\mu,\tau}$.
L	Supernova distance.
$R_{\text{NS}}, M_{\text{NS}}$	Radius and mass of a neutron star.
Δt_{tof}	Mass induced time-of-flight delay.
dn^{em}/dt	Rate of neutrino emission, i.e. number of neutrinos of any energy emitted per unit of time.
$F(E)$	Neutrino spectrum at the source.
p	Pinching parameter, $p \propto \langle E^2 \rangle / \langle E \rangle$.
$\overrightarrow{\nu}_W$	Neutrino flavor eigenstates.

Symbol	Definition
$\vec{\nu}_M$ ($\vec{\nu}_M^m$)	Neutrino mass eigenstates in vacuum (in matter).
$U_{\alpha i}$	entries of the MNS matrix.
μ_i	In matter effective neutrino masses.
γ	Adiabaticity parameter.
$P_{H,L}$ ($\bar{P}_{H,L}$)	Supernova mantle jumping probabilities.
$p_{\alpha i}$ ($\bar{p}_{\alpha i}$)	Supernova mantle conversion probabilities $\equiv P(\nu_\alpha \rightarrow \nu_i)$.
$P_{\alpha\beta}$ ($P_{\bar{\alpha}\bar{\beta}}$)	Conversion probabilities $\equiv P(\nu_\alpha \rightarrow \nu_\beta)$.
p_{\oplus} (\bar{p}_{\oplus})	Conversion probabilities in the Earth.
$S_\alpha(E, t)$	Total flux of neutrino flavor α at the source, i.e. number of neutrinos α emitted per unit of time and per unit of energy.
$S_\alpha^{\text{det}}(E, t)$	Total flux of neutrino flavor α arriving to the detector, i.e. number of neutrinos α arriving per unit of time and per unit of energy.
\bar{E}_α	Average energy of neutrinos α at the source.
$d^2n_\alpha/dE dt$	Total rate of neutrino flavor α in the detector, i.e. number of neutrinos α detected per unit of time and per unit of energy.
$f_E(E)$	Time-integrated energy spectrum.
$f_t(t)$	Energy-integrated time profile.
\mathcal{M}	A supernova emission model. If the model can be parametrized with a set of parameters $\{\theta\}$ the model is represented by $\mathcal{M}(\theta)$.

Symbol **Definition**

 \mathcal{D} Data set, i.e. set of energy and time pairs $\{E_i, t_i\}$.

 $f(E, t)$ Probability distribution function used to describe the signal (model density probability).

 \mathcal{L} Likelihood function.

 $\phi(t)$ Flux model.

 $\mathcal{G}(x; \mu, \sigma)$ Normal distribution with mean μ and standard deviation σ .

 $\tilde{f}(E, t)$ Regularized model density probability.

 $\hat{\mathcal{L}}$ Profile Likelihood.

C.2 List of abbreviations

Abrev. Definition	
SN	Supernova/Supernovae.
TOF	Time-of-flight.
LTE	Local Thermodynamic Equilibrium.
MNS	Maki-Nakagawa-Sakata matrix.
NH	Normal hierarchy.
IH	Inverted hierarchy.
LF	Likelihood function.
log-LF	Logarithm of Likelihood Function.
ML	Maximum Likelihood analysis.
MC	Monte Carlo.
CR	Credible regions (credible region probability).
PL	Profile likelihood.
SK	Super-Kamiokande.
KL	KamLAND.
HK	Hyper-Kamiokande.

References

- [1] G. Gamow and M. Schoenberg, “The possible role of neutrinos in stellar evolution,” *Phys. Rev.* **58** (1940) 1117.
- [2] S. Chandrasekhar, “The highly collapsed configurations of a stellar mass (second paper),” *Mon. Not. Roy. Astron. Soc.* **95** (Jan., 1935) 207–225.
- [3] G. G. Raffelt, M. T. Keil, R. Buras, H.-T. Janka, and M. Rampp, “Supernova neutrinos: Flavor-dependent fluxes and spectra,” [astro-ph/0303226](#).
- [4] H.-T. Janka, R. Buras, K. Kifonidis, T. Plewa, and M. Rampp, “Core collapse and then? the route to massive star explosions,” [astro-ph/0212316](#).
- [5] R. Buras, M. Rampp, H. T. Janka, and K. Kifonidis, “Improved models of stellar core collapse and still no explosions: What is missing?,” *Phys. Rev. Lett.* **90** (2003) 241101, [astro-ph/0303171](#).
- [6] H.-T. Janka, R. Buras, K. Kifonidis, A. Marek, and M. Rampp, “Core-collapse supernovae at the threshold,” [astro-ph/0401461](#).
- [7] H. A. Bethe and R. Wilson, James, “Revival of a stalled supernova shock by neutrino heating,” *Astrophys. J.* **295** (1985) 14–23.
- [8] **Super-Kamiokande** Collaboration, Y. Fukuda *et al.*, “Evidence for oscillation of atmospheric neutrinos,” *Phys. Rev. Lett.* **81** (1998) 1562–1567, [hep-ex/9807003](#).
- [9] **Super-Kamiokande** Collaboration, Y. Fukuda *et al.*, “Measurement of the flux and zenith-angle distribution of upward through-going muons by super-kamiokande,” *Phys. Rev. Lett.* **82** (1999) 2644–2648, [hep-ex/9812014](#).

- [10] **MACRO** Collaboration, M. Ambrosio *et al.*, “Measurement of the atmospheric neutrino-induced upgoing muon flux using macro,” *Phys. Lett.* **B434** (1998) 451–457, [hep-ex/9807005](#).
- [11] **MACRO** Collaboration, M. Ambrosio *et al.*, “Low energy atmospheric muon neutrinos in macro,” *Phys. Lett.* **B478** (2000) 5–13, [hep-ex/0001044](#).
- [12] **Soudan 2** Collaboration, M. Sanchez *et al.*, “Observation of atmospheric neutrino oscillations in soudan 2,” *Phys. Rev.* **D68** (2003) 113004, [hep-ex/0307069](#).
- [13] **SNO** Collaboration, Q. R. Ahmad *et al.*, “Measurement of the charged current interactions produced by b-8 solar neutrinos at the sudbury neutrino observatory,” *Phys. Rev. Lett.* **87** (2001) 071301, [nucl-ex/0106015](#).
- [14] **Kamiokande** Collaboration, Y. Fukuda *et al.*, “Solar neutrino data covering solar cycle 22,” *Phys. Rev. Lett.* **77** (1996) 1683–1686.
- [15] B. T. Cleveland *et al.*, “Measurement of the solar electron neutrino flux with the homestake chlorine detector,” *Astrophys. J.* **496** (1998) 505–526.
- [16] **GALLEX** Collaboration, W. Hampel *et al.*, “Gallex solar neutrino observations: Results for gallex iv,” *Phys. Lett.* **B447** (1999) 127–133.
- [17] **GNO** Collaboration, M. Altmann *et al.*, “Gno solar neutrino observations: Results for gno i,” *Phys. Lett.* **B490** (2000) 16–26, [hep-ex/0006034](#).
- [18] **Super-Kamiokande** Collaboration, S. Fukuda *et al.*, “Solar b-8 and he p neutrino measurements from 1258 days of super-kamiokande data,” *Phys. Rev. Lett.* **86** (2001) 5651–5655, [hep-ex/0103032](#).
- [19] **SAGE** Collaboration, J. N. Abdurashitov *et al.*, “Measurement of the solar neutrino capture rate by the russian-american gallium solar neutrino experiment during one half of the 22-year cycle of solar activity,” *J. Exp. Theor. Phys.* **95** (2002) 181–193, [astro-ph/0204245](#).
- [20] **Super-Kamiokande** Collaboration, M. B. Smy *et al.*, “Precise measurement of the solar neutrino day/night and seasonal variation in super-kamiokande-i,” *Phys. Rev.* **D69** (2004) 011104, [hep-ex/0309011](#).
- [21] **SNO** Collaboration, S. N. Ahmed *et al.*, “Measurement of the total active b-8 solar neutrino flux at the sudbury neutrino observatory with enhanced neutral current sensitivity,” *Phys. Rev. Lett.* **92** (2004) 181301, [nucl-ex/0309004](#).

- [22] **KamLAND** Collaboration, K. Eguchi *et al.*, “First results from kamland: Evidence for reactor anti- neutrino disappearance,” *Phys. Rev. Lett.* **90** (2003) 021802, [hep-ex/0212021](#).
- [23] **KamLAND** Collaboration, T. Araki *et al.*, “Measurement of neutrino oscillation with kamland: Evidence of spectral distortion,” [hep-ex/0406035](#).
- [24] **K2K** Collaboration, Y. Oyama, “K2k (kek to kamioka) neutrino oscillation experiment at kek-ps,” [hep-ex/9803014](#).
- [25] H. Paes and T. J. Weiler, “Absolute neutrino mass determination,” *Phys. Rev.* **D63** (2001) 113015, [hep-ph/0101091](#).
- [26] S. M. Bilenky, C. Giunti, J. A. Grifols, and E. Masso, “Absolute values of neutrino masses: Status and prospects,” *Phys. Rept.* **379** (2003) 69–148, [hep-ph/0211462](#).
- [27] J. Bonn *et al.*, “Results from the mainz neutrino mass experiment,” *Prog. Part. Nucl. Phys.* **48** (2002) 133–139.
- [28] V. M. Lobashev *et al.*, “Direct search for neutrino mass and anomaly in the tritium beta-spectrum: Status of troitsk neutrino masséperiment,” *Nucl. Phys. Proc. Suppl.* **91** (2001) 280–286.
- [29] H. V. Klapdor-Kleingrothaus *et al.*, “Latest results from the heidelberg-moscow double-beta-decay experiment,” *Eur. Phys. J. A* **12** (2001) 147–154, [hep-ph/0103062](#).
- [30] H. V. Klapdor-Kleingrothaus, I. V. Krivosheina, A. Dietz, and O. Chkvorets, “Search for neutrinoless double beta decay with enriched ge- 76 in gran sasso 1990-2003,” *Phys. Lett.* **B586** (2004) 198–212, [hep-ph/0404088](#).
- [31] **16EX** Collaboration, C. E. Aalseth *et al.*, “The igex ge-76 neutrinoless double-beta decay experiment: Prospects for next generation experiments,” *Phys. Rev.* **D65** (2002) 092007, [hep-ex/0202026](#).
- [32] S. Hannestad, “Neutrinos in cosmology,” *New J. Phys.* **6** (2004) 108, [hep-ph/0404239](#).
- [33] S. Hannestad, “Neutrino masses and the number of neutrino species from wmap and 2dfgrs,” *JCAP* **0305** (2003) 004, [astro-ph/0303076](#).

- [34] O. Elgaroy and O. Lahav, “The role of priors in deriving upper limits on neutrino masses from the 2dfgrs and wmap,” *JCAP* **0304** (2003) 004, [astro-ph/0303089](#).
- [35] P. Crotty, J. Lesgourgues, and S. Pastor, “Current cosmological bounds on neutrino masses and relativistic relics,” *Phys. Rev.* **D69** (2004) 123007, [hep-ph/0402049](#).
- [36] J. F. Beacom, N. F. Bell, and S. Dodelson, “Neutrinoless universe,” *Phys. Rev. Lett.* **93** (2004) 121302, [astro-ph/0404585](#).
- [37] G. T. Zatsepin, “Possibility of determining the upper limit of the neutrino mass from the time of flight,” *JETP Lett.* **8** (1968) 205.
- [38] S. Pakvasa and K. Tennakone, “Neutrinos of non-zero rest mass,” *Phys. Rev. Lett.* **28** (1972) 1415.
- [39] T. Piran, “Neutrino mass and detection of neutrino supernova bursts,” *Phys. Lett.* **B102** (1981) 299–302.
- [40] Z. F. Seidov, “The supernova neutrino pulse shape in the scintillation detector,” *Astrophysics and Space Science* **81** (Jan., 1982) 483–488.
- [41] K. S. Hirata *et al.*, “Observation in the kamiokande-ii detector of the neutrino burst from supernova sn1987a,” *Phys. Rev.* **D38** (1988) 448–458.
- [42] **IMB** Collaboration, J. C. Van Der Velde *et al.*, “Neutrinos from sn1987a in the imb detector,” *Nucl. Instrum. Meth.* **A264** (1988) 28–31.
- [43] E. N. Alekseev, L. N. Alekseeva, I. V. Krivosheina, and V. I. Volchenko, “Detection of the neutrino signal from sn1987a in the lmc using the inr baksan underground scintillation telescope,” *Phys. Lett.* **B205** (1988) 209–214.
- [44] D. N. Schramm, “Neutrinos from supernova sn1987a,” *Comments Nucl. Part. Phys.* **17** (1987) 239.
- [45] W. D. Arnett and J. L. Rosner, “Neutrino mass limits from sn1987a,” *Phys. Rev. Lett.* **58** (1987) 1906.
- [46] J. N. Bahcall and S. L. Glashow, “Upper limit on the mass of the electron-neutrino,” *Nature* **326** (1987) 476.

- [47] D. N. Spergel and J. N. Bahcall, “The mass of the electron-neutrino: Monte carlo studies of sn1987a observations,” *Phys. Lett.* **B200** (1988) 366.
- [48] L. F. Abbott, A. De Rujula, and T. P. Walker, “Constraints on the neutrino mass from the supernova data: A systematic analysis,” *Nucl. Phys.* **B299** (1988) 734.
- [49] T. J. Loredo and D. Q. Lamb, “Bayesian analysis of neutrinos observed from supernova sn 1987a,” *Phys. Rev.* **D65** (2002) 063002, [astro-ph/0107260](#).
- [50] D. Fargion, “Time delay between gravitational waves and neutrino burst from a supernova explosion: a test for the neutrino mass,” *Nuovo Cim. Lett.* **31** (1981) 499–500, [hep-ph/0110061](#).
- [51] N. Arnaud *et al.*, “Gravity wave and neutrino bursts from stellar collapse: A sensitive test of neutrino masses,” *Phys. Rev.* **D65** (2002) 033010, [hep-ph/0109027](#).
- [52] T. Totani, “Electron neutrino mass measurement by supernova neutrino bursts and implications on hot dark matter,” *Phys. Rev. Lett.* **80** (1998) 2039–2042, [astro-ph/9801104](#).
- [53] J. F. Beacom, R. N. Boyd, and A. Mezzacappa, “Technique for direct-ev scale measurements of the mu and tau neutrino masses using supernova neutrinos,” *Phys. Rev. Lett.* **85** (2000) 3568–3571, [hep-ph/0006015](#).
- [54] J. F. Beacom, R. N. Boyd, and A. Mezzacappa, “Black hole formation in core collapse supernovae and time- of-flight measurements of the neutrino masses,” *Phys. Rev.* **D63** (2001) 073011, [astro-ph/0010398](#).
- [55] R. Mayle, J. R. Wilson, and D. N. Schramm, “Neutrinos from gravitational collapse,” *Astrophys. J.* **318** (1987) 288–306.
- [56] A. Burrows, D. Klein, and R. Gandhi, “The future of supernova neutrino detection,” *Phys. Rev.* **D45** (1992) 3361–3385.
- [57] M. T. Keil, *Supernova neutrino spectra and applications to flavor oscillations*. PhD thesis, 2003. [astro-ph/0308228](#).
- [58] D. N. Spergel, T. Piran, A. Loeb, J. Goodman, and J. N. Bahcall, “A simple model for neutrino cooling of the lmc supernova,” *Science* **237** (1987) 1471.

[59] H. T. Janka, “When do supernova neutrinos of different flavors have similar luminosities but different spectra?,” *Astropart. Phys.* **3** (1995) 377–384, [astro-ph/9503068](#).

[60] S. E. Woosley, J. R. Wilson, G. J. Mathews, R. D. Hoffman, and B. S. Meyer, “The r process and neutrino heated supernova ejecta,” *Astrophys. J.* **433** (1994) 229–246.

[61] R. Buras, “Private communication.”

[62] G. G. Raffelt, “Mu- and tau-neutrino spectra formation in supernovae,” *Astrophys. J.* **561** (2001) 890–914, [astro-ph/0105250](#).

[63] M. T. Keil, G. G. Raffelt, and H.-T. Janka, “Monte carlo study of supernova neutrino spectra formation,” *Astrophys. J.* **590** (2003) 971–991, [astro-ph/0208035](#).

[64] G. G. Raffelt, *Stars as laboratories for fundamental physics: The astrophysics of neutrinos, axions, and other weakly interacting particles*. Chicago, USA: Univ. Pr. (1996) 664 p.

[65] H. Minakata and H. Nunokawa, “Inverted hierarchy of neutrino masses disfavored by supernova 1987a,” *Phys. Lett.* **B504** (2001) 301–308, [hep-ph/0010240](#).

[66] C. Lunardini and A. Y. Smirnov, “Supernova neutrinos: Earth matter effects and neutrino mass spectrum,” *Nucl. Phys.* **B616** (2001) 307–348, [hep-ph/0106149](#).

[67] A. S. Dighe and A. Y. Smirnov, “Identifying the neutrino mass spectrum from the neutrino burst from a supernova,” *Phys. Rev.* **D62** (2000) 033007, [hep-ph/9907423](#).

[68] M. Aglietta *et al.*, “Effects of neutrino oscillations on the supernova signal in lvd,” *Nucl. Phys. Proc. Suppl.* **110** (2002) 410–413, [astro-ph/0112312](#).

[69] K. Takahashi and K. Sato, “Earth effects on supernova neutrinos and their implications for neutrino parameters,” *Phys. Rev.* **D66** (2002) 033006, [hep-ph/0110105](#).

[70] C. Lunardini and A. Y. Smirnov, “Probing the neutrino mass hierarchy and the 13-mixing with supernovae,” *JCAP* **0306** (2003) 009, [hep-ph/0302033](#).

- [71] A. S. Dighe, M. T. Keil, and G. G. Raffelt, “Identifying earth matter effects on supernova neutrinos at a single detector,” *JCAP* **0306** (2003) 006, [hep-ph/0304150](#).
- [72] Z. Maki, M. Nakagawa, and S. Sakata, “Remarks on the unified model of elementary particles,” *Prog. Theor. Phys.* **28** (1962) 870.
- [73] **Particle Data Group** Collaboration, S. Eidelman *et al.*, “Review of particle physics,” *Phys. Lett.* **B592** (2004) 1.
- [74] T. K. Kuo and J. Pantaleone, “Neutrino oscillations in matter,” *Rev. Mod. Phys.* **61** (1989) 937.
- [75] G. L. Fogli, E. Lisi, D. Montanino, and A. Palazzo, “Supernova neutrino oscillations: A simple analytical approach,” *Phys. Rev.* **D65** (2002) 073008, [hep-ph/0111199](#).
- [76] L. Wolfenstein, “Neutrino oscillations in matter,” *Phys. Rev.* **D17** (1978) 2369.
- [77] S. P. Mikheev and A. Y. Smirnov, “Resonant amplification of neutrino oscillations in matter and solar neutrino spectroscopy,” *Nuovo Cim.* **C9** (1986) 17–26.
- [78] J. N. Bahcall, M. C. Gonzalez-Garcia, and C. Pena-Garay, “Solar neutrinos before and after neutrino 2004,” *JHEP* **08** (2004) 016, [hep-ph/0406294](#).
- [79] T. K. Kuo and J. Pantaleone, “Supernova neutrinos and their oscillations,” *Phys. Rev.* **D37** (1988) 298.
- [80] S. P. Mikheev and A. Y. Smirnov, “3 nu oscillations in matter and solar neutrino data,” *Phys. Lett.* **B200** (1988) 560–564.
- [81] E. K. Akhmedov, “Parametric resonance of neutrino oscillations and passage of solar and atmospheric neutrinos through the earth,” *Nucl. Phys.* **B538** (1999) 25–51, [hep-ph/9805272](#).
- [82] A. Strumia and F. Vissani, “Precise quasielastic neutrino nucleon cross section,” *Phys. Lett.* **B564** (2003) 42–54, [astro-ph/0302055](#).
- [83] E. Nardi and J. I. Zuluaga, “Exploring the sub-ev neutrino mass range with supernova neutrinos,” *Phys. Rev.* **D69** (2004) 103002, [astro-ph/0306384](#).

- [84] T. Totani, K. Sato, H. E. Dalhed, and J. R. Wilson, “Future detection of supernova neutrino burst and explosion mechanism,” *Astrophys. J.* **496** (1998) 216–225, [astro-ph/9710203](#).
- [85] E. Nardi and J. I. Zuluaga, “Constraints on neutrino masses from a galactic supernova neutrino signal at present and future detectors,” *Nucl. Phys. B* **731** (2005) 140–163, [hep-ph/0412104](#).
- [86] R. W. Mayle, J. R. Wilson, and M. Tavani, “Pions, supernovae, and the supranuclear matter density equation of state,” *Astrophys. J.* **418** (1993) 398–404.
- [87] H.-T. Janka and W. Hillebrandt, “Neutrino emission from type II supernovae - an analysis of the spectra,” *Astron. and Astrophys.* **224** (Oct., 1989) 49–56.
- [88] M. Rampp, *Radiation Hydrodynamics with Neutrinos: Stellar Core Collapse and the Explosion Mechanism of Type II Supernovae*. PhD thesis, 2000.
- [89] M. Rampp and H. T. Janka, “Spherically symmetric simulation with boltzmann neutrino transport of core collapse and post-bounce evolution of a 15 solar mass star,” *Astrophys. J.* **539** (2000) L33–L36, [astro-ph/0005438](#).
- [90] M. Rampp and H. T. Janka, “Radiation hydrodynamics with neutrinos: Variable eddington factor method for core-collapse supernova simulations,” *Astron. Astrophys.* **396** (2002) 361, [astro-ph/0203101](#).
- [91] R. Buras, H.-T. Janka, M. T. Keil, G. G. Raffelt, and M. Rampp, “Electron-neutrino pair annihilation: A new source for muon and tau neutrinos in supernovae,” *Astrophys. J.* **587** (2003) 320–326, [astro-ph/0205006](#).
- [92] K. Nakamura, “Hyper-kamiokande: A next generation water cherenkov detector,” *Int. J. Mod. Phys. A* **18** (2003) 4053–4063.
- [93] L. Oberauer, “Low energy neutrino physics after sno and kamland,” *Mod. Phys. Lett. A* **19** (2004) 337–348, [hep-ph/0402162](#).
- [94] **KATRIN** Collaboration, A. Osipowicz *et al.*, “Katrín: A next generation tritium beta decay experiment with sub-ev sensitivity for the electron neutrino mass,” [hep-ex/0109033](#).
- [95] **KATRIN** Collaboration, C. Weinheimer, “Katrín, a next generation tritium beta decay experiment in search for the absolute neutrino mass scale,” *Prog. Part. Nucl. Phys.* **48** (2002) 141–150.

- [96] O. Cremonesi, “Neutrinoless double beta decay: Present and future,” *Nucl. Phys. Proc. Suppl.* **118** (2003) 287–296, [hep-ex/0210007](#).
- [97] G. D’Agostini, “Bayesian inference in processing experimental data: Principles and basic applications,” *Rept. Prog. Phys.* **66** (2003) 1383–1420, [physics/0304102](#).
- [98] D. Sivia, *Data analysis: A Bayesian tutorial*. Oxford, UK: Oxford Science Publications (1998).
- [99] R. Cox, “Probability, frequency and reasonable expectation,” *American Journal of Physics* **14** (1946) 1–13.
- [100] V. Dose, “Bayes in five days.” CIPS, MPI fr Plasmaphysik, Garching, Germany, Reprint 83, May 2002.
- [101] U. Seljak and M. Zaldarriaga, “A line of sight approach to cosmic microwave background anisotropies,” *Astrophys. J.* **469** (1996) 437–444, [astro-ph/9603033](#).
- [102] J. Zuluaga, “Programming with sung: reference manual,” 2004. <http://www.sungweb.tk>.
- [103] “Gnu scientific library (gsl).” GNU Project, <http://www.gnu.org/software/gsl>.
- [104] “CERNLIB libraries.” Computing and Network division, CERN. <http://cernlib.web.cern.ch/cernlib/libraries.html>.
- [105] T. William and C. Kelley, “Gnuplot.” <http://www.gnuplot.info>.
- [106] W. H. Press, B. P. Flannery, S. A. Teukolsky, and W. T. Vetterling, *Numerical Recipes: The Art of Scientific Computing*. Cambridge University Press, Cambridge (UK) and New York, 2nd ed., 1992.